

2

Semiannual Technical Report

AD-A267 305



Growth and Doping of $Al_xGa_{1-x}N$ Films by Electron Cyclotron Resonance Assisted Molecular Beam Epitaxy

ONR Grant No. N00014-92-J-1436
(May 1, 1992 - April 30, 1993)

P.I. Theodore D. Moustakas

Department of Electrical,
Computer, and Systems Engineering

Boston Univeristy
Boston, MA 02215
617-353-5431

DTIC
ELECTE
JUL 27 1993
S E D

Approved for Public Release; Distribution Unlimited

May 30, 1992

93-16819



104PF

93 7 28 102

Table of Contents

1 Summary of results during the funding period	2
1.1 Heteroepitaxial growth of GaN by ECR-assisted MBE	2
1.2 Heteroepitaxial growth of AlN by ECR-assisted MBE	3
1.3 n- and p-doping of GaN films	3
1.4 Growth of High mobility GaN films and Transport Mechanism in GaN	3
1.5 Ohmic contacts & Processing of GaN	3
1.6 Atomic Structure Studies	4
1.7 Photoluminescence Studies	4
1.8 Conduction Electron Spin Resonance Studies	4
2 Figures	5
Figure 1 : Optical Spectra of Plasma	6
Figure 2 : Surface Morphology v. Power for GaN	7
Figure 3 : RHEED v. Power for GaN	8
Figure 4 : RHEED of AlN	9
Figure 5 : SEM of AlN	10
Figure 6 : XRD of AlN	11
Figure 7 : Mobility of GaN	12
Figures 8 : Photoluminescence spectra for GaN	13(a,b,c)
3 References	14
4 Publication List	15

Appendix A: "Growth of GaN by ECR-assisted MBE"

Appendix B: "Growth and Doping of GaN films by ECR-Assisted MBE"

Appendix C: "High Mobility GaN Films Produced by ECR-Assisted MBE"

Appendix D: "Electron Transport mechanism in Gallium Nitride"

Appendix E: "Metal Contacts to Gallium Nitride"

Appendix F: "Heteroepitaxy, Polymorphism, and Faulting in GaN Thin Films on Silicon and Sapphire Substrates"

Appendix G: "Conduction Electron Spin Resonance in Zinc-Blende GaN Thin Films"

DTIC QUALITY INSPECTED 5

Accession For	
NTIS CRA&I	<input checked="" type="checkbox"/>
DTIC TAB	<input type="checkbox"/>
U. announced	<input type="checkbox"/>
Justification	
By	
Distribution /	
Availability Codes	
Dist	Avail and/or Special
A-1	

1 Summary of results during the funding period

During this funding year the work was focused on the heteroepitaxial growth and doping of GaN films by the method of Electron Cyclotron Resonance microwave plasma assisted Molecular Beam Epitaxy. Work was also initiated in the growth of AlN. A brief description of specific accomplishments are listed below:

1.1 Heteroepitaxial growth of GaN by ECR-assisted MBE.

The N₂ ECR plasmas employed in the growth of GaN were investigated by optical emission spectroscopy. Figure 1 shows one such spectrum. It is obvious that both neutral and ionic species are present in such plasmas.

The heteroepitaxial growth of GaN on a variety of substrates [Si(100), Si(111), sapphire (c, α , R-planes)] by the ECR-MBE method was investigated, using a two step growth process for GaN which specifically separates the nucleation and growth phases. Since the nucleation rate depends exponentially on $1/T$ it is clear that the nucleation dominated regime occurs at low temperatures. Thus, we developed a low temperature buffer which covers uniformly the substrate due to the large nucleation rate. The growth of the rest of the film occurs at relatively higher temperatures and should be close to homoepitaxy. Under equilibrium conditions, homoepitaxy should proceed in the layer-by-layer mode without the formation of nuclei. However, due to imperfections of the buffer layer, nuclei may form at the surface edges and steps at small contact angles. Recently we were able to form GaN films in their zincblende structure on Si (001) with an extremely low two-dimensional nucleation rate (~ 20 nuclei/ $\mu\text{m}^2 \cdot \text{h}$) and lateral growth rate 100 times the vertical growth rate. Thus, under these conditions, the growth is quasi *layer-by-layer*. (1,2)

More recently, studies of GaN growth on sapphire (0001) indicate a complete layer-by-layer growth and atomically smooth surfaces. This was accomplished by optimizing ion assisted growth. Figure 2 shows the effect of ion assistace (microwave power in the discharge) in the transition from an island growth or Volmer-Weber mode (a) to a layer-by-layer or Frank-Van der Merwe growth mode (b) and to a layer-by-layer followed by island or Stranski-Krastanov growth mode (c). Figure 3 shows the corresponding RHEED studies of these films, which also indicate that the first two films have atomically smooth surfaces while the third film has a rough surface.

Besides the GaN-buffer, we have recently developed an AlN buffer not by a deposition process but by nitridation of the sapphire substrate. We found that the conversion of Al₂O₃ surface to AlN requires exposing the substrate, held at 850°C, to an ECR nitrogen plasma for approximately 10-15 min. This AlN layer appears to be atomically smooth based on the elongated RHEED pattern(2,3). We found that the GaN-buffer, which is usually grown at lower temperatures (approximately 400°C), is atomically smooth, when grown on the top of this AlN buffer. Furthermore, GaN films grown on the combination of AlN-GaN buffers were found to have the best surface morphology with lateral growth rate much higher than the vertical growth rate. The best films were found to have a rocking curve around the main

peak with FWHM of 10 min. Details of these results are presented in Appendix A and B.

1.2 Heteroepitaxial growth of AlN by ECR-assisted MBE.

The growth of AlN has not yet been optimized. In the initial studies we attempted to grow AlN on (0001) sapphire at relatively low temperatures (800°C) so that the growth of AlN would be comparable with that of GaN. The RHEED pattern, surface morphology, and XRD diffraction of such a film are shown in Figures 4, 5, and 6, respectively. These data indicate that the AlN grown so far is inferior to our GaN films.

These studies were interrupted temporarily due to the failure of two Al-Knudsen cells. In both cases the heating elements failed, presumably due to exposure to a nitrogen atmosphere at very high temperatures (nitridation).

1.3 n- and p-doping of GaN films.

Plasma modes with high nitrogen plasma density were identified which allow the growth of semi-insulating GaN films (resistivity at 300°K of $10^{12}\Omega\cdot\text{cm}$).

Such GaN films were doped n-type with Si, a common dopant in MBE growth. Silicon was incorporated as a donor with a net carrier concentration of $N_D - N_A = 2 \times 10^{18}\text{cm}^{-3}$.

GaN films produced under the growth conditions which lead to intrinsic films were also doped p-type by the incorporation of Mg. Carrier concentrations up to 2×10^{19} were also obtained without requiring an additional annealing step as reported previously (4,5). These studies are presented in Appendix B.

1.4 Growth of High mobility GaN films and transport mechanism in GaN.

We have been able to grow auto-doped GaN films systematically with carrier concentrations from 10^{19} to $2 \times 10^{17}\text{cm}^{-3}$. Simultaneously, the electron mobility increased from about $20\text{ cm}^2/\text{V}\cdot\text{sec}$ to $210\text{ cm}^2/\text{V}\cdot\text{sec}$. These results are illustrated in Figure 7. It is interesting to note that this curve extrapolates to a mobility of $600\text{ cm}^2/\text{V}\cdot\text{sec}$ reported for GaN films grown by the MOCVD method (5). Based on the temperature dependent transport measurements, a picture of simultaneous transport in the conduction band and the autodoping centers has emerged. When the concentration of the autodoping centers becomes less than the concentration of the deep defects, the material becomes fully compensated, leading to hopping conduction in the deep compensating defects, accounting for the low electron mobility in these films(7). Details on these studies are presented in Appendix C and D

1.5 Ohmic Contacts / Processing of GaN.

Reactive Ion Etching (RIE) techniques have been developed to process GaN films. Etching was carried out in Freon 12, at $200\text{Å}/\text{min}$ and selectivity 3:1 for GaN/photoresist (8).

The rectification properties of various metal contacts to GaN were investigated. A direct correlation between the metal work functions and barrier height to GaN was found, a result attributed to the ionic character of GaN. Thus, ohmic contacts to both n- and p-type GaN can be made by choosing metals with the appropriate work functions (Al for n-type and Au for p-type) (9). Details on these studies can be found in Appendix E.

1.6 Atomic Structure Studies.

The structure of GaN films grown on a variety of substrates [Si(100), Si(111), sapphire (c, α , R-planes)] was studied with four-circle X-ray diffractometry. These studies allowed us to determine the presence of secondary phases, the direction and quality of orientational ordering in and out of the substrate plane and the homogeneous and inhomogeneous strains in the film. Our studies show that wurtzite and zincblende GaN polymorphs often coexist in films which grow with their close-packed stacking planes parallel to the substrate. The evidence suggests that the zincblende phase may nucleate at stacking faults (4). Details on these studies are described in Appendix F.

1.7 Photoluminescence Studies.

A photoluminescence system was set up using a pulsed N₂ laser as the excitation source. The laser has a photon energy of 3.678eV, pulse width of 10ns, repetition rate of 40Hz, and a listed peak power of 25KW.

Figure 8 shows typical photoluminescence spectra of undoped, Mg p-type doped, and Si n-type doped GaN films. These data clearly indicate that doping modifies the photoluminescence transitions. These studies are still in progress and will be pursued during the second funding year.

1.8 Conduction Electron Spin Resonance Studies.

Electron Spin Resonance in zincblende GaN thin films were conducted at temperatures below 100°K. The observed resonance has an isotropic g-value of 1.9533 which, in the investigated temperature range, was attributed to non-localized electrons in a band of auto-doping centers (N-vacancies). The g-value agrees with the value calculated using a five-band model and the same theory predicts an effective mass of $m^*/m = 0.15$. Details of these studies are presented in Appendix G.

2 Figures

Optical Emission Spectra of ECR Nitrogen Plasma

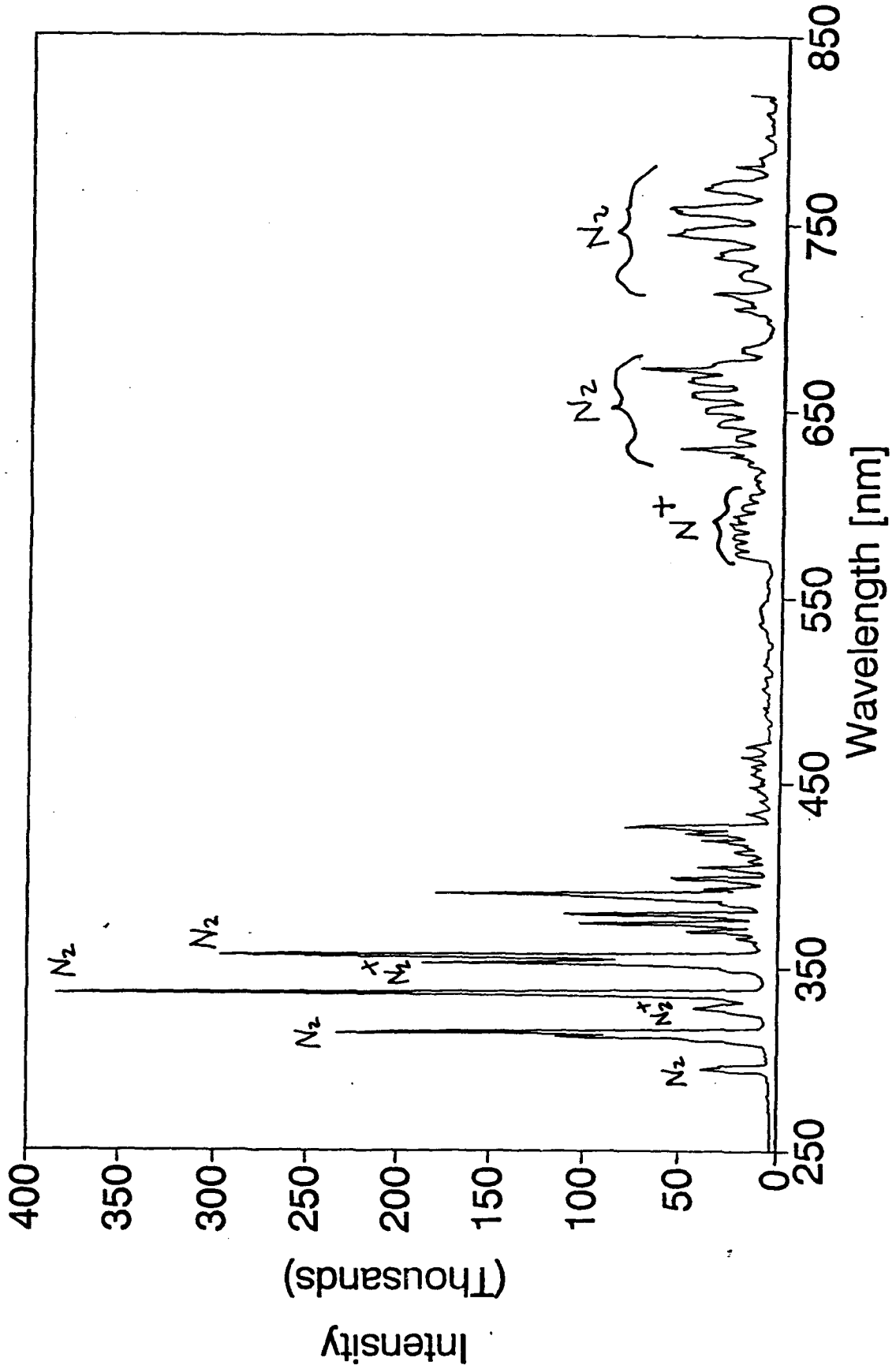
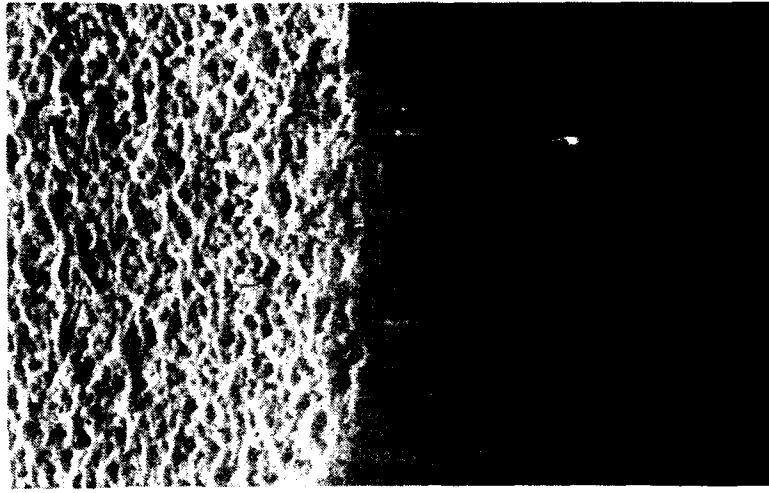


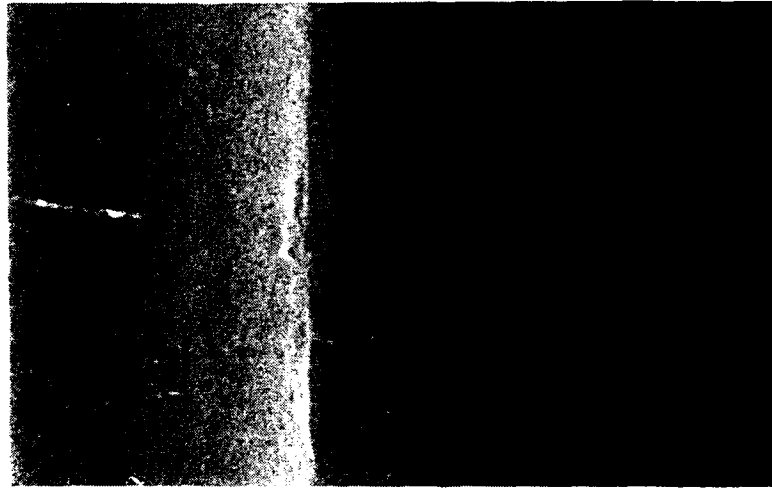
Figure 1.

Figure 2.

Suface Morphology v. Plasma Power



25W



25.000 14m

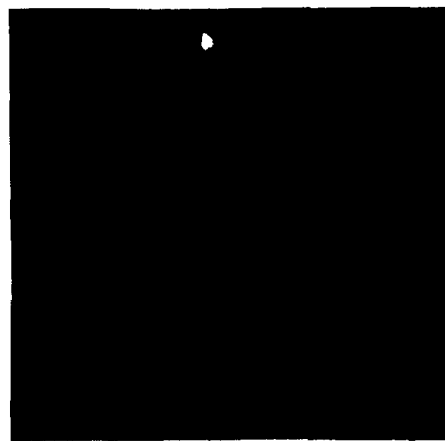
20W



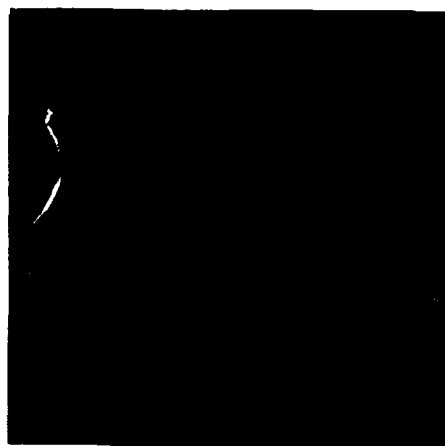
18W

Figure 3.

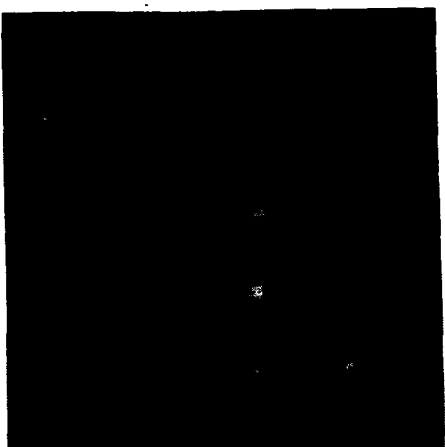
RHEED v. Plasma Power



18W



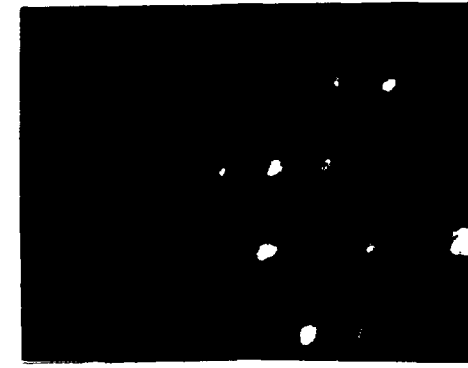
20W



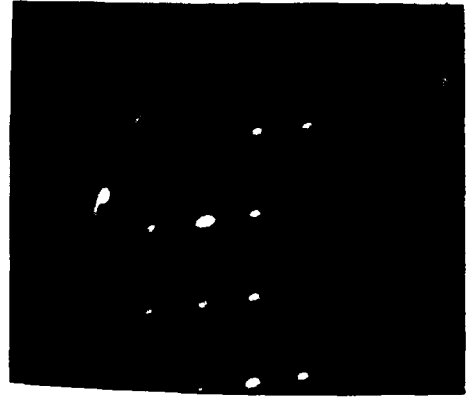
25W

Figure 4.

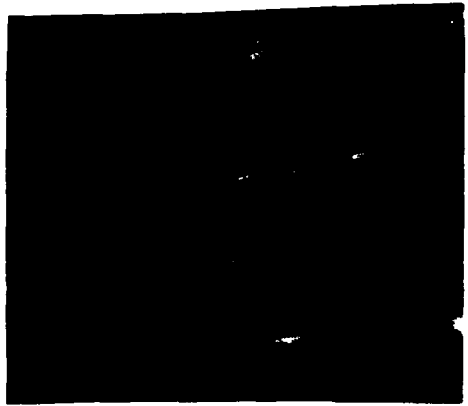
RHEED During Growth of AlN



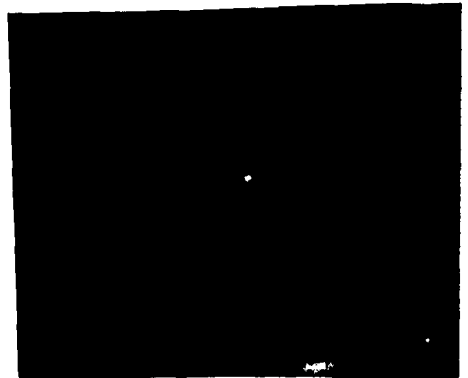
8 hr



35 min



5 min



Substrate after

Plasma

Nitridation

Figure 5.

Surface Morphology of AlN

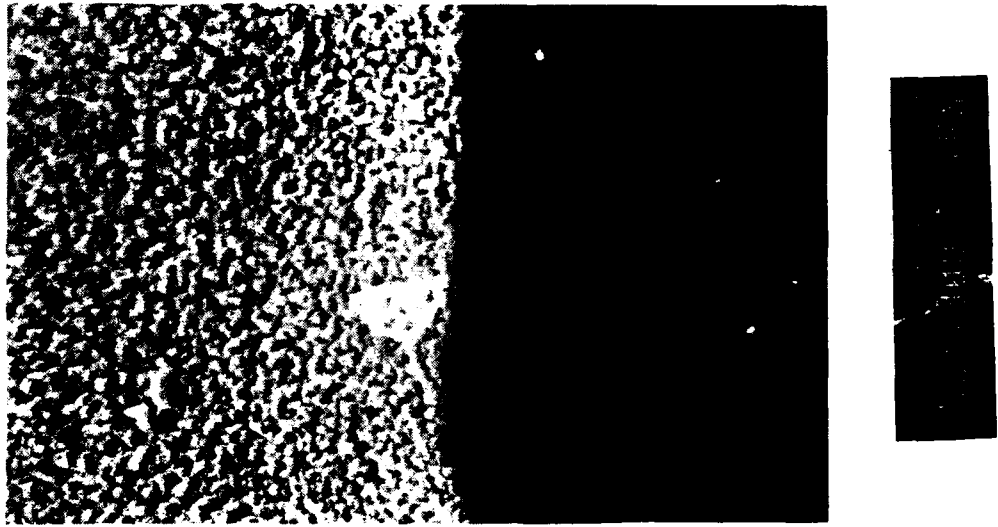


Figure 6.

$\theta/2\theta$ XRD and θ -Rocking
Curve for an AlN Film

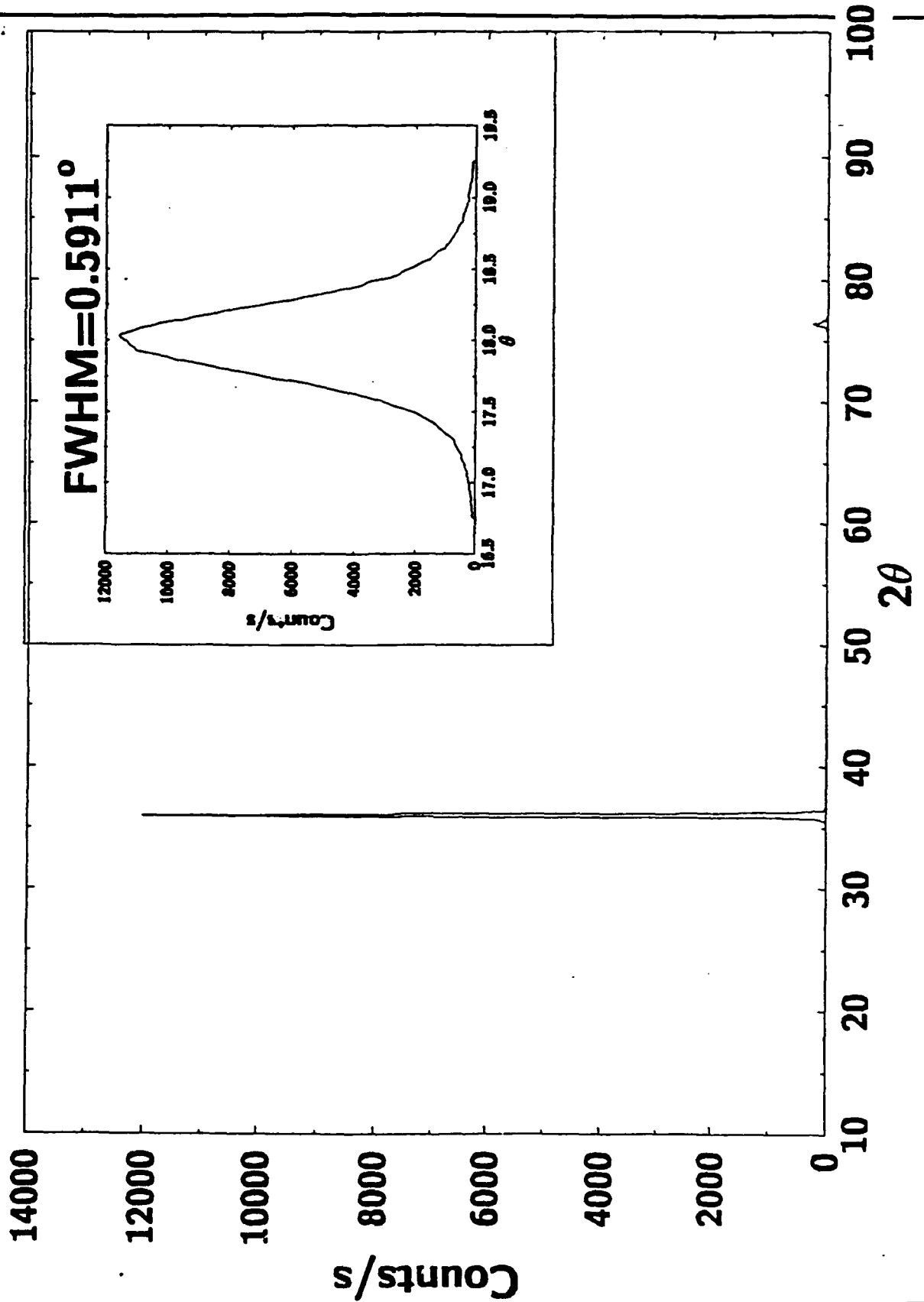
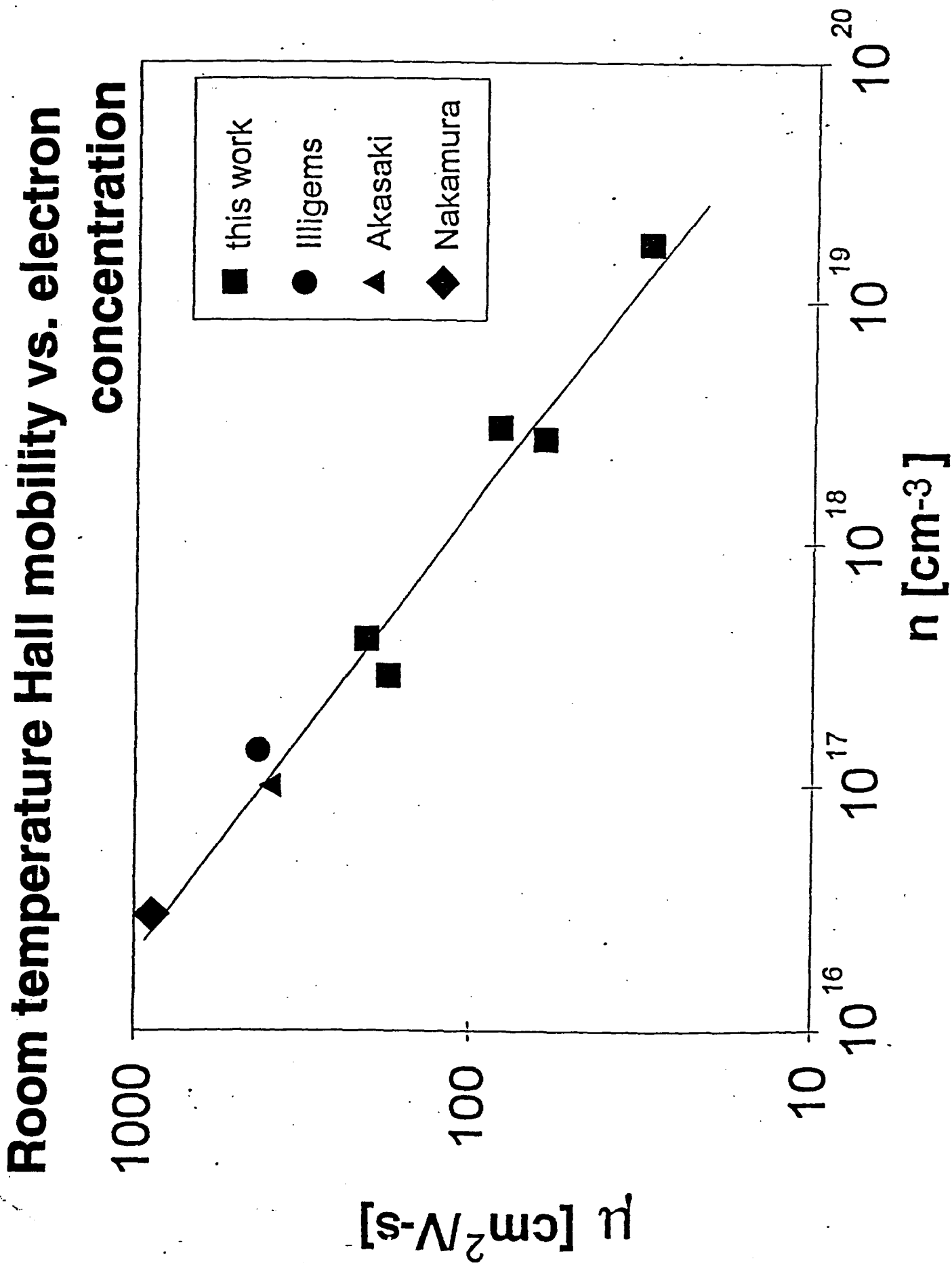
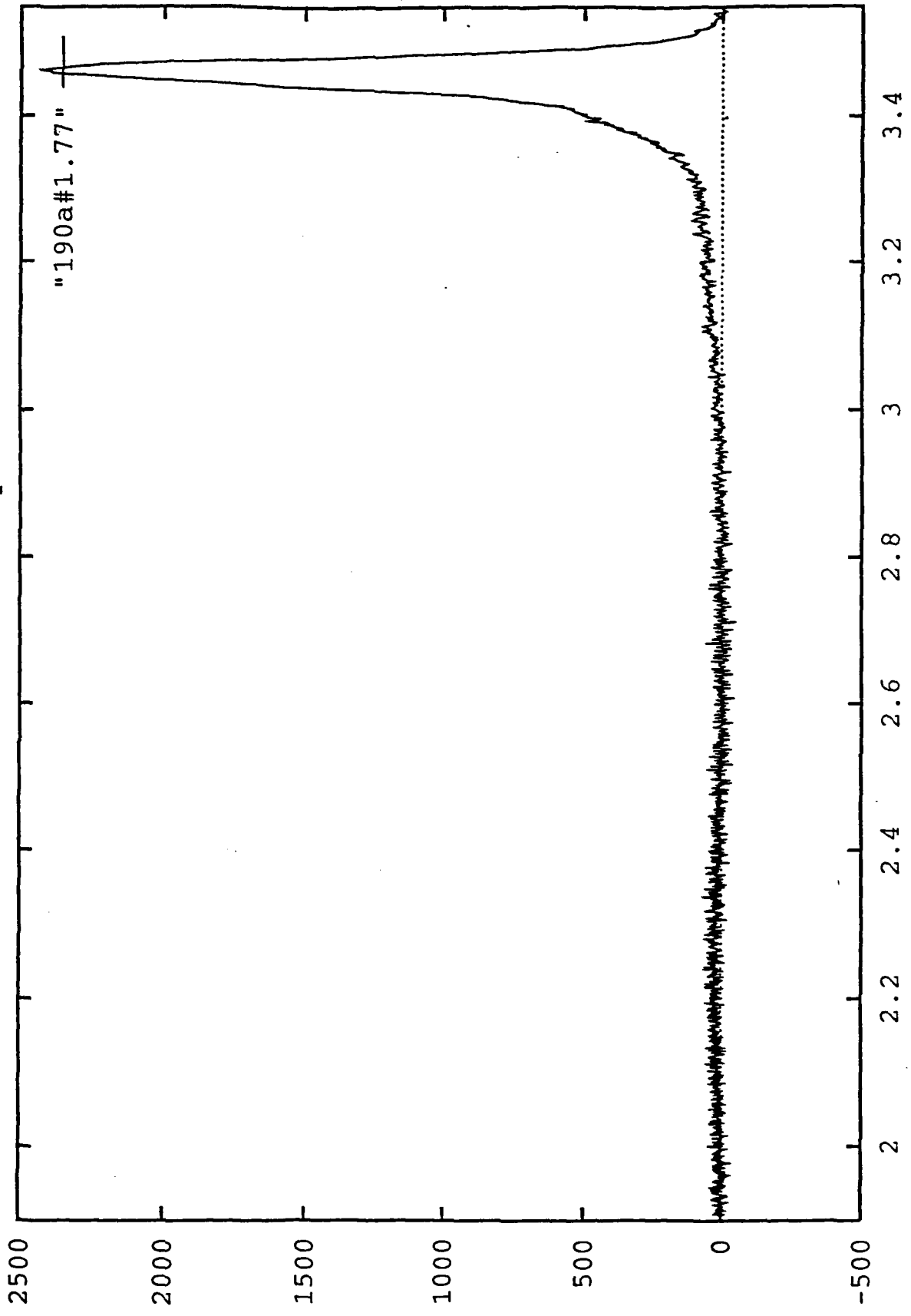


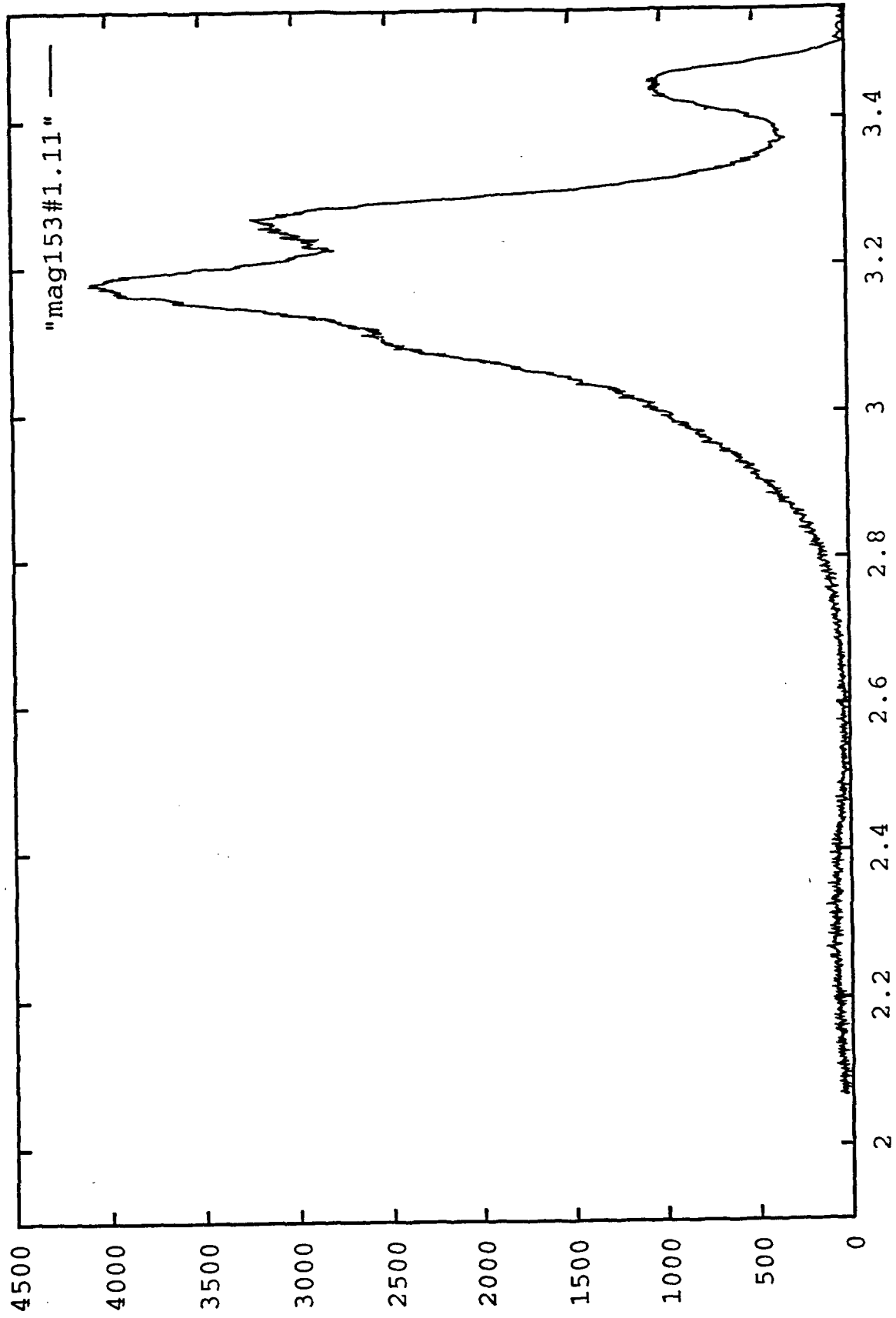
Figure 7.



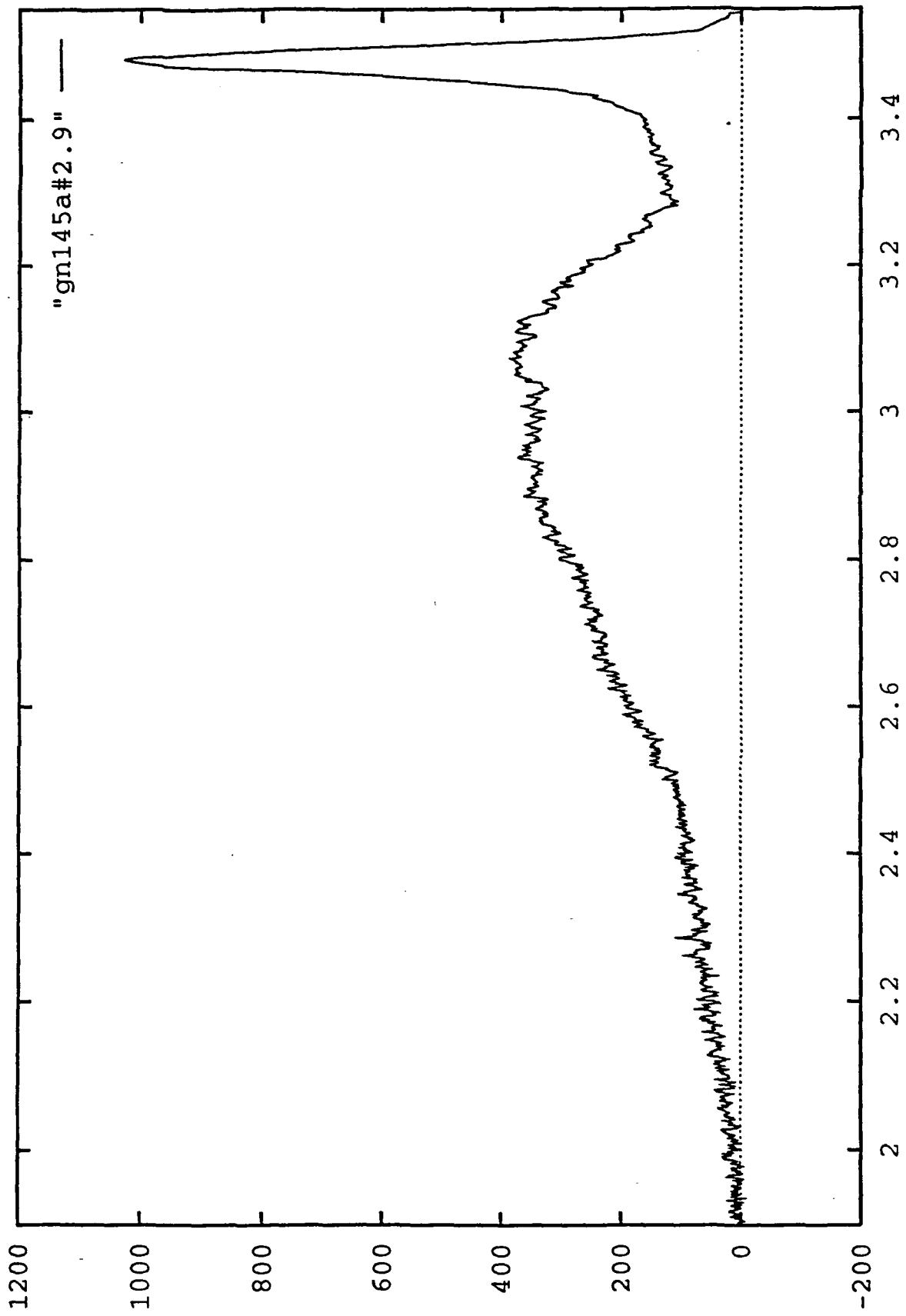
8a. Photoluminescence Spectra for Undoped GaN .



8b. Photoluminescence Spectra for p-type Doped GaN .



8c. Photoluminescence Spectra for n-type Doped GaN .



3 References

1. "Epitaxial growth and characterization of zinc-blende gallium nitride on (001) silicon," T. Lei, T.D. Moustakas, R.J. Graham, Y. He, and S.J. Berkowitz, *J. Appl. Phys.* **71**, 4933 (1992).
2. "Growth of GaN by ECR-Assisted MBE," T.D. Moustakas, T. Lei, and R.J. Molnar, *Physica B*, **185**, 36 (1993).
3. "A Comparative Study of GaN Films Grown on Different Faces of Sapphire by ECR-Assisted MBE," T.D. Moustakas, R.J. Molnar, T. Lei, G. Menon, and C.R. Eddy Jr., *Mat. Res. Soc. Symp. Proc. Vol. 242*, 427 (1992).
4. "Thermal Annealing Effects on P-Type Mg-Doped GaN films," S. Nakamura, T. Mukai, M. Senoh, and N. Iwasa, *Jpn. J. Appl. Phys. Vol. 31*, L139 (1992).
5. "Conductivity Control of AlGa_N, Fabrication of AlGa_N/GaN Multiheterostructures and Their Application to UV/Blue Light Emitting Devices," I. Akasaki and H. Amano, *Mat. Res. Soc. Symp. Proc. Vol. 242*, 383 (1992).
6. "High mobility GaN films produced by ECR-assisted MBE," R.J. Molnar, T. Lei, and T.D. Moustakas, *Mat. Res. Soc. Proc.*, 281 (1993).
7. "Electron Transport Mechanism in Gallium Nitride," R.J. Molnar, T. Lei, and T.D. Moustakas, *Appl. Phys. Lett.*, **62**, 72 (1993).
8. "Ohmic Contacts and Schottky Barriers on Gallium Nitride," J. Foresi, M.S. Thesis (Boston University, 1992).
9. "Metal Contacts to Gallium Nitride," J. Foresi and T.D. Moustakas, *Appl. Phys. Lett.*, **62**, 2859 (1993).
10. "Heteroepitaxy, Polymorphism, and Faulting in GaN Thin Films on Silicon and Sapphire Substrates," T. Lei, K.F. Ludwig Jr, and T.D. Moustakas, *J. Appl. Phys.*, accepted for publication (Oct. 1993).

4 Publication List

"Growth of GaN by ECR-Assisted MBE"
T.D. Moustakas, T. Lei, and R.J. Molnar
Physica B, 185, 36 (1993)
Appendix A

"Growth and Doping of GaN Films by ECR-Assisted MBE"
T.D. Moustakas and R.J. Molnar
Mat. Res. Soc. Proc., vol 281 (1993).
Appendix B

"Electron Transport Mechanism in Gallium Nitride"
R.J. Molnar, T. Lei, and T.D. Moustakas
Appl. Phys. Lett., 62, 72 (1993)
Appendix C

"High Mobility GaN Films produced by ECR-Assisted MBE"
R.J. Molnar, T. Lei, and T.D. Moustakas
Mat. Res. Soc. Proc., vol 281
Appendix D

"Metal Contacts to Gallium Nitride"
J.S. Foresi and T.D. Moustakas
Appl. Phys. Lett, 62, 2859 (1993)
Appendix E

"Heteropitaxy, Polymorphism, and Faulting in GaN Thin Films on Silicon and Sapphire"
T. Lei, K.F. Ludwig, and T.D. Moustakas
J. Appl. Phys., accepted (1993)
Appendix F

"Conduction electron spin resonance in zinc-blende GaN thin films"
M. Fanciulli and T.D. Moustakas
Phys. Rev. B (submitted)
Appendix G

"P-type doping of GaN"
R.J. Molnar and T.D. Moustakas
Bull. of Amer. Phys. Soc., 38, 445 (1993)

"Conduction Electron Spin Resonance in Zinc-Blende GaN Thin Films"
M. Fanciulli, T. Lei, and T.D. Moustakas
Bull. of Amer. Phys. Soc., 38, 621 (1993)

"Potential of III-V Nitrides for Optical and Electronic Applications"
T.D. Moustakas
183rd Meeting of ECS, Extended Abstracts, vol 93-1, 955 (1993)

Appendix A:

Growth of GaN by ECR-assisted MBE
Published in *Physica B* 185, 36 (1993).

Growth of GaN by ECR-assisted MBE

T.D. Moustakas, T. Lei and R.J. Molnar

Molecular Beam Epitaxy Laboratory, Department of Electrical, Computer and Systems Engineering, Boston University, MA, USA

High-quality GaN films have been grown on a variety of substrates by electron cyclotron resonance microwave plasma-assisted molecular beam epitaxy (ECR-MBE). The films were grown in two steps. First, a GaN-buffer was grown at low temperature and then the rest of the film was grown at higher temperatures. We found that this method of growth leads to a relatively small two-dimensional nucleation rate (~ 20 nuclei/ μm^2 h) and high lateral growth rate (100 times faster than the vertical growth rate). This type of quasi-layer-by-layer growth results in a smooth surface morphology to within 100 Å. Growth on Si(100) leads to single-crystalline GaN films having the zinc-blende structure. Growth on Si(111) leads to GaN films having the wurtzitic structure with a large concentration of stacking faults. The crystallographic orientation and the surface morphology of GaN films on sapphire depends on the orientation of sapphire. To this date, the best films were grown on the basal plane of sapphire.

1. Introduction

The family of refractory nitrides (InN, GaN and AlN), their solid solutions and heterojunctions are one of the most promising families of electronic materials. All three are direct bandgap semiconductors with their energy gaps covering the region from 1.95 eV (InN) and 3.5 eV (GaN) to 6.28 eV (AlN). Thus, the growth of high-quality crystals and successful doping of these materials should lead to applications in optoelectronic devices from the visible to the ultraviolet part of the electromagnetic spectrum, as well as in devices for high-power and high-temperature electronics [1–2]. GaN, in particular, is predicted to have a high electron drift velocity, so it should also be suitable for high-frequency and microwave devices [3].

GaN films have been grown by many growth techniques, including chemical vapor deposition [4–7], metal-organic chemical vapor deposition [8–15], molecular beam epitaxy [16–25] and a number of plasma-assisted processes [26–30]. A

variety of substrates such as silicon, spinel, silicon carbide and various crystallographic orientations of sapphire have been used in these studies. Most of the films grown are wurtzitic (α -GaN) and have n-type conductivity with high carrier concentration [31], which is believed to result from nitrogen vacancies [31–32] or oxygen impurity incorporation [33]. P-type conductivity has been reported recently on Mg-doped GaN films [34–35].

Zincblende GaN (β -GaN), which is the thermodynamically metastable phase of GaN, is hoped to be more amenable to doping than the wurtzitic GaN, since all of the III–V compounds that can be efficiently doped n-type or p-type are cubic [2]. β -GaN has been epitaxially stabilized on a β -SiC and MgO(100) substrate [18–19], which are closely lattice-matched to β -GaN and on a GaAs [36–37] and Si substrate [21–25] which have significant mismatch to β -GaN.

In this paper, we review the growth of GaN films by the electron cyclotron resonance microwave plasma-assisted molecular beam epitaxy. Particular emphasis is placed on the growth of this material in two temperature steps, a method developed recently in our laboratory for the growth of GaN. [21–25,38]. Films have been

Correspondence to: T.D. Moustakas, Molecular Beam Epitaxy Laboratory, Department of Electrical, Computer and Systems Engineering, Boston University, Boston, MA 02215, USA.

grown on Si(100), Si(111) and various faces of sapphire.

2. Experimental methods

The deposition system used in this study is schematically illustrated in fig. 1. Two ECR sources were used. The first (Astex 8" model 1000) was used for the growth of GaN on Si(100) and Si(111). The second (Astex compact model) was used for the growth of GaN on sapphire. The base pressure in the overall system was 10^{-11} Torr. A reflection high-energy electron diffraction (RHEED) setup is an integral part of the apparatus. A conventional Knudsen effusion cell was used to evaporate gallium. Atomic and ionic nitrogen were produced by passing molecular nitrogen through the ECR source. Part of

the molecular nitrogen was also introduced downstream the ECR source. Typically, 10% of the molecular nitrogen gas is converted into atomic nitrogen. Due to this high decomposition rate, a source pressure of about 10^{-4} Torr is sufficient for the growth of stoichiometric films. The magnetic field configuration for the 8" source under optimized conditions for the growth of GaN films is illustrated in fig. 2. The on-axis ECR condition ($H = 875$ G) is about 40 cm above the substrate. The compact ECR source fits inside an effusion cell and thus the distance from the front of the source to the substrate is only 12 cm.

The structure and microstructure of the films were studied by reflection high-energy electron diffraction (RHEED), X-ray diffraction and scanning electron microscopy (SEM). X-ray diffraction studies were performed using a diffrac-

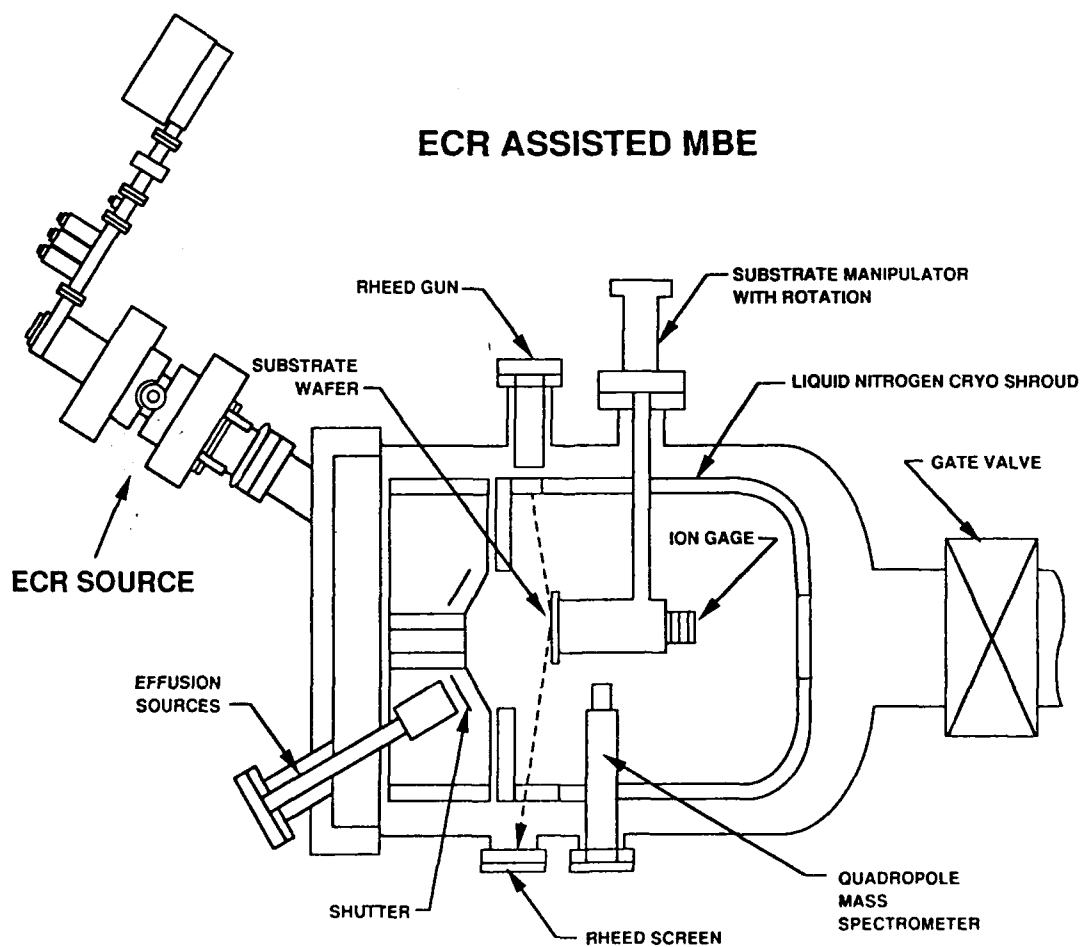


Fig. 1. Schematic of the deposition system.

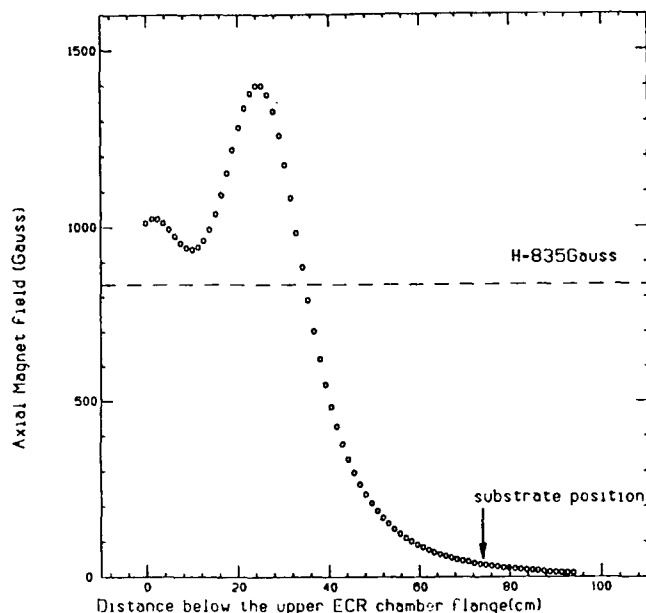


Fig. 2. Magnetic field configuration under optimized growth conditions.

tometer with four-circle geometry. This allows us to perform ϕ -scans at a reflection peak (hkl), corresponding to planes not parallel to the substrate to probe in-plane ordering. Additionally, standard θ - 2θ scans were performed to probe the ordering normal to the substrate.

Si(001) and Si(111) substrates (n-type, p-type or undoped) were used in these studies. They were ultrasonically degreased in solvents and etched in buffered HF to remove the oxides,

prior to their introduction into the MBE unit. In the preparation chamber, the substrates were outgassed for 15 minutes at 850°C.

The sapphire substrates were subjected to the following cleaning steps prior to the growth of the GaN films. They were sequentially cleaned in ultrasonic baths of trichloroethylene, acetone and isopropanol for removal of hydrocarbon residues from the surface, etched in $H_3PO_4:H_2SO_4$ (1:3) for the removal of surface contaminants and mechanical damage due to polishing and finally rinsed in de-ionized water. After these steps, the substrates were blown dry with nitrogen, mounted on a molybdenum block and transferred to the introduction chamber of the MBE system. In the preparation chamber, the substrates were heated to 850°C for approximately half an hour and then transferred to the growth chamber where they were subjected to bombardment by nitrogen plasma for approximately half an hour at 700°C.

3. Experimental results

3.1. Growth on Si(100)

Following clearing, the Si substrate was examined by studying its RHEED pattern in the growth chamber at 400°C. Figure 3 shows typical

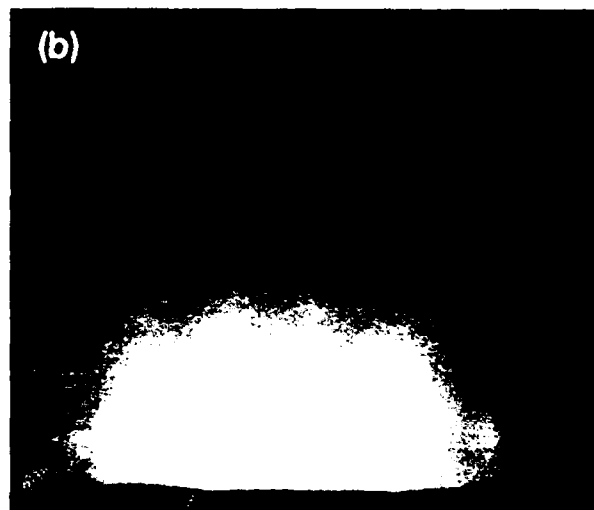
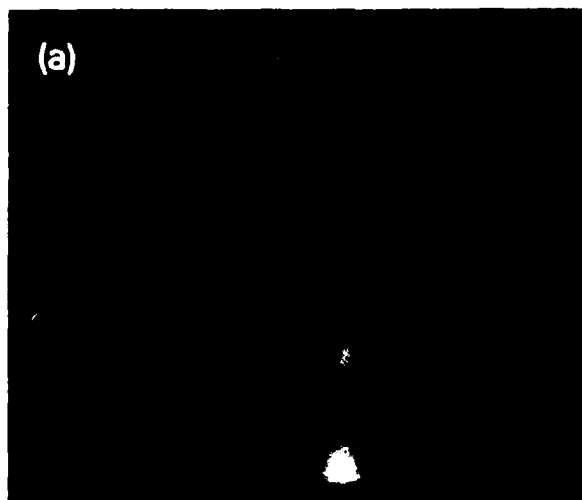


Fig. 3. RHEED patterns of Si(001) substrates after the routine preparation; (a) for [100] azimuthal incidence of the electron beam; (b) for [110] azimuthal incidence of the electron beam.

RHEED patterns of the Si substrate with the electron beam incident along the $[100]$ and $[110]$ directions. These results clearly indicate that the $\text{Si}(001)$ surface is unreconstructed (i.e. 1×1). We find that such an unreconstructed $\text{Si}(001)$ surface is required to epitaxially grow a single crystalline GaN-buffer. Outgassing of the Si substrate at lower temperatures, for example 600°C , leads to an irregular pattern with few diffraction spots, which we were unable to index with any reconstruction pattern. A GaN-buffer grown on such a surface would generally be polycrystalline with the wurtzitic structure. It is conceivable that epitaxy of GaN should take place on a well-ordered unreconstructed surface, but not on an irregular disordered surface.

After the substrate preparation and characterization, a GaN-buffer layer of about 300 \AA to 900 \AA thick was deposited at a temperature of 400°C for 10 to 30 minutes. Figure 4 shows the RHEED patterns at two azimuthal incidence angles of the electron beam for the GaN buffer layer. The diffraction spots were relatively broad, signifying that the thin buffer layer is very defective. This is expected due to the large lattice mismatch between the film and the substrate. However, the symmetry of the patterns indicates that the buffer layer has the zincblende

structure with the $[001]$ direction perpendicular to the substrate.

Following the deposition and characterization of the GaN-buffer the substrate was heated to a higher temperature, typically 600°C , and a GaN film of about $1 \mu\text{m}$ thick was grown at a growth rate about $2000 \text{ \AA}/\text{h}$. Shown in fig. 5(a) and (b) are typical RHEED patterns of a GaN film about $1 \mu\text{m}$ thick grown on a p-type substrate for $[100]$ and $[110]$ azimuthal incidence of the electron beam. The results are similar when the growth takes place on undoped substrates. These results clearly indicate that the GaN film has the zincblende structure, with its (001) crystallographic planes parallel to the substrate surface. The diffraction spots of this pattern are significantly sharper and elongated, which suggests that the final GaN film has a better crystalline quality and a smoother surface morphology than the GaN-buffer.

The RHEED pattern of a GaN film grown on a p-type substrate under slightly lower nitrogen pressure is shown in fig. 6. The streak-like pattern is characteristic of two-dimensional scattering, indicating that the GaN film is close to atomically smooth. Such elongated RHEED patterns were frequently observed when the growth took place on n-type substrates. This may sug-

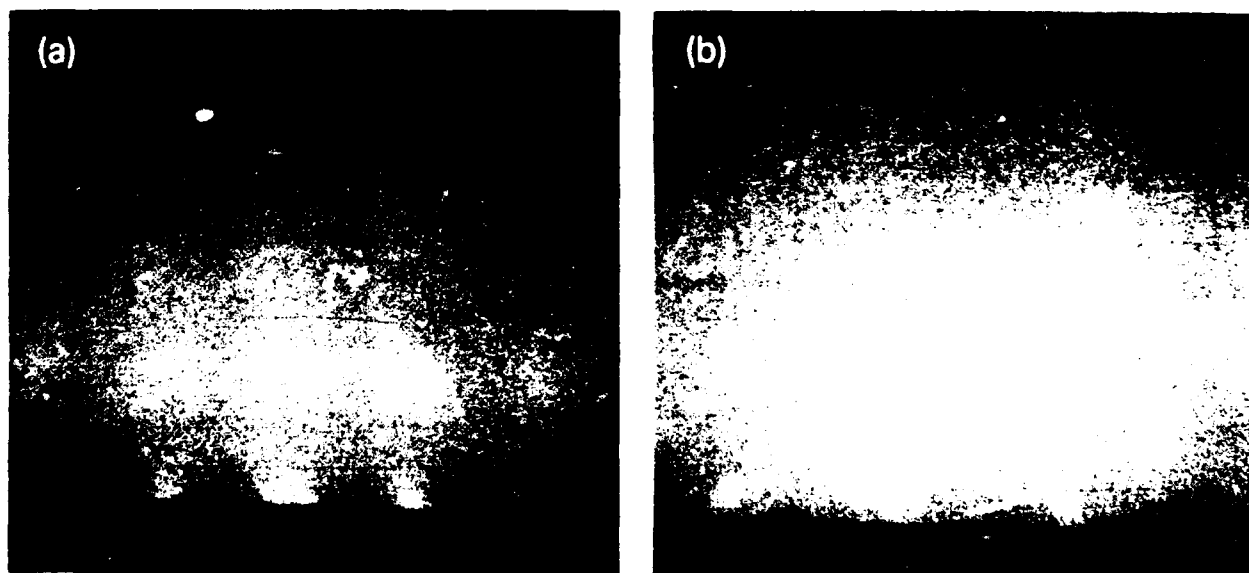


Fig. 4. RHEED patterns of GaN buffer grown at 400°C for 10 minutes; (a) for $[100]$ azimuthal incidence of the electron beam; (b) for $[110]$ azimuthal incidence of the electron beam.

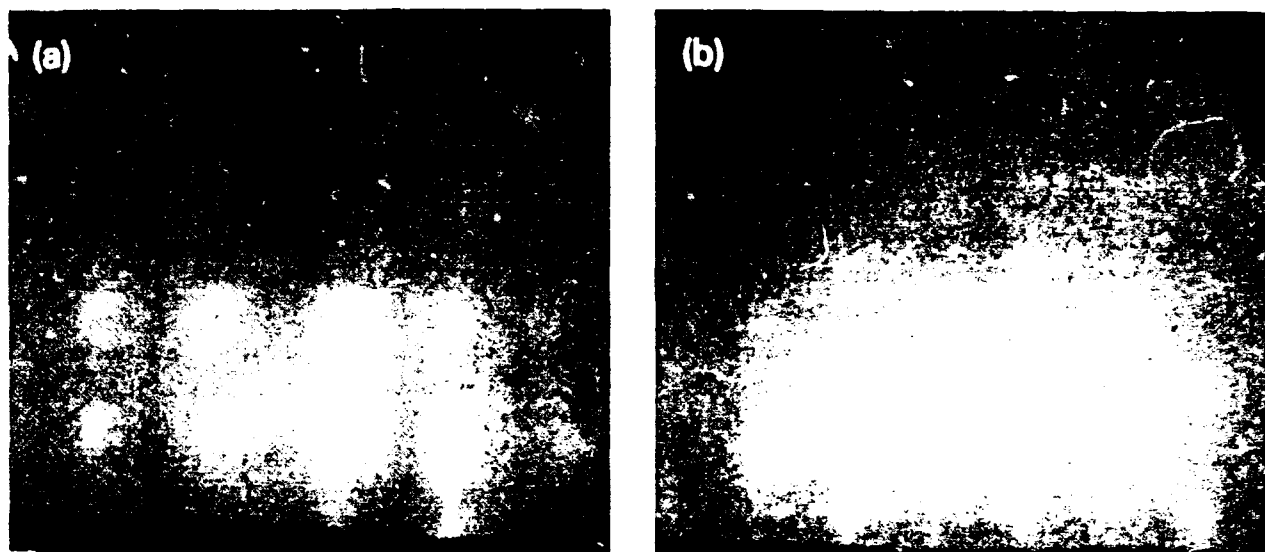


Fig. 5. Typical RHEED patterns of a GaN films on p-type or undoped substrate; (a) for $[100]$ azimuthal incidence of the electron beam; (b) for $[110]$ azimuthal incidence of the electron beam.

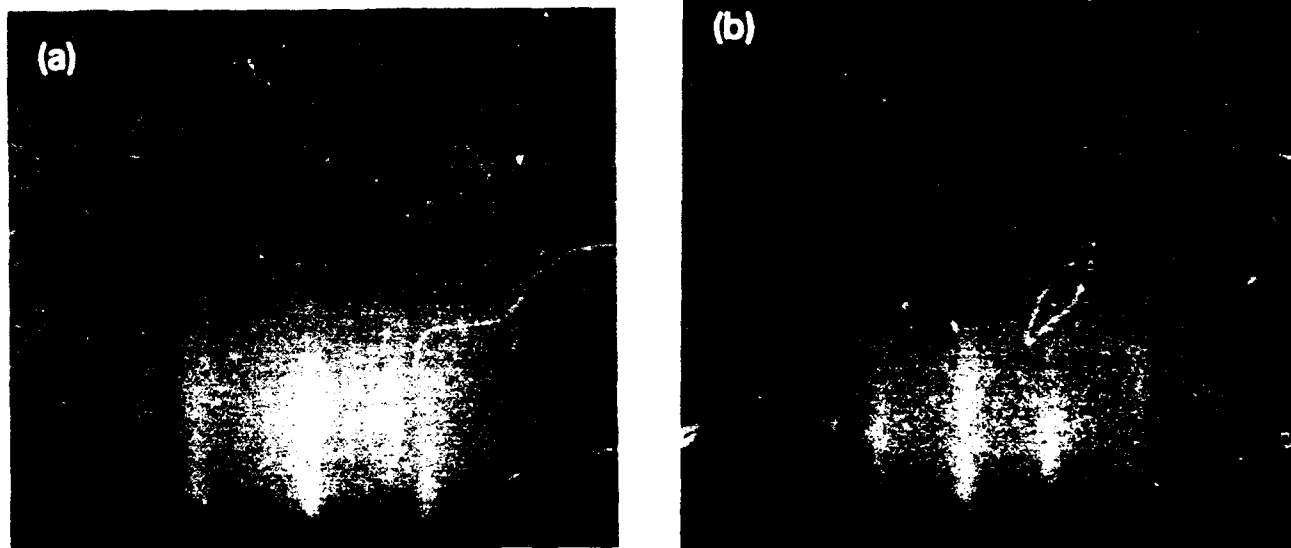


Fig. 6. The RHEED patterns of a GaN film with smooth-surface morphology; (a) for $[100]$ azimuthal incidence of the electron beam; (b) for $[110]$ azimuthal incidence of the electron beam.

gest that GaN wets to the n-type substrate better than the p-type substrate. Morimoto and co-workers reported that in vapor phase growth, GaN adhered to n-type silicon, but not to p-type silicon substrates.

In a few cases, the Si substrate was first bombarded with nitrogen plasma prior to the formation of the GaN buffer. The lack of a RHEED pattern indicates that either an amorphous SiN film was formed on the substrate or that the

surface was disordered. The GaN buffer grown on nitrogen-plasma bombarded substrates were found to be polycrystalline having the wurtzitic structure with the (0002) preferred orientation.

Shown in fig. 7 are the surface morphology and the cross-sectional view of a β -GaN film on a p-type silicon substrate studied by SEM. It can be seen that the film has a relatively flat surface, roughened with many well-oriented rectangular shaped 'tiles', which reflect the symmetry of the

β -GaN(001) surface. The cross-sectional view shows no evidence of columnar morphology, which is another indication that the film is single crystalline.

Detailed electron microscopy studies [23] have shown that the tiles in fig. 7 are oriented along the [110] and [1 $\bar{1}$ 0] directions. This presumably arises because the GaN surfaces corresponding to those directions are more closely packed than the [100] and [010] surfaces and therefore have lower surface energy.

Shown in fig. 8(a) is the morphology of the

GaN film, whose RHEED pattern was discussed in fig. 6. The surface morphology of a film on an n-type substrate is shown in fig. 8(b). Both of these surfaces are smooth with steps approximately 100 Å thick, which resulted from a layer-by-layer growth [23]. These results suggest that additional optimization of the growth process could lead to atomically smooth surfaces.

From the data of fig. 8, we can calculate the two-dimensional nucleation rate and the lateral growth rate. Let J be the nucleation rate, s be the average area of the plateau, h the height of

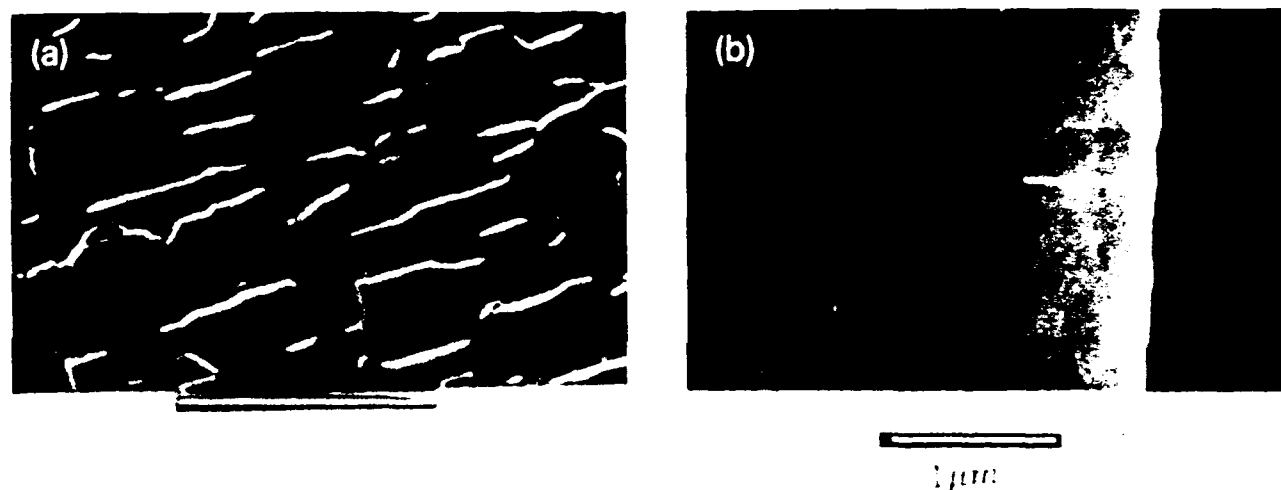


Fig. 7. Surface morphology of a GaN thin film on p-type Si substrate; (a) front view; (b) cross-sectional view.

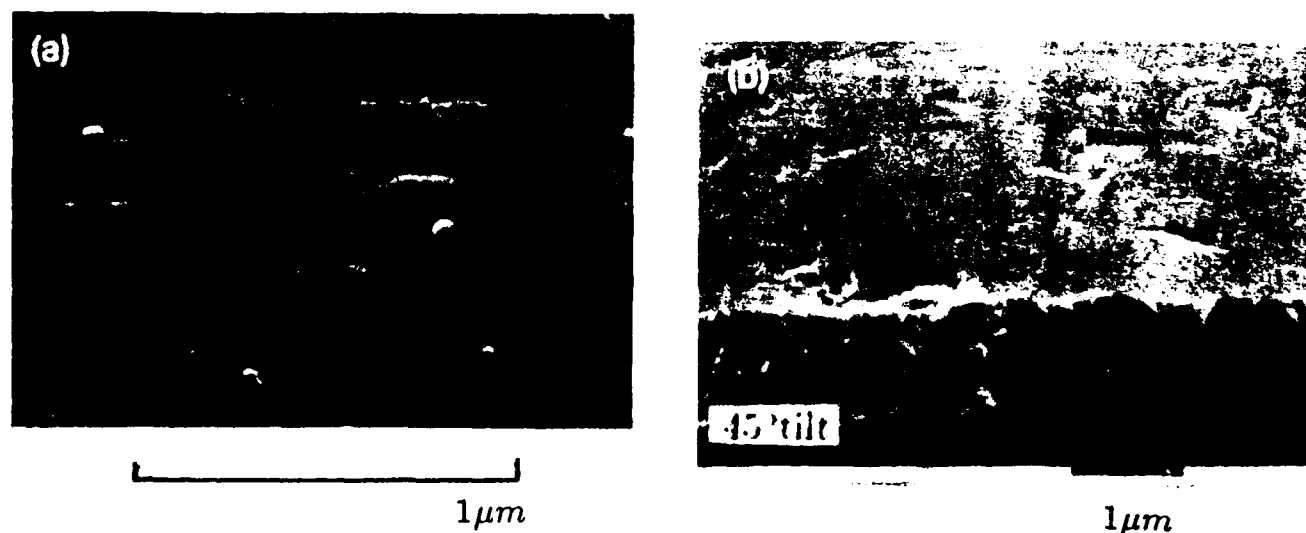


Fig. 8. SEM surface morphology of a smooth GaN thin film; (a) on a p-type substrate; (b) on an n-type substrate.

the plateau, and t the time for the plateau to grow, which is limited by nucleation. Then, we have

$$\sqrt{s} \approx v_l t = \frac{v_l}{(Js)}, \quad (1)$$

$$h \approx v_n t = \frac{v_n}{(Js)}, \quad (2)$$

where v_l and v_n are the lateral and vertical growth rates respectively. From the data of fig. 8, we have $\sqrt{s} \approx 1 \mu\text{m}$ and $h \approx 100 \text{ \AA}$. If we use the known vertical growth rate $v_n = 2000 \text{ \AA/h}$, then from eqs. (1) and (2) we obtain $v_l \approx 100v_n$ and $J \approx 20 \text{ nuclei}/(\mu\text{m}^2 \text{ h})$.

These data indicate that this two-step method of film growth leads to quasi-layer-by-layer growth with a very small two-dimensional nucleation rate and high lateral growth rate.

The structure of the films was confirmed by convergent beam electron diffraction (CBED) and selected area diffraction (SAD). These studies were published elsewhere [23]. In this paper, we focus on the X-ray diffraction studies of the films.

The X-ray diffraction in fig. 9 shows a strong peak at $2\theta = 40.1$ degrees, whose d -spacing is 2.25 \AA , which is due to the (002) reflection from β -GaN. Hence, the lattice constant to β -GaN

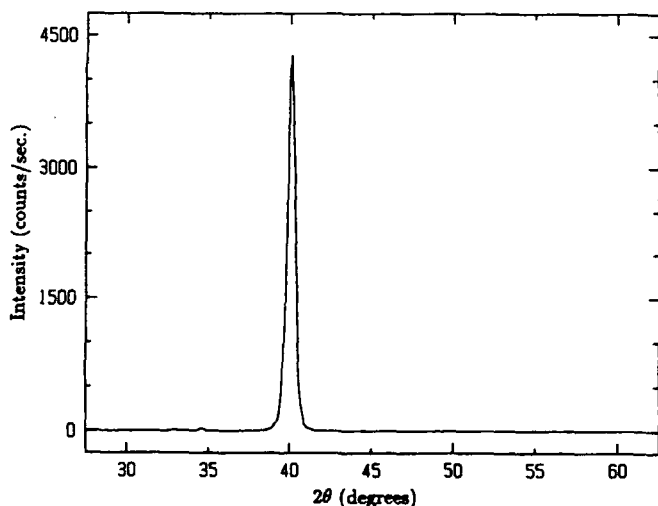


Fig. 9. X-ray diffraction using Cu- K_α radiation of a β -GaN film.

was found to be 4.50 \AA , in good agreement with the electron diffraction data [23]. A small peak was also observed at $2\theta = 34.6^\circ$, which is due to the d -spacing of (111) β -GaN or (0002) α -GaN. This suggests that the GaN film has some misoriented domains. These domains may have developed in the early stages of the buffer layer deposition as revealed by TEM imaging [39]. Similar structural faults have also been observed in the interface between GaN epitaxy on GaAs(100) [37]. We have also observed these misoriented domains in almost all of our samples. The consistent appearance of the misoriented domains in GaN-Si and GaN-GaAs heteroepitaxy is very likely to be related to the large lattice mismatch between the GaN and the substrate. Because of the large lattice mismatch, the interface of GaN and the substrate is under significant strain; therefore, it might be favorable for the system to introduce dislocations or misorientations of GaN to reduce the interfacial energies. In zincblende or wurtzitic structures, the [111] or [0002] planes are the most closely packed, and hence have the lowest surface energies. Therefore, the introduction of [111] or [0002] oriented GaN would lower the surface energy at the GaN-vapor interface, and would not necessarily increase the energy for the GaN-substrate interface, since it was strained significantly. However, the [111] or [0002] oriented GaN domains would grow slower than the [001] oriented GaN grains stabilized by introduction of dislocations. As a result, they were buried in the interface region as the film grew.

The X-ray rocking curve of the [002] peak of a GaN film $4 \mu\text{m}$ thick was found to have a full width at half maximum (FWHM) of approximately 60 minutes, which measures the orientation spread perpendicular to the substrate. This is significantly narrower than that of GaN on GaAs [37], but much broader than that of β -GaN on MgO substrates [19] and α -GaN on [0001] sapphire substrates as discussed later.

The ϕ -scan for the zincblende GaN was performed at the $[\bar{1}11]$ reflection, and is shown in fig. 10. The data clearly show that the peak repeats itself every 90 degrees, consistent with the cubic symmetry of this material. The FWHM

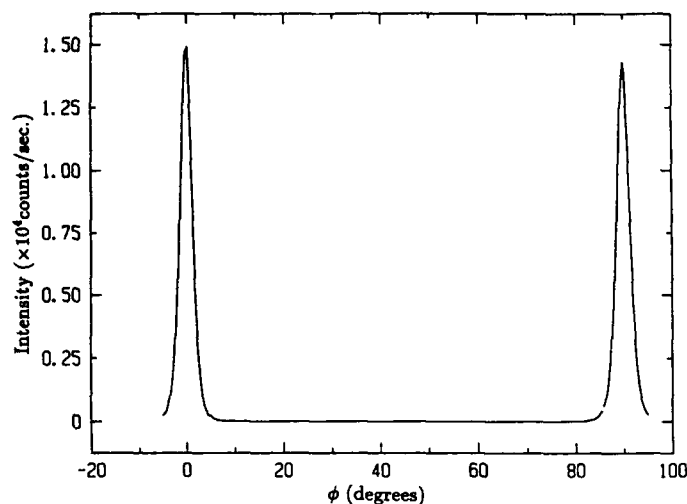


Fig. 10. ϕ -scan at $(\bar{1}11)$ for a zincblende GaN film.

of these peaks, which measures the in-plane orientation spread, was found to be 2.5 degrees.

3.2. Growth on Si(1 1 1)

Growth on Si(1 1 1) followed the same steps as described previously in the growth on Si(0 0 1). Figure 11 shows the RHEED pattern for a GaN film on Si(1 1 1). The data indicate that the film has the wurtzitic structure with the $[0001]$ planes parallel to the substrate. The sharpness of

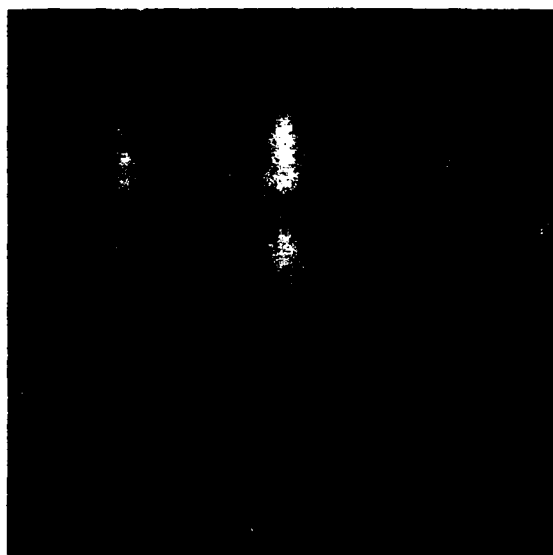


Fig. 11. RHEED patterns for a GaN film on Si(1 1 1) with $[1\bar{1}\bar{2}0]$ electron azimuthal incidence.

the diffraction spots indicate good crystalline quality of the film.

Figure 12 shows a θ - 2θ scan for a GaN film on Si(1 1 1). The single peak at 34.6 degrees corresponds to $[0002]$ reflection of the wurtzitic GaN; thus, the lattice constant in the c -direction is 5.18 Å.

The ϕ -scan for the wurtzitic GaN shown in fig. 13 was performed at the $[1\bar{1}02]$ reflection. Clearly, this peak repeats every 60 degrees, consistent with the 3 mm symmetry of the rotation axis. The FWHM is found to be 1.9 degrees,

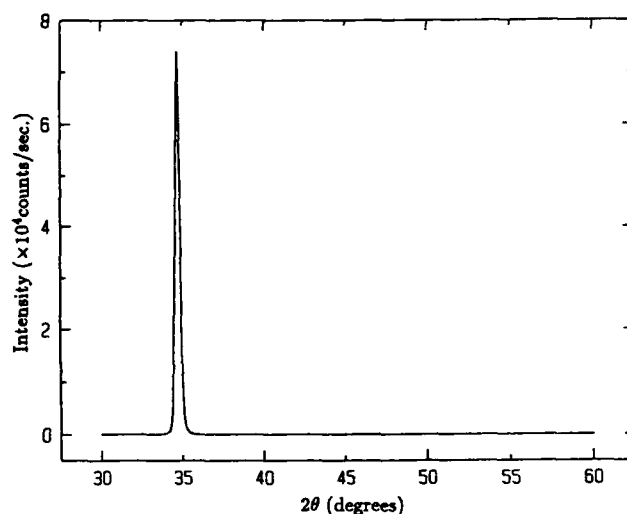


Fig. 12. θ - 2θ scans for a wurtzitic GaN film on Si(1 1 1).

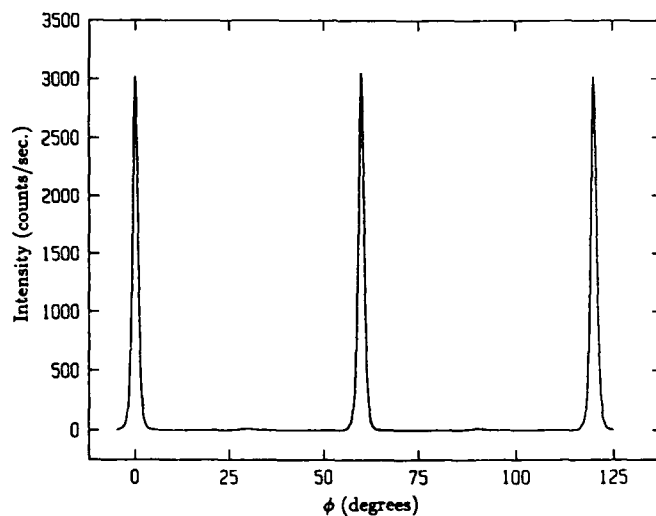


Fig. 13. ϕ -scan for a wurtzite GaN film on Si(1 1 1).

while the FWHM of the θ - 2θ rocking curve at the [0002] peak is found to be 0.9 degrees.

The XRD data of fig. 12 and fig. 13 appear to indicate that the α -GaN film on Si(111) is a single crystal. However, any stacking faults along the growth direction of the GaN film on Si(111) cannot be easily detected in the normal θ - 2θ scans [40]. Such stacking faults are very common defects in materials with the FCC or HCP structures growing along the [111] and [0002] directions [40]. Such stacking faults, if they exist in the wurtzitic GaN films on Si(111), should give rise to a certain amount of cubic GaN component with the [111] planes parallel to the substrate. To explore this possibility, we rotated the sample in such a way that the X-ray diffraction corresponds to the [002] reflection of the zincblende structure, and indeed a peak was detected at $2\theta = 40$ degrees. This is shown in a θ - 2θ scan around this peak (see fig. 14).

To obtain a stronger reflection, ϕ -scans on these cubic domains were performed at the $\bar{1}11$ peak, which is shown in fig. 15. These data reveal a repetition every 60 degrees. Since the [111] axis in the zincblende structure is only a 3-fold rotational axis, the ϕ -scan should show a repetition every 120 degrees instead of every 60 degrees. This can be accounted for if there are two kinds of stacking sequences, namely the

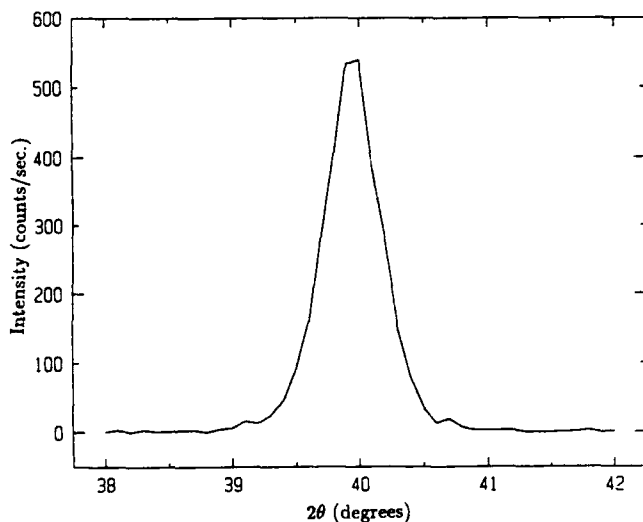


Fig. 14. θ - 2θ scan at the (002) reflection of cubic GaN grains in GaN on Si(111).

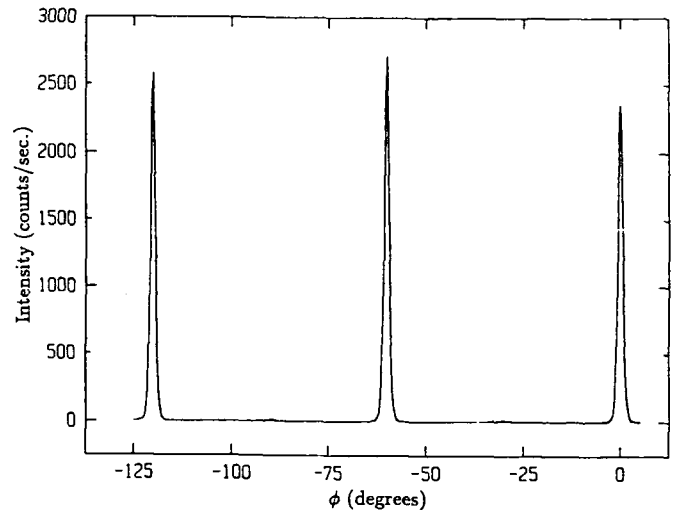


Fig. 15. ϕ -scan at the $(\bar{1}11)$ peak of cubic GaN components.

ABC... and CBA... sequence. The fact that the peak at $\phi = 60$ degrees is of comparable intensity to the other two peaks suggests that the two types of stacking sequences occur with an equal probability, as is expected.

The existence of the cubic GaN domains in the wurtzite structures implies the existence of a high concentration of stacking faults. This could be due to the fact that the cohesive energies of wurtzite and zincblende GaN are comparable, so that the formation energy of a stacking fault is negligible. If this is true, then all of the [0002] oriented GaN films have a considerable amount of stacking faults. This is currently being investigated by XRD studies of GaN on [11 $\bar{2}$ 0] and [0001] sapphire substrates. However, one should not rule out that the high concentration of stacking faults in GaN on Si(111) is related to strain resulting from the large lattice mismatch between GaN and Si, which could lead to a reduction of the formation energy of stacking faults due to structural deformation.

3.3. Growth on a sapphire substrate

GaN films were also grown on the c -plane [0001], a -plane [11 $\bar{2}$ 0] and r -plane [1 $\bar{1}$ 02] of sapphire. Figure 16 shows RHEED patterns of

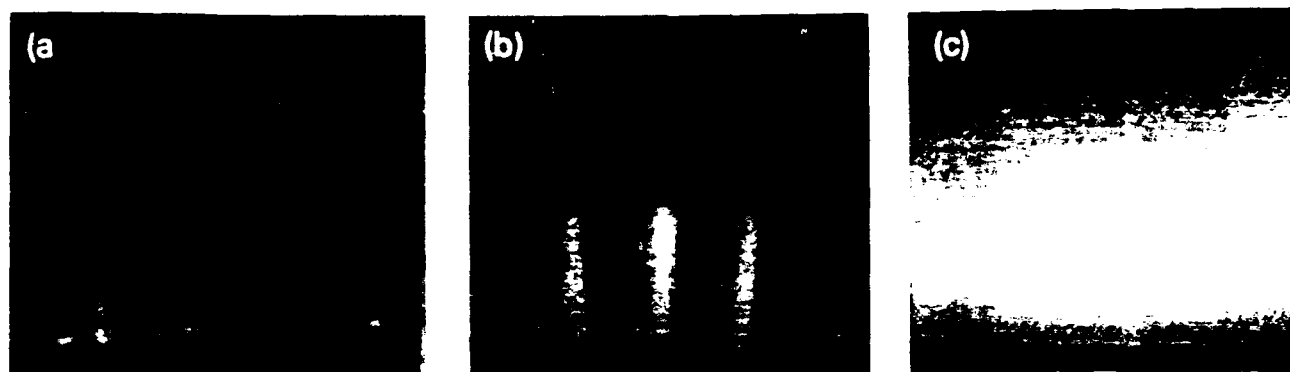


Fig. 16. RHEED patterns of the sapphire substrates after exposure to the nitrogen plasma: (a) *c*-plane, (b) *a*-plane, (c) *r*-plane.

the three types of substrates after exposure to the nitrogen plasma. The data indicate that the surface of the substrates were nitrated and from the diffraction patterns, the lattice constant of the AlN was estimated to be $a = 3.1 \text{ \AA}$. Furthermore, the streakiness of the diffraction patterns, in particular those of the *c*-plane and *a*-plane sapphire substrates, suggests that the AlN layers are atomically smooth.

Figure 17 shows RHEED patterns of the GaN-buffer on the three types of substrates. The data indicate that the GaN-buffer is single crystalline on all three types of substrates. The GaN films grown on the *c*-plane and *a*-plane sapphire substrates have their *c*-plane $[0001]$ parallel to the substrates, while the GaN films grown on the *r*-plane of sapphire have their *a*-plane $[11\bar{2}0]$ parallel to the substrate. The streakiness of the diffraction patterns of the GaN-buffers on the

c-plane and *a*-plane sapphire substrates suggests that the GaN-buffer on these substrates are atomically smooth.

Figure 18 shows RHEED patterns of the GaN films at the end of each run. These reveal the same epitaxial relationship between GaN films and the substrates as the corresponding GaN-buffers discussed in fig. 17. Also, the films on the *c*-plane and *a*-plane sapphire substrates are atomically smooth.

Figure 19 shows the surface morphology of GaN films grown on the three types of substrates. The films on the *a*-plane have the smoothest surface morphology. The surface morphology of GaN films on the *c*-plane consists of interconnected tiles several thousand angstroms in size. The GaN films grown on the *r*-plane sapphire were found to have the roughest surface morphology. The pyramidal surface morphology

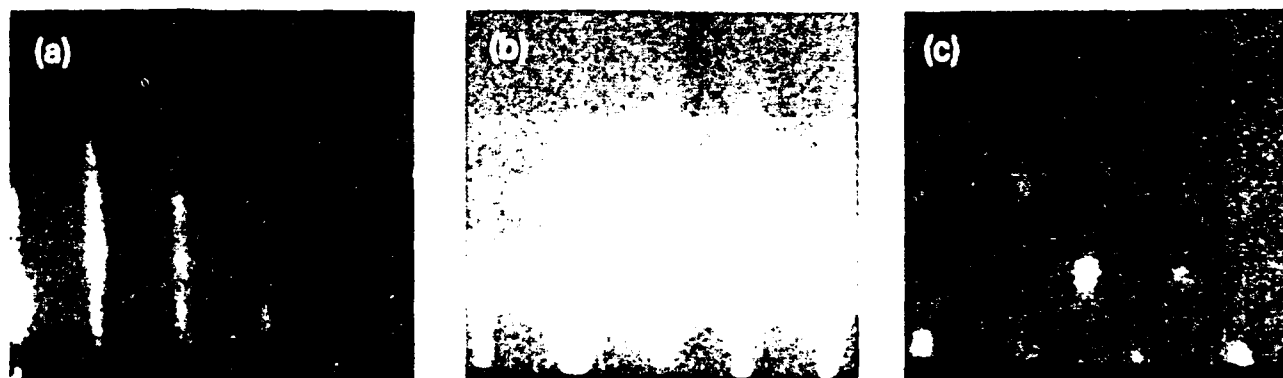


Fig. 17. RHEED patterns of the GaN-buffer on the various sapphire substrates: (a) *c*-plane, (b) *a*-plane, (c) *r*-plane.

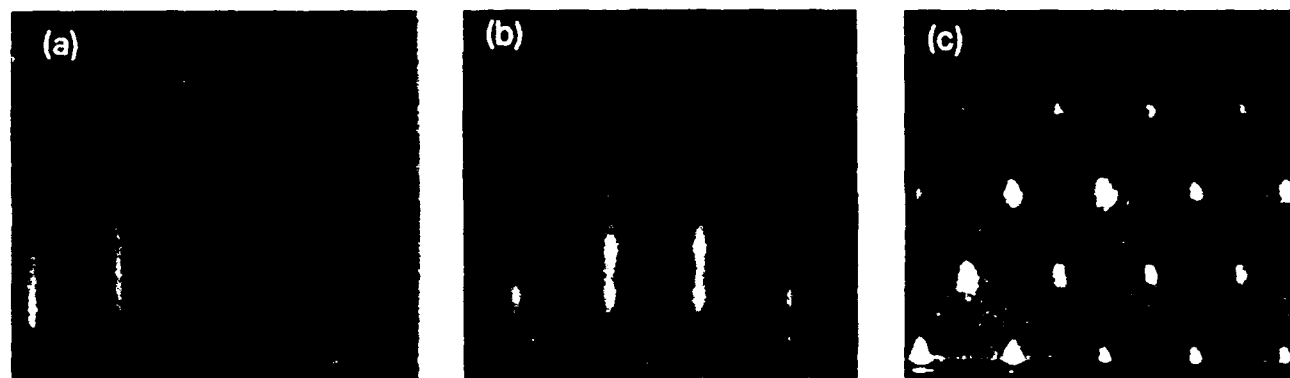


Fig. 18. RHEED patterns of the GaN films after growth on the various sapphire substrates: (a) *c*-plane, (b) *a*-plane, (c) *r*-plane.

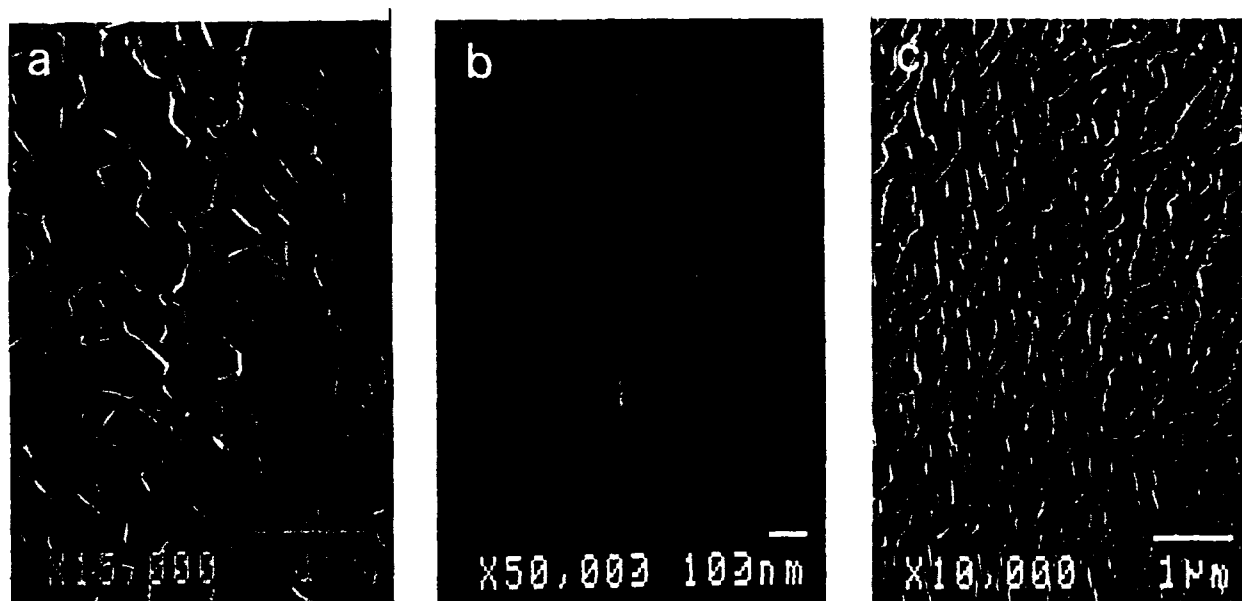


Fig. 19. SEM surface morphology of GaN films grown on various sapphire substrates: (a) *c*-plane, (b) *a*-plane, (c) *r*-plane.

is likely to be related to the fact that the *a*-plane of GaN is bounded by two prism planes under equilibrium growth conditions.

Figure 20 shows the θ - 2θ XRD and the θ -rocking curve at the main reflection peak of the GaN films grown on the three types of substrates. The main reflection peak for the GaN films grown on the *c*-plane and *a*-plane sapphire occurs at $2\theta = 34.6$ degrees, corresponding to the [0002] reflection. This confirms that films were grown with their *c*-planes parallel to the substrate. The main diffraction peak of the GaN film on the *r*-plane of sapphire occurs at $2\theta =$

57.8 degrees corresponding to the GaN [11 $\bar{2}$ 0] reflection. This confirms the RHEED study that the *a*-plane of the GaN film is parallel to the substrate. The rocking curve of the GaN film on the *c*-plane of sapphire has the smallest width (FWHM = 10 min), indicating the crystalline quality of these films to be the best. Such films were also found to have the highest electron mobility ($\mu > 200$ cm²/V s) among films grown by MBE processes.

The epitaxial relationship of the GaN films to the *c*-plane of sapphire is to be expected. However, the epitaxial relationship of the GaN films

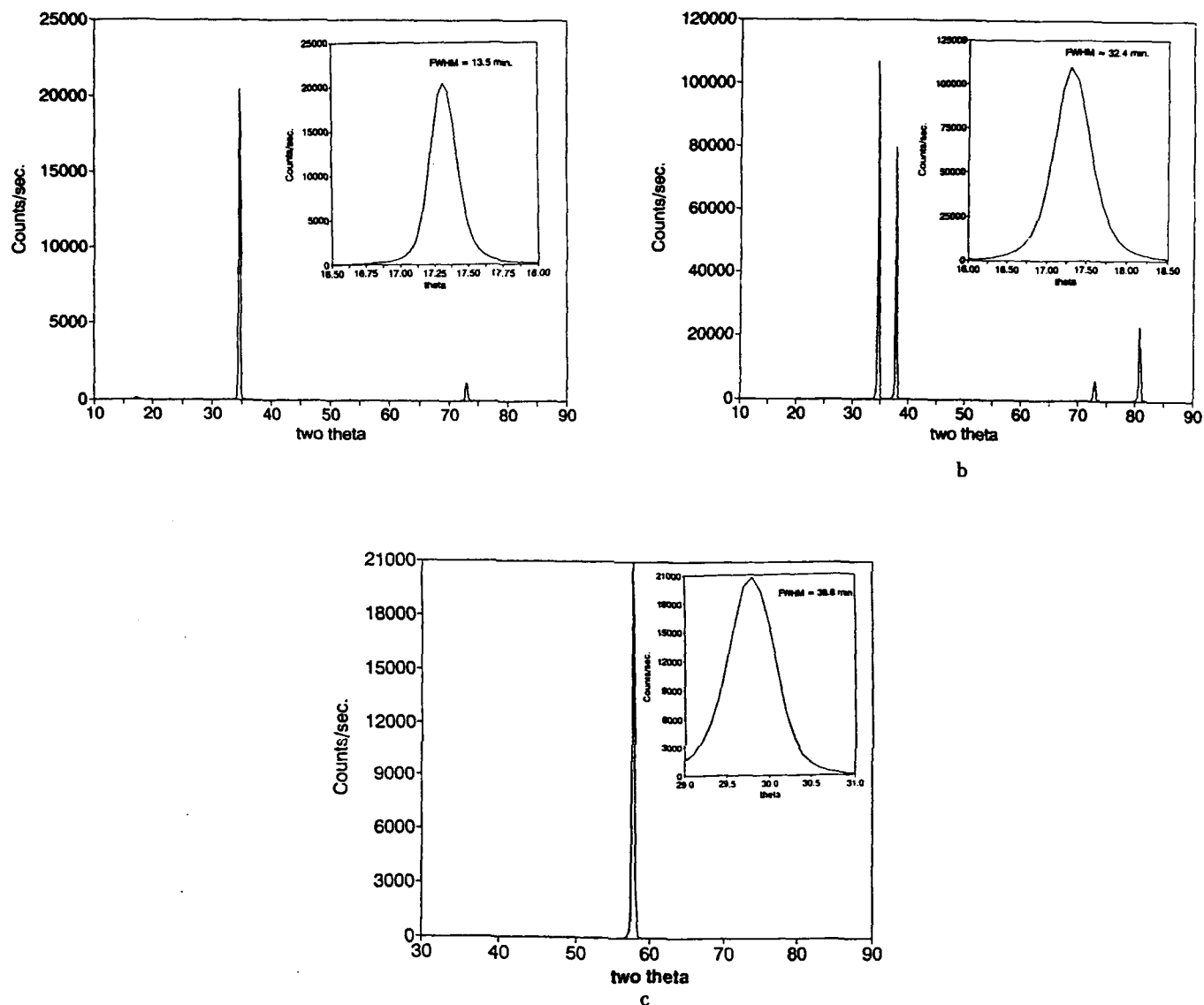


Fig. 20. θ - 2θ XRD of the GaN film on various sapphire substrates: (a) *c*-plane, (b) *a*-plane, (c) *r*-plane. The inserts show the corresponding rocking curves.

on the *a*-plane and *r*-plane of sapphire is not obvious. This epitaxial relationship can be accounted for as follows: The *a*-plane sapphire has a rectangular unit cell with dimensions $12.97 \text{ \AA} \times 8.23 \text{ \AA}$, two of which can accommodate a number of unit cells of GaN basal planes as illustrated in fig. 21(a). This results in 1.6% lattice mismatch along $[0001]$ of sapphire and 0.6% along the $[1\bar{1}00]$ axis of the sapphire substrate. The *r*-plane of sapphire substrate has a unit cell with dimensions $4.75 \text{ \AA} \times 15.34 \text{ \AA}$,

which accommodates three unit cells of the *a*-plane of GaN as illustrated in fig. 21(b). This results in 16% lattice mismatch along the $[11\bar{2}0]$ of sapphire and 1.3% along the $[1\bar{1}01]$ of sapphire.

4. Conclusion

In conclusion, a two-step growth process has been developed for the heteroepitaxial growth of

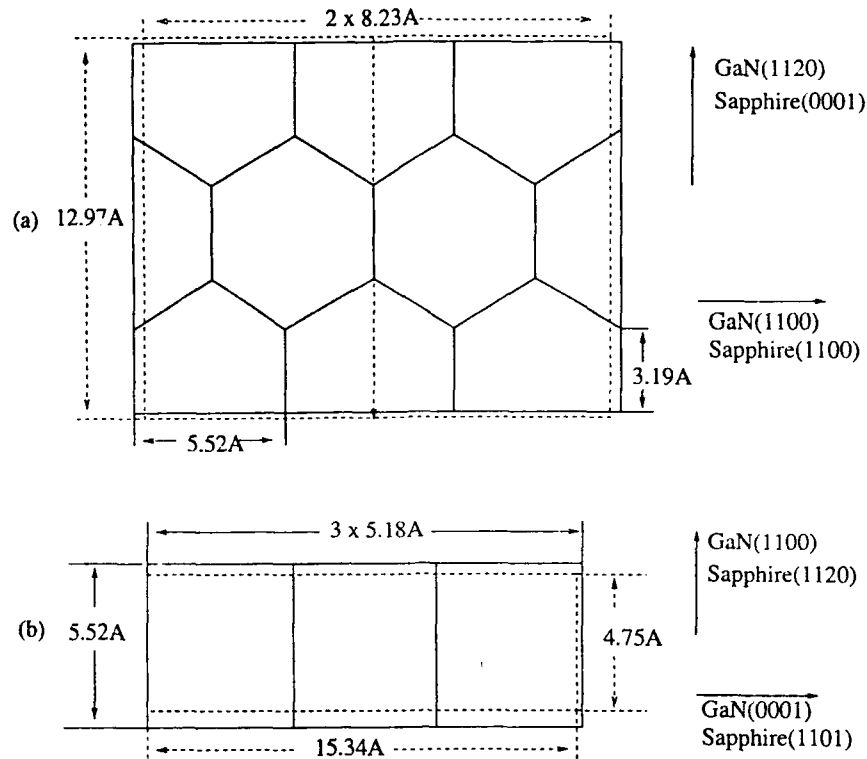


Fig. 21. Epitaxial relationship between GaN and (a) the a -plane of sapphire, (b) the r -plane of sapphire.

GaN films. This method was found to lead to films with smooth surface morphology, which we interpreted as resulting from a quasi-layer-by-layer growth. Using this process GaN films were grown on a variety of substrates by the ECR-assisted MBE method.

GaN films were successfully grown on Si(001) and (111) substrates, using this two-step process. The films on Si(001) are single-crystalline and epitaxially stabilized in the zincblende structure, while those on Si(111) have the wurtzite structure. Although RHEED suggest that the wurtzitic GaN on Si(111) is single-crystalline, a considerable amount of cubic phase was detected by XRD studies, and was attributed to a larger concentration of stacking faults along the growth direction.

GaN films were also grown on c -plane, a -plane and r -plane sapphire. The growth process involves the conversion of the sapphire surface into AlN by plasma nitridation. The XRD studies indicate that GaN films on c -plane sapphire have the best crystalline quality.

Acknowledgements

We are grateful to Prof. Karl Ludwig for stimulating discussions and help with the XRD studies. This work was supported by the Office of Naval Research (Grant No. N00014-92-J-1436).

References

- [1] R.F. Davis, Proc. IEEE 79 (1991) 702; R.F. Davis, Z. Sitar, B.E. Williams, H.S. Kong, H.J. Kim, J.W. Palmour, J.A. Edmond, J. Ryu, J.T. Glass and C.H. Carter Jr., Mat. Sci. Eng. B 1 (1988) 77.
- [2] J.I. Pankove, MRS Symp. Proc. 162 (1990) 515.
- [3] P. Das and D.K. Ferry, Solid State Electron. 19 (1976) 851.
- [4] H.P. Maruska and J.J. Tietjen, Appl. Phys. Lett. 15 (1969) 327.
- [5] J.I. Pankove, Phys. Rev. Lett. 34 (1975) 809.
- [6] R. Madar, G. Jacob, J. Hallis and R. Fruchart, J. Cryst. Growth 31 (1975) 197.
- [7] B. Monemar, O. Lagerstedt and H.P. Giskason, J. Appl. Phys. 51 (1980) 625.

- [8] T. Sasaki and S. Zembutsu, *J. Appl. Phys.* 61 (1986) 2533.
- [9] M.A. Khan, R.A. Skogman, R.G. Schulze and M. Gershenzon, *Appl. Phys. Lett.* 42 (1983) 430.
- [10] M.A. Khan, J.N. Kuznia, J.M. Van Hove, D.T. Olson, S. Krishnankutty and R.M. Kolbas, *Appl. Phys. Lett.* 58 (1991) 526.
- [11] M.A. Khan, J.M. Hove, J.N. Kuznia and D.T. Olston, *Appl. Phys. Lett.* 58 (1991) 2408.
- [12] M. Manasewit, F.M. Erdmann and W.I. Simpson, *J. Electrochem. Soc.* 118 (1971) 1864.
- [13] H. Amano, N. Sawasaki, I. Akasaki and Y. Toyoda, *Appl. Phys. Lett.* 48 (1986) 353.
- [14] T. Kawabata, T. Matsuda and Susumu Koike, *J. Appl. Phys.* 56 (1984) 2367.
- [15] T. Duffy, C.C. Wang, G.D. O'Clock, J. S.H. McFarelane and P.I. Zanzucchig, *J. Electron. Mater.* 2 (1973) 359.
- [16] H. Gotoh, T. Suga, H. Susuki and M. Kimata, *Jpn. J. Appl. Phys.* 20 (1981) L545.
- [17] S. Yoshida, S. Misawa and S. Gonda, *Appl. Phys. Lett.* 42 (1983) 427.
- [18] M.J. Paisley, Z. Sitar, J.B. Posthil and R.F. Davis, *J. Vac. Sci. Technol.* 7 (1989) 701.
- [19] R.C. Powell, G.A. Tomasch, Y.W. Kim, J.A. Thornton and J.E. Greene, *MRS Symp. Proc.* 162 (1990) 525.
- [20] Z. Sitar, M.J. Paisley, B. Yan and R.F. Davis, *MRS Symp. Proc.* 162 (1990) 537.
- [21] T. Lei, M. Fanciulli, R. Molnar, Y. He, T.D. Moustakas and J. Scanlon, *Bull. Am. Phys. Soc.* 36 (1991) 543.
- [22] T. Lei, M. Fanciulli, R.J. Molnar, T.D. Moustakas, R.J. Graham and J. Scanlon, *Appl. Phys. Lett.* 58 (1991) 944.
- [23] T. Lei, T.D. Moustakas, R.J. Graham, Y. He and S.J. Berkowitz, *J. Appl. Phys.* 71 (1992) 4933.
- [24] T. Lei and T.D. Moustakas, *Mat. Res. Soc. Proc.* 242 (1992) 433.
- [25] T.D. Moustakas, R.J. Molnar, T. Lei, G. Menon and C.R. Eddy Jr., *Mat. Res. Soc. Proc.* 242 (1992) 427.
- [26] T.P. Humphreys, C.A. Sukow, R.J. Nemanich, J.B. Posthil, R.A. Rudder, S.V. Hattangady and R.J. Markunas, *MRS Symp. Proc.* 162 (1990) 531.
- [27] E. Lashimi, B. Mathur, A.B. Bhattacharya and V.P. Bhargava, *Thin Solid Films* 74 (1980) 77.
- [28] S. Zembutsu and T. Sasaki, *Appl. Phys. Lett.* 48 (1986) 870.
- [29] S. Zembutsu and M. Kobayashi, *Thin Solid Films* 129 (1985) 289.
- [30] J. Knights and R.A. Lujan, *J. Appl. Phys.* 49 (1978) 129.
- [31] J.I. Pankove, S. Bloom and G. Harbeke, *RCA Rev.* 36 (1975) 163.
- [32] O. Lagerstedt and B. Monemar, *J. Appl. Phys.* 45 (1974) 2266.
- [33] W. Seifert, R. Franzheld, E. Butter, H. Sobotta and V. Riede, *Cryst. Res. Technol.* 18 (1983) 383.
- [34] H. Amano, M. Kito, K. Hiramatsu and I. Akasaki, *Jpn. J. Appl. Phys.* 28 (1989) L2112-L2114.
- [35] S. Nakamura, *Jpn. J. Appl. Phys.* 30 (1991) L1705.
- [36] M. Mizuta, S. Fujieda, Y. Matsumoto and T. Kawamura, *Jpn. J. Appl. Phys.* 25 (1986) L945.
- [37] S. Strite, J. Ruan, Z. Li, N. Manning, A. Salvador, H. Chen, D.J. Smith, W.J. Choyke and H. Morkoc, *J. Vac. Sci. Technol. B* 9 (1991) 1924.
- [38] G. Menon, MSc thesis, Boston University (1990).
- [39] S.N. Basu, private communications.
- [40] B.E. Warren, *X-ray Diffraction* (Addison-Wesley, New York, 1969).

Appendix B:

Growth and Doping of GaN Films by ECR-Assisted MBE
To be published in *Materials Research Society Proceedings* **281** (1993).

GROWTH AND DOPING OF GaN FILMS BY ECR-ASSISTED MBE

T.D. Moustakas and R.J. Molnar

Molecular Beam Epitaxy Laboratory, Department of Electrical, Computer, and Systems Engineering, Boston University, Boston, MA 02215.

ABSTRACT

We report on growth, doping, and characterization studies of GaN films produced by the Electron Cyclotron Resonance microwave plasma assisted Molecular Beam Epitaxy. The films were grown heteroepitaxially on sapphire (0001), whose surface was converted into atomically smooth AlN by plasma nitridation. The GaN films were grown in two temperature steps, a process found to promote the layer-by-layer growth mode. ECR plasma conditions to grow either n-type autodoped or semi-insulating GaN film were identified. The structure and microstructure as well as the electrical properties of these two classes of films are discussed. A systematic dependence between electron mobility and net carrier concentration was found, which predicts that the mobility of GaN with a net carrier concentration of 10^{14}cm^{-3} is about $10^4\text{cm}^2/\text{V}\cdot\text{s}$. The insulating films were intentionally doped either p-type or n-type by incorporation of Mg or Si during film growth. Hole or electron concentrations at 300K between $10^{18} - 10^{19}\text{cm}^{-3}$ have been obtained without requiring any post-growth treatment.

INTRODUCTION

The family of refractory nitrides (InN, GaN, AlN) is one of the most promising classes of optoelectronic materials. The three binaries are direct band-gap semiconductors and their energy gaps cover the spectral region from 1.95eV (InN) and 3.4eV (GaN) to 6.28eV (AlN). The successful development of these materials would lead to devices such as light emitting diodes, lasers, and light detectors, operating in the spectral region from the visible to ultraviolet. Due to their unique physical properties (high energy gap, high thermal conductivity, high saturation velocity), these materials are also expected to be used in the fabrication of devices for high temperature, high power, and high frequency applications. Heterojunctions, quantum wells, and superlattices based on these materials are expected to show novel low dimensional electronic behavior due both to the strong quantum confinement and to the lack of defects associated with the transition from direct to indirect semiconductors, a problem common in GaAs / $\text{Al}_x\text{Ga}_{1-x}\text{As}$ structures.

The majority of the published work deals mostly with the synthesis and characterization of these materials. Early work dealing primarily with bulk growth is reviewed in "Refractory Semiconductor Materials" (1) and recent results were presented in the MRS symposium on "Wide Band-Gap Semiconductors" (2) as well as in reviews by Pankove (3) and Davis (4).

The synthesis of bulk crystals of GaN and AlN by equilibrium processes (1) has led only to the growth of millimeter size single crystals. Vapor phase synthesis of III-V nitrides has focused on heteroepitaxial growth, primarily on (0001) sapphire. The most important recent development is the discovery that AlN (5-8) and GaN (9-12) buffers lead to lateral growth which significantly improves the surface morphology as well as the optical and electrical properties of the films. Another recent significant development was the epitaxial stabilization of cubic-GaN of selective substrates, including β -SiC (13), GaAs (14), MgO (15), and Si (10,11).

GaN films have been grown by many growth techniques, including CVD (16), MOCVD (17), and MBE (18). All these methods produced n-type GaN films, a result attributed to nitrogen vacancies due to thermal decomposition of GaN at the high growth temperature. To reduce the growth temperature, plasma assisted deposition methods were developed (9-11,13-15) which lead to the growth of semi-insulating GaN films. The early effort at p-type doping were unsuccessful (19) due to compensation by n-type defects. With improvements in film quality, recent reports indicate the possibility of p-type doping and the resulting fabrication of efficient light emitting

devices (7,20).

In this paper, we report our progress in the growth, doping, and characterization of GaN films by the Electron Cyclotron Resonance microwave plasma assisted Molecular Beam Epitaxy (ECR-MBE).

EXPERIMENTAL METHODS

The deposition system used in this study is schematically illustrated in Figure 1. It consists of a Varian GenII MBE unit with an ASTeX compact ECR source inserted into one of the effusion cell ports. The pressure in the overall system is 10^{-11} Torr. A Reflection High Energy Electron Diffraction (RHEED) setup is an integral part of the apparatus. Ga and dopant elements (Si and Mg) are evaporated from conventional Knudsen effusion cells, while active nitrogen is produced by passing molecular nitrogen through the ECR source at a total pressure of 10^{-4} Torr. The growth rate of the GaN films is controlled by varying the flux of Ga. The stoichiometry of the films is controlled by varying the microwave power in the ECR discharge, which affects the flux of the active nitrogen. Generally, microwave power of 35 Watts or higher was found to lead to semi-insulating GaN films (stoichiometric) for growth rates up to 6500 \AA/h . For higher growth rates or smaller microwave power in the discharge, the flux of active nitrogen is insufficient for the growth of stoichiometric films and excess gallium in the films is phase separated in the form of Ga droplets (21). The films discussed in this paper were grown at growth rates of $2000\text{-}2500 \text{ \AA/h}$, and microwave power levels appropriate for the growth of conducting or insulating films. n-type and p-type doping of GaN films was accomplished by subliming Si or Mg respectively during the growth process.

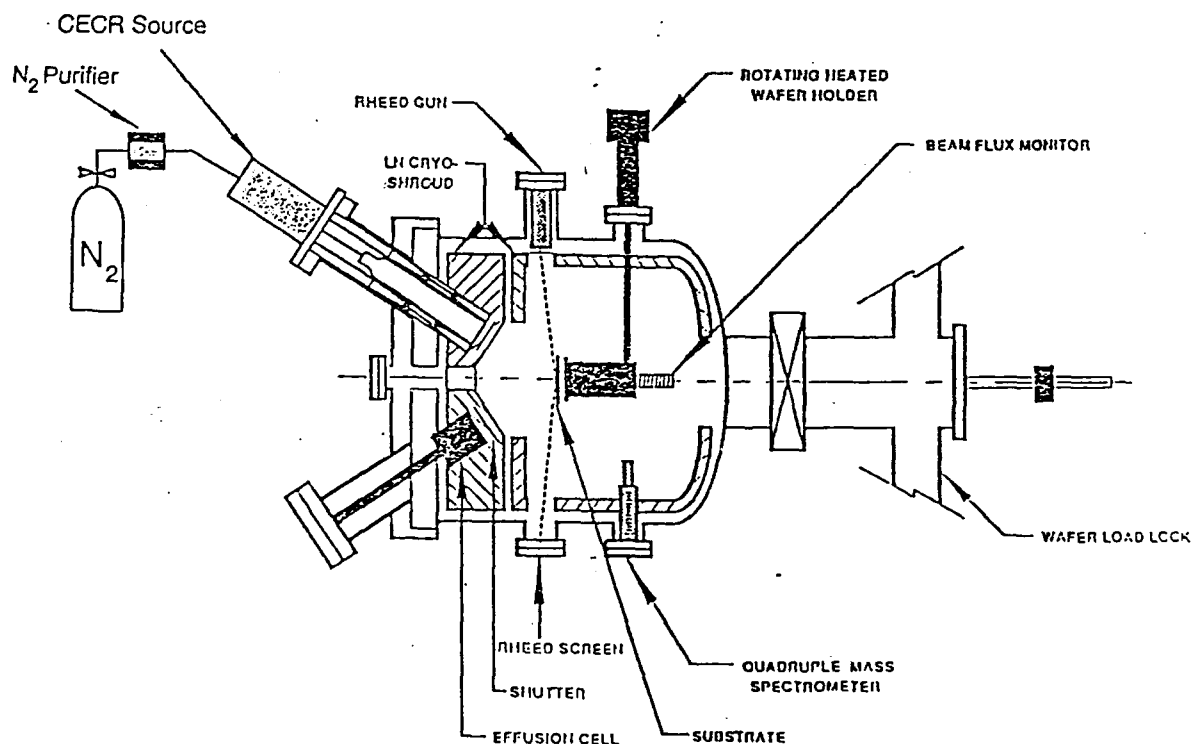


Figure 1. ECR-MBE growth chamber.

The GaN films were grown on the c-plane (0001) of sapphire. The substrates were degreased and etched in $H_3PO_4 : H_2SO_4(1 : 3)$ for the removal of surface contaminants and mechanical damage due to polishing, and finally were rinsed in de-ionized water. After these steps, the substrates were blown dry with nitrogen, mounted on a BN block and transferred to the introduction chamber of the MBE system. In the preparation chamber, the substrates were heated to 850°C for approximately half an hour and then transferred to the growth chamber where they were subjected to bombardment by nitrogen plasma for approximately half an hour at 800°C.

The structure and microstructure of the films were studied by RHEED, XRD, and SEM. To measure the transport coefficients, the samples were abrasively etched into Van der Pauw lamillas and electrical contacts were formed by soldering gold wires with indium.

EXPERIMENTAL RESULTS AND DISCUSSION

A. Film Growth

We found that exposure of the substrate to a nitrogen plasma results in nitridation of the surface of the substrate and its conversion into AlN. The AlN thin film was found to be a single crystal and its RHEED pattern is illustrated in Figure 2a. The streakiness of the diffraction pattern suggests that the AlN film is atomically smooth. Similar nitridation has also been observed when the α -plane (11 $\bar{2}$ 0) and the r-plane(1 $\bar{1}$ 02) of sapphire were exposed to a nitrogen plasma (22,23).

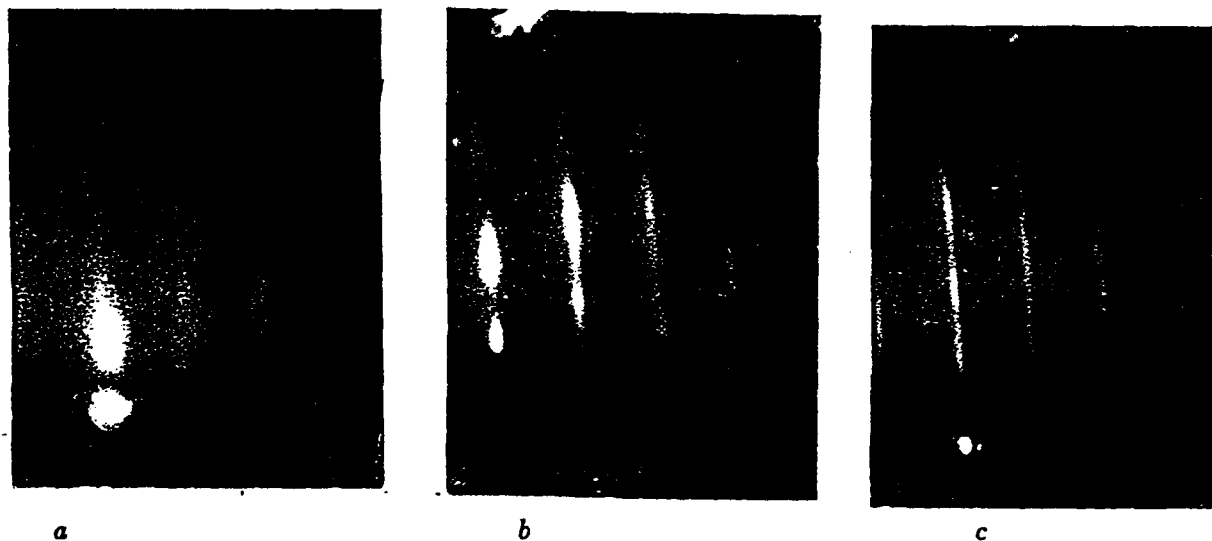


Figure 2. RHEED patterns taken at various steps during growth: (a) substrate after plasma nitridation (b) after the growth of the GaN buffer (c) after growth at high temperature.

The GaN film was grown on the previously formed AlN film following a two temperature step process developed in our laboratories over the past few years (9-11, 22-24). In this process a GaN-buffer, approximately 200Å thick, is grown first at a relatively low temperature (500°C) followed by a higher temperature growth (800°C) of the rest of the film. Figures 2b and 2c show the RHEED patterns of the GaN buffer and the GaN film after the completion of the growth. The streakiness of these diffraction patterns also indicate that both the thin GaN-buffer as well as the thick GaN film are atomically smooth. The diffraction pattern of Figure 2c tends to be spotty under deposition conditions which lead to semi-insulating GaN films. This is consistent with the surface morphology of these films as discussed later. This method of film growth, using a GaN-buffer, has also been used for the growth of GaN films by the MOCVD method (12) and the reports indicate significant improvements in the quality of such films as well.

B. Surface Morphology

The surface morphology of GaN films was found to depend strongly on the ECR plasmas. In low power plasmas, which lead to n-type autodoped GaN films, the surface morphology is flat as shown in Figure 3a. These data are in agreement with the RHEED data of Figure 2c. Furthermore, the cross-sectional view shows no evidence of columnar morphology. These findings suggest that lateral growth in these films is significantly higher than the vertical growth. In a similar study on the growth of GaN on Si(100), we were able to resolve steps of approximately 100Å on the top of the plateaus and by comparing this with the area of the plateaus, we concluded that the lateral growth rate is larger than the vertical growth rate by a factor of 100, and that the two dimensional nucleation rate was found to be 20 nuclei/ $\mu\text{m}^2\text{h}$ (11,23). Based on these findings, we characterized the growth on Si(100) as quasi layer-by-layer growth. The evidence from the data presented in here is that growth on (0001) sapphire proceeds via the layer-by-layer mode.

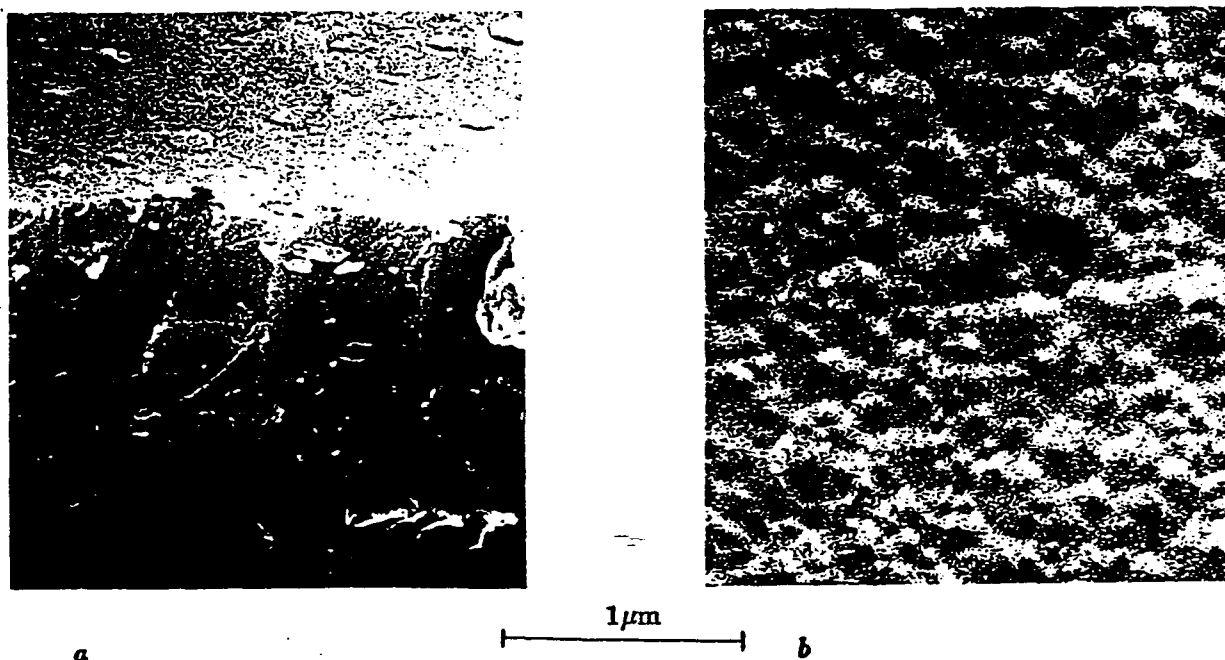


Figure 3. SEM surface morphologies (a) conducting film (b) insulating film

Higher power plasmas, which lead to semi-insulating films, result to some degree of surface roughening. The surface morphology of such a film is shown in Figure 3b. At this moment, we do not know whether the change in growth mode, under the two plasma conditions, is related to the change in surface mobility of the absorbed atoms or to the kinetics of growth due to the change in concentration of active nitrogen at the growing surface.

C. Film Structure

A comprehensive study on the structure of GaN films on silicon and sapphire substrates has been published elsewhere (25). Here, we present data on GaN films grown on (0001) sapphire substrates and discuss only $\theta - 2\theta$ scans and rocking curves around the main diffraction peak.

Figure 4 shows the $\theta - 2\theta$ scan and the θ -rocking curve at the main reflection peak for a GaN film grown under lower power plasma conditions (conducting films). There are two peaks in the $\theta - 2\theta$ scans, one at $2\theta = 34.6^\circ$ corresponding to the (0002) reflection, and the second at $2\theta = 72^\circ$ which is the second order harmonic. The θ -rocking curve of the (0002) peak, shown in the insert of Figure 4, has a FWHM of 10 minutes, which is comparable to the best reported in the literature (26) for films grown by other deposition methods. These data confirm that the

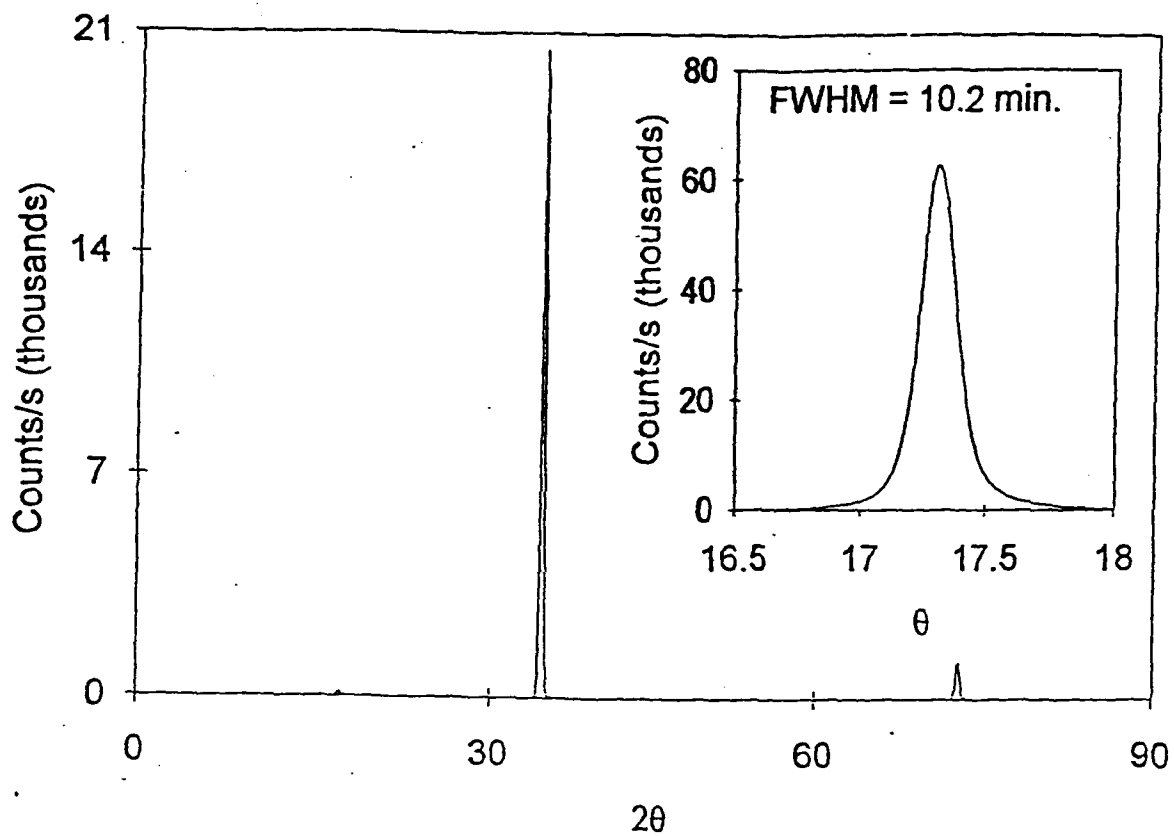


Figure 4. XRD of a conducting GaN film. The insert shows the rocking curve around the main peak.

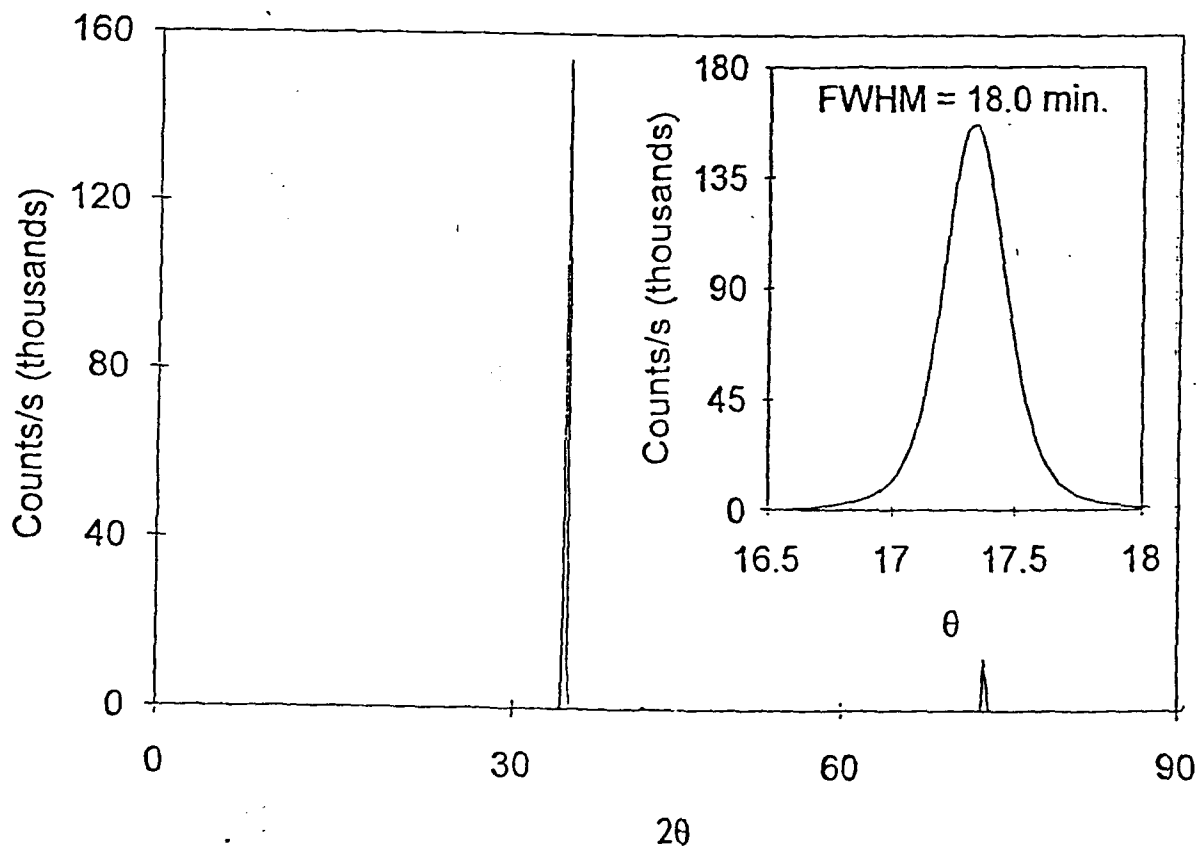


Figure 5. XRD of a semi-insulating GaN film. The insert shows the rocking curve around the main peak.

GaN films were grown with their c-plane parallel to the substrate. The epitaxial relationship between GaN and (0001) sapphire was discussed by Lee *et. al.* (25). The GaN basal unit cell is oriented 30° away from the sapphire unit cell in epitaxial relationship with a smaller hexagonal unit cell consisting of the Al atoms in the sapphire substrate.

Figure 5 shows a $\theta - 2\theta$ scan and the θ -rocking curve for a GaN film grown under higher power plasma conditions (insulating films).

D. Electrical Properties

GaN films grown by various methods were generally found to be heavily doped n-type ($10^{18} - 10^{20} \text{cm}^{-3}$). Recently, GaN films grown by the MOCVD method with either an AlN-buffer (7) or with a GaN-buffer (12) were found to have carrier concentrations in the range of $10^{16} - 10^{17} \text{cm}^{-3}$ and electron mobilities as high as $900 \text{cm}^2/\text{V}\cdot\text{s}$.

As discussed earlier, GaN films grown by the ECR method can be made either conducting or insulating by choosing the power level in the ECR discharge. Films grown at relatively low power levels (< 35 Watts) were found to be autodoped with n-type conductivity, while those grown at higher power levels in the ECR discharge were found to be insulating. Since the power in the ECR discharge controls the amount of active nitrogen, the observed trend in the electrical behavior together with the presence of phase separated gallium in the conducting films, suggest that the origin of autodoping centers in GaN is indeed due to N-vacancies. In the following, we review the electrical properties of both conducting and insulating GaN films. Details on these studies were published elsewhere (27,28).

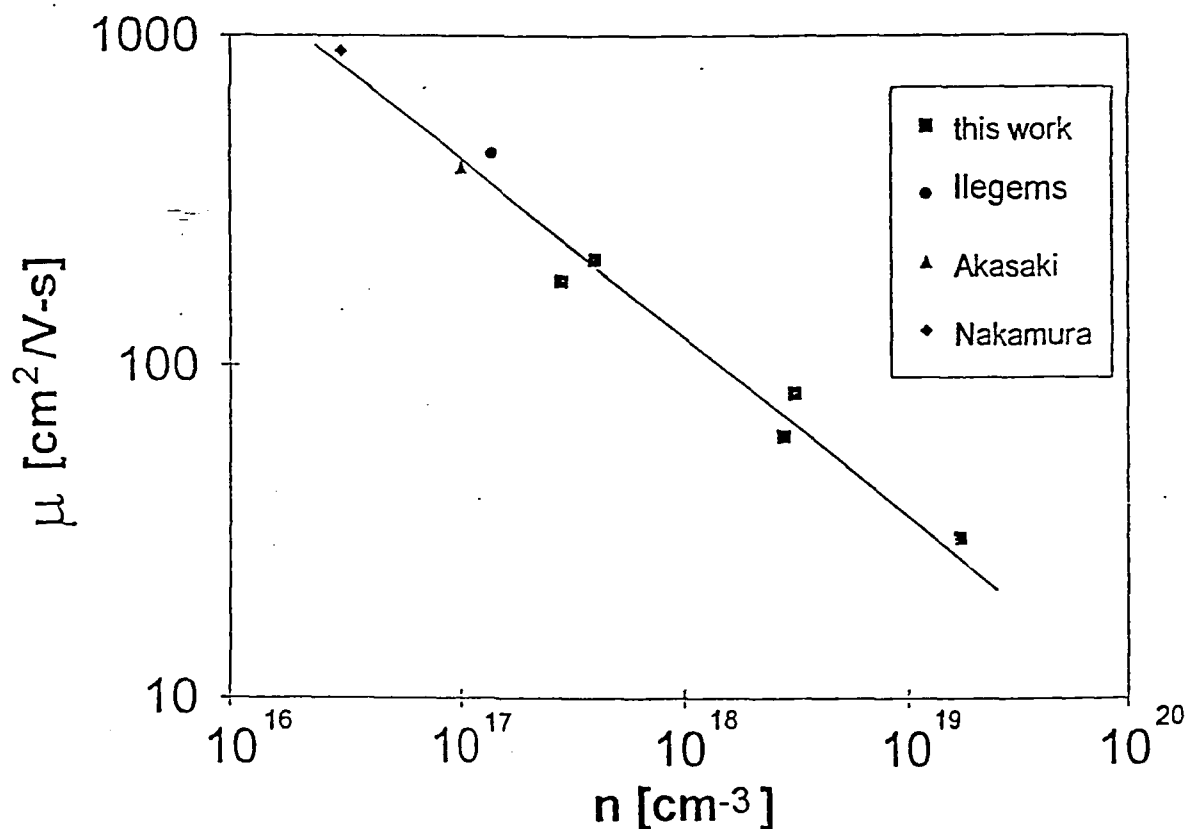


Figure 6. Electron mobilities vs. electron concentration for a number of GaN films.

A number of n-type GaN films were produced by keeping the power in the ECR discharge constant (active nitrogen overpressure fixed) and gradually reducing the flux of the Ga-beam. The electron mobility vs net carrier concentration at 300K for these films is shown in Figure 6. Shown in the same Figure are also the results reported for GaN films produced by various

CVD methods (7,29,30). It is important to note that all data follow the same trend which can be extrapolated to predict the electron mobility of relatively pure and defect free GaN films. For example, films with carrier concentrations of 10^{14}cm^{-3} are predicted to have a mobility of $10^4\text{cm}^2/\text{V}\cdot\text{s}$, which is comparable with that of GaAs.

The electron transport mechanism in our films was investigated by studying the temperature dependence of the Hall coefficient and of the resistivity (27,28). The analysis of these data indicate that the ionization energy of the autodoping centers is 20 to 30 meV. These autodoping centers form a band when their concentration is larger than 10^{17}cm^{-3} and conduction in this band was found to dominate the transport at low temperatures. In fact for heavily autodoped films ($5 \times 10^{18}\text{cm}^{-3}$), transport in this band dominates even at room temperature.

GaN films with net carrier concentrations less than 10^{16}cm^{-3} were also produced. Paradoxically, such films were found to have low electron mobilities ($\leq 1\text{cm}^2/\text{V}\cdot\text{s}$). This result can be accounted for as follows: When the concentration of the autodoping centers becomes less than the concentration of the deep defects, the material becomes fully compensated and thus conduction is dominated by hopping transport in the deep compensating defects. This suggests that the concentration of deep defects in our films is of the order of 10^{16}cm^{-3} . This may also be true for films grown by the MOCVD methods, since the best films grown by this method have net carrier concentrations of $3 \times 10^{16}\text{cm}^{-3}$ (30). These deep defects are probably related to heteropitaxial growth, such as dislocations.

E. Doping

Early efforts to dope GaN films with Zn or other group II-elements led to compensated films. Recently, Akasaki and co-workers (7) reported that Mg compensated GaN films can be converted to p-type when irradiated with a beam of low energy electrons (LEEBI). Subsequently, Nakamura and co-workers (31) demonstrated that similar results can be obtained by thermal annealing in a nitrogen atmosphere and attributed the acceptor activation to thermal removal of H_2 which ties up the Mg in the form of Mg-H complexes.

GaN films produced by the ECR-MBE methods were doped p- or n-type by incorporation of Mg or Si respectively during film growth. Hall effect measurements on Mg-doped films indicate that the films are p-type and that carrier concentrations at 300K between $10^{18} - 10^{19}\text{cm}^{-3}$ have been obtained without requiring any post growth annealing treatment (32). These films have electrical conductivities of between 0.1 to $1.0 \Omega^{-1}\text{cm}^{-1}$. The magnitude of the hole mobility at room temperature was found to be $0.6 \text{cm}^2/\text{V}\cdot\text{s}$ and was not strongly dependent on temperature. The carrier concentration vs inverse temperature for one of the samples is shown in Figure 7. We believe that the scatter in the data is due to difficulties in measuring the Hall coefficient of a low mobility material. The conductivity measurements, which are far more consistent, are shown in Figure 8. Since the electron mobility, at this level of doping, was found to be temperature independent, we can use the conductivity data to extract the activation energy for the carrier concentration. From the high temperature data of Figure 8. ($>150\text{K}$), an activation energy for the conductivity of $\Delta E=0.15\text{eV}$ was calculated. This is in agreement with the results of Akasaki (33) for LEEBI activated Mg-doped GaN films grown by the MOCVD method. The low temperature data in Figures 7 and 8 are consistent of impurity conduction (34).

The concentration of holes in a semiconductor with an acceptor concentration N_A and donor concentration N_D ($N_A > N_D$) is given by the expression (35):

$$\frac{p(N_D + p)}{N_A - N_D - p} = 2N_V \exp \left[-\frac{(E_A - E_V)}{kT} \right] \quad (1)$$

where N_V is the effective density of states at the valence band

$$N_V = 2 \left(\frac{m_h^* kT}{2\pi \hbar^2} \right)^{3/2} \quad (2)$$

Equation (1) has two approximations. If $p \ll N_D$, Eq. (1) takes the form

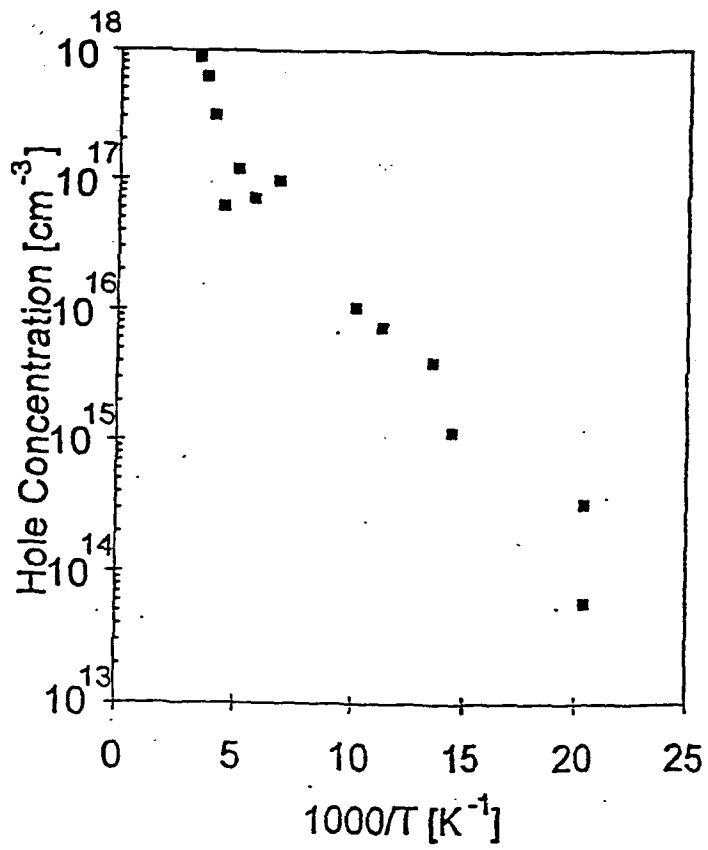


Figure 7. Hole concentration vs $1/T$ for a Mg-doped GaN film.

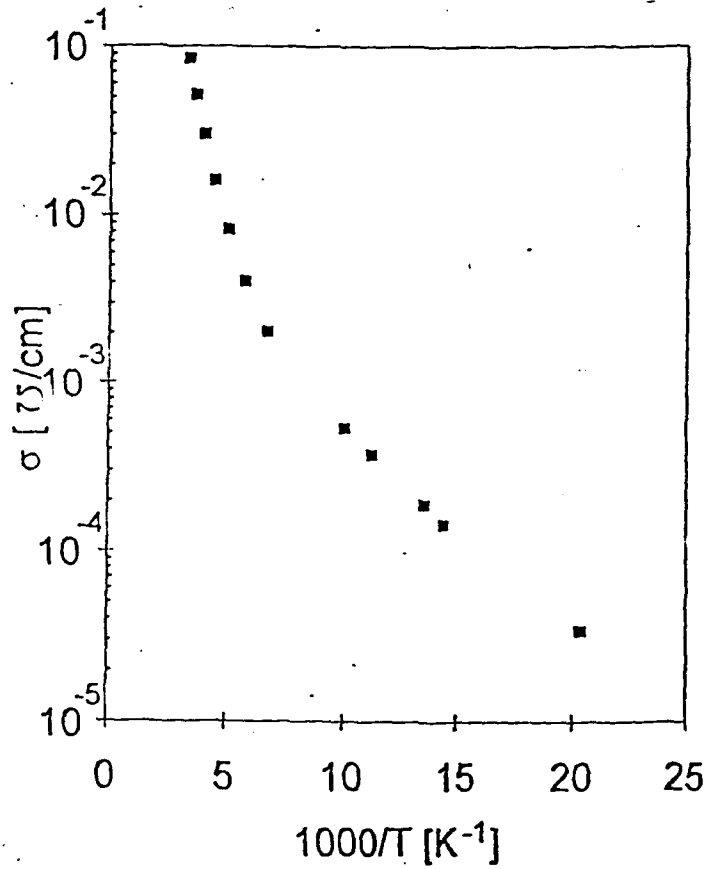


Figure 8. Conductivity vs $1/T$ for the same GaN film discussed in in Figure 7.

$$p = 2N_v \frac{(N_A - N_D)}{N_D} \exp \left[-\frac{(E_A - E_V)}{kT} \right] \quad (3)$$

In this case the plot of $\ln(pT^{-3/2})$ vs inverse temperature should have a slope equal to the ionization energy of acceptors ($E_A - E_V$).

If $p \gg N_D$, then Equation (1) takes the form

$$p = (2N_v N_A)^{1/2} \exp \left[-\frac{(E_A - E_V)}{2kT} \right] \quad (4)$$

In this case, the exponential involves only half of the ionization energy.

The evidence suggests that N-vacancies in GaN act as donors and their concentration depends on the overpressure of active nitrogen during film growth. The films in this study were grown under high N-overpressure and thus N_D should be very low. If this is true, Equation (4) should be applicable in the high temperature region of the experimental data and $E_A - E_V = 0.30\text{eV}$. However, one cannot rule out that the kinetics of the formation of N-vacancies is modified in the presence of Mg, and that $N_D \gg p$ in the investigated temperature range. If this is true, then Equation (3) is applicable and $E_A - E_V = 0.15\text{eV}$. Further studies are required to determine the ionization energy of Mg in GaN.

The activation of Mg-acceptors without any post-growth annealing is not inconsistent with Nakamura's proposal for the formation of Mg-H complexes in GaN:Mg films grown by the MOCVD method (36), since the concentration of H_2 is low in MBE growth. However, one should not rule out the possibility of ion assisted doping phenomena present in our method.

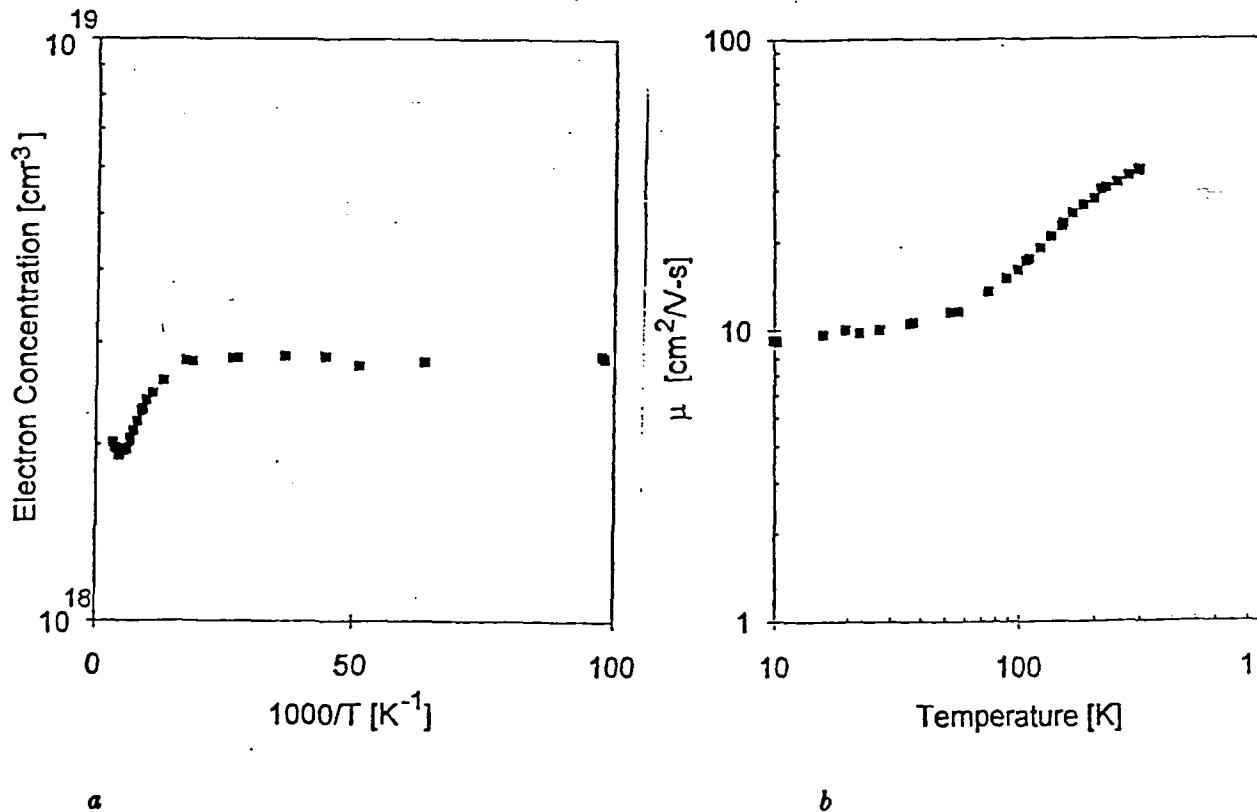


Figure 9. (a) Electron concentration vs $1/T$ and (b) electron mobility vs T for a GaN film doped with Si.

Hall effect measurements on Si doped films indicate that the films are n-type. Net carrier concentration at 300K between $10^{18} - 10^{19}\text{cm}^{-3}$ have been obtained. The temperature dependence of the carrier concentration and electron mobility for one of the Si-doped films is shown in

Figures 9a and 9b. The carrier concentration was computed from the measured values of the Hall coefficient, R_H , using the equation

$$n = \frac{1}{eR_H} \quad (5)$$

Equation (5) assumes electron conduction in one band. However, as discussed previously (27), the data of Figure 9 are consistent with two-band conduction (conduction and impurity bands).

CONCLUSIONS

We discussed the growth of GaN on sapphire (0001). The surface of the substrate was first converted to atomically smooth AlN by plasma nitridation and the GaN film was grown on the top of this AlN-buffer using a two temperature step process. It was shown that this process promotes growth in the layer-by-layer mode. Plasma conditions to grow either conducting or insulating films were identified and the effect of these conditions on the structure, microstructure, and electrical properties were discussed. The insulating films were doped p-type or n-type by incorporating Mg or Si respectively. Carrier concentrations in the range of $10^{18} - 10^{19} \text{cm}^{-3}$ were obtained without requiring any post growth annealing.

ACKNOWLEDGEMENTS

This work was supported by the office of Naval Research (grant number N0014-92-j-1436). We are grateful to Karl Ludwig for collaboration in XRD, and to Max Yoder for discussions and encouragement.

REFERENCES

1. Refractory Semiconductor Materials, edited by N.A. Garjunaova and D.N. Nasledov (Consultant Bureau, New York, 1966)
2. Wide Band-Gap Semiconductors, Mat. Res. Soc. Symp. Proc., Vol. 242, edited by T.D. Moustakas, J.I. Pankove, and Y. Hamakura (1992).
3. J.I. Pankove, Mat. Res. Soc. Proc., Vol. 162, 516 (1990)
4. R.F. Davis, Proc. of the IEEE, 79, 702 (1991)
5. H. Amano, N. Sawaki, I. Akasaki, and Y. Toyoda, Appl. Phys. Lett., 48, 353 (1986)
6. H. Amano, I. Akasaki, H. Hiramatsu, N. Koide, and N. Sawaki, Thin Solid Films, 163, 415 (1988)
7. J. Akasaki and H. Amano, reference 2, p. 383
8. M. Asif Khan, J.N. Kuznia, J.M. Van Hove, D.T. Olson, S. Krishnankutty, R.M. Kolba, Appl. Phys. Lett., 58, 526 (1991)
9. G. Menon, Master Thesis, Boston University (1990); G. Menon, R. Molnar, S.J. Berkowitz, and T.D. Moustakas, Bull. APS 36, 544 (1991)
10. T. Lei, M. Fanciulli, R.J. Molnar, T.D. Moustakas, R.J. Graham, and J. Scanlon, Appl. Phys. Lett., 59, 944 (1991)
11. T. Lei, T.D. Moustakas, R.J. Graham, T. He, and S.R. Berkowitz, J. Appl. Phys., 71, 4933 (1992)

12. S. Nakamura, Jpn. J. Appl. Phys. 30, L1705 (1991)
13. M.J. Paisley, Z. Sitar, J.B. Posthill, and R.F. Davis, J. Vac. Sci. and Technol., A7, 701 (1989)
14. G. Martin, S. Strite, J. Thornston, and H. Morkoc, Appl. Phys. Lett., 58, 2375 (1991)
15. R.C. Powell, G.A. Tomasch, Y.W. Kim, J.A. Thornton and J.E. Greene, MRS Symp. Proc. 162, 525 (1990)
16. H.P. Maruska and J.J. Tietjen, Appl. Phys. Lett. 15, 327 (1969)
17. H.M. Manasevit, F.M. Erdmann, and W.I. Simpson, J. Electrochem. Soc. 118, 1864 (1971)
18. S. Yoshida, S. Misawa, Y. Fujii, S. Tanaka, S. Hayakawa, S. Gonda, and A. Itoh, J. Vac. Sci. Technol., 16, 990 (1979)
19. J.I. Pankove, J.E. Berkeyheiser and E.A. Miller, J. Appl. Phys., 45 1280 (1974)
20. S. Nakamura, T. Mukai, and M. Senoh, Jpn. J. Appl. Phys. L1998 (1991)
21. C.R. Eddy Jr., T.D. Moustakas, and J. Scanlon, J. Appl. Phys. 73 (Jan. 1993)
22. T.D. Moustakas, R.J. Molnar, T. Lei, G. Menon, and C.R. Eddy Jr., Reference 2, p 427.
23. T.D. Moustakas, T. Lei, and R.J. Molnar, Physica B; Condensed Matter (1993)
24. T. Lei and T.D. Moustakas, Reference 2, p. 433
25. T. Lei, K.F. Ludwig, and T.D. Moustakas, J. Appl. Phys. (submitted for publication)
26. T. Sasaki and S. Zembutsu, J. Appl. Phys. 61, 2533 (1987)
27. R.J. Molnar, T. Lei, and T.D. Moustakas, Appl. Phys. Lett. 62 (Jan. 1993).
28. R.J. Molnar, T. Lei, and T.D. Moustakas (this volume)
29. M. Ilegems, J. Cryst. Growth 13/14, 360 (1972)
30. S. Nakamura, T. Mukai, and M. Senoh, J. Appl. Phys. 71, 5543 (1992)
31. S. Nakamura, M. Senoh, and T. Makai, Jpn. J. Appl. Phys., L1708 (1992)
32. R.J. Molnar and T.D. Moustakas, Appl. Phys. Lett. (submitted for publication)
33. I. Akasaki, H. Amano, N. Koide, M. Kotaki, and K. Mannabe (to be published)
34. N.F. Mott, T.D. Twose, Advances in Physics 10, 107 (1961)
35. N.B. Hannay, Semiconductors (Reinhold Publishing Corp., New York, 1960)
36. S. Nakamura, N. Iwasa, M. Senoh, and T. Mukai, Jpn. J. Appl. Phys., 31 (1992)

Appendix C:

High Mobility GaN Films Produced by ECR-Assisted MBE
To be published in *Materials Research Society Proceedings* 281 (1993).

HIGH MOBILITY GaN FILMS PRODUCED BY ECR-ASSISTED MBE

R.J. Molnar, T. Lei, and T.D. Moustakas

Molecular Beam Epitaxy Laboratory, Department of Electrical, Computer, and Systems Engineering, Boston University, Boston, MA 02215

ABSTRACT

High electron mobility autodoped GaN films were produced by the ECR assisted MBE method. The net electron concentration was varied systematically from 2×10^{19} to $2 \times 10^{17} \text{cm}^{-3}$ by controlling the active nitrogen overpressure. Correspondingly, the electron mobility increased from 20 to $210 \text{cm}^2 \text{V}^{-1} \text{sec}^{-1}$. The line through the experimental data also predicts the electron mobilities of GaN films produced by the CVD methods.

INTRODUCTION

GaN films, produced by a variety of vapor phase methods, are autodoped n-type, a result attributed to the formation of nitrogen vacancies during film growth. In general, the net carrier concentration in such films was reported to be in the range of $10^{18} - 10^{20} \text{cm}^{-3}$ (1). Recently, GaN films grown by the MOCVD method either with an AlN-buffer (2), or with a GaN-buffer (3) were found to have carrier concentrations of between $10^{16} - 10^{17} \text{cm}^{-3}$ and electron mobilities as high as $900 \text{cm}^2 \text{V}^{-1} \text{sec}^{-1}$.

In this paper, we report for the first time the growth of high mobility autodoped GaN films by Electron Cyclotron Resonance assisted Molecular Beam Epitaxy (ECR-MBE). The transport mechanism in these films was investigated by studying the temperature dependence of the Hall constant and resistivity.

EXPERIMENTAL METHODS

The thin film deposition system used in this study consists of a Varian GenII MBE unit with an ASTeX compact ECR source inserted in one of the effusion cell ports. A conventional Knudsen effusion cell was used to evaporate Ga, while active nitrogen was provided by passing molecular nitrogen through the ECR source.

The GaN films were grown on the c-plane (0001) of sapphire. The substrates were degreased and etched in $\text{H}_3\text{PO}_4 : \text{H}_2\text{SO}_4 (1 : 3)$ for the removal of surface contaminants and mechanical damage due to polishing and finally rinsed in de-ionized water. After these steps, the substrates were blown dry with nitrogen, mounted on a BN block, and transferred to the introduction chamber of the MBE system. In the preparation chamber, the substrates were heated to 850°C for approximately half an hour and then transferred to the growth chamber where they were subjected to bombardment by nitrogen plasma for approximately half an hour at 800°C . As discussed elsewhere (4,5), this resulted in the formation of an atomically smooth AlN layer. The GaN film was grown on the top of this AlN-buffer in two temperature steps as described elsewhere (4,5). First, a thin ($\sim 200 \text{\AA}$) GaN-buffer was grown at 500°C and the rest of the film, typically $2 \mu\text{m}$ thick, was grown at 800°C . This two step process leads to quasi layer-by-layer growth.(5)

The samples were abrasively etched into Van der Pauw lamella and electrical contacts were formed by soldering gold wires with indium. The samples' conductivities and Hall constants were measured as a function of temperature.

RESULTS AND DISCUSSION

Although the films were not intentionally doped, Hall effect measurements indicate that they have n-type conductivity. The magnitude of the electron mobility vs. the net electron concentration at 300K for the investigated films is shown in Figure 1. Also shown in the same figure are the results reported for GaN films produced by CVD methods (2,3,6). It is important to note that all data follow the same trend, which can be extrapolated to predict the electron mobility of relatively pure and defect free GaN-films. For example, a GaN film with net carrier concentration of 10^{14}cm^{-3} is predicted from this graph to have an electron mobility of about $10^4\text{cm}^2\text{V}^{-1}\text{sec}^{-1}$, which is comparable with that of GaAs.

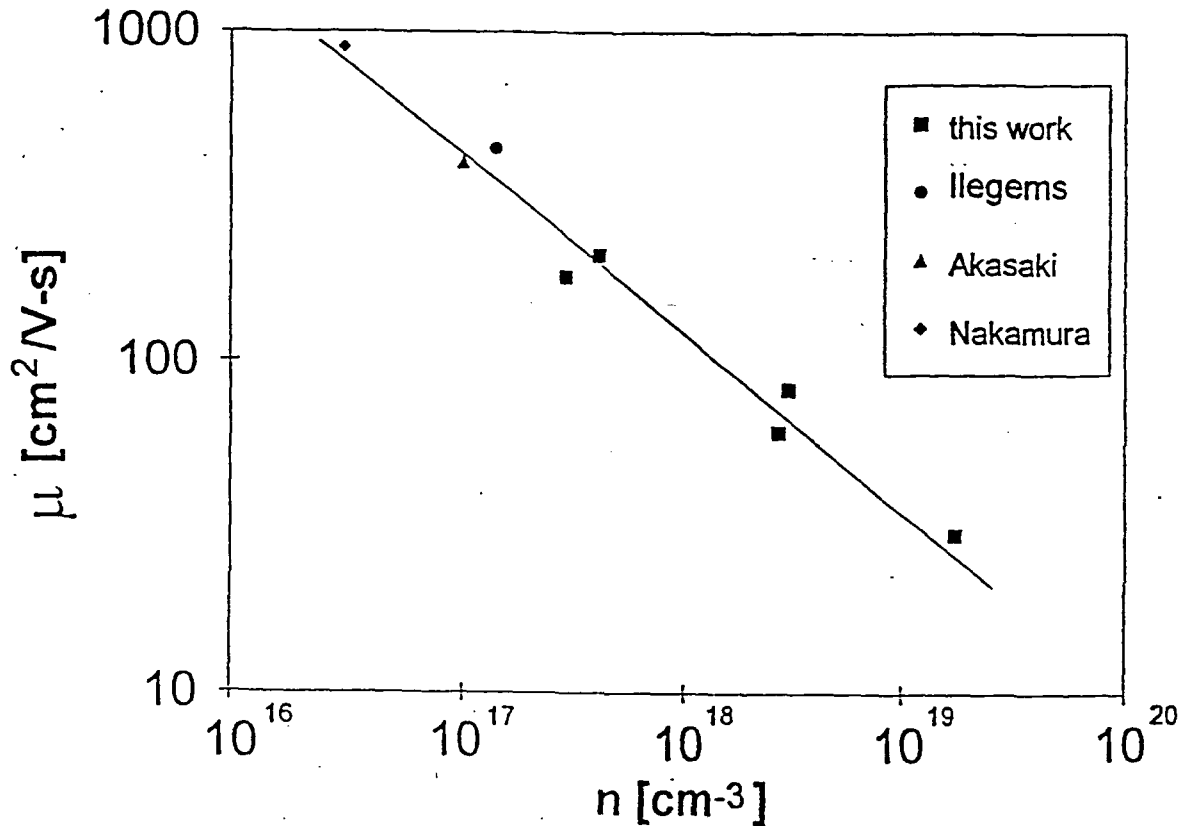


Figure 1. Electron mobility vs. net carrier concentration at 300K for a number of GaN films.

The electron concentrations in Figure 1 were calculated from the expression

$$n = \frac{1}{eR_H} \quad (1)$$

where R_H is the Hall constant. Equation (1) assumes electron conduction in one band. As discussed previously (7), this assumption is valid at 300K, but at lower temperatures, conduction in the autodoping centers (presumably nitrogen vacancies) becomes dominant. This is illustrated in Figures 2 and 3, where we plot the Hall coefficient and resistivity of the most insulating of our films vs $1/T$. As discussed previously (7), these data indicate that at about 100K, the transport switches from the conduction band to the band of the autodoping centers. Thus, in general, the Hall constant and resistivity of these films should be described by two band expressions:

$$R_H = \frac{n_c \mu_c^2 + n_d \mu_d^2}{(n_c \mu_c + n_d \mu_d)^2 e} \quad (2)$$

$$\rho = \frac{1}{n_c e \mu_c + n_d e \mu_d} \quad (3)$$

where n_c and n_d are the concentrations of conducting carriers in the conduction band and the band of the autodoping centers respectively; μ_c and μ_d are their corresponding mobilities. Equations (2) and (3) can account for the experimental behavior of Figures 2 and 3. Similar behavior was reported also by Ilegems (6) and Akasaki (2) for the GaN films grown by CVD methods. Nakamura (3), on the other hand, who produced GaN films with the smallest carrier concentration ($3 \times 10^{16} \text{cm}^{-3}$) sees only transport in the conduction band down to 40K.

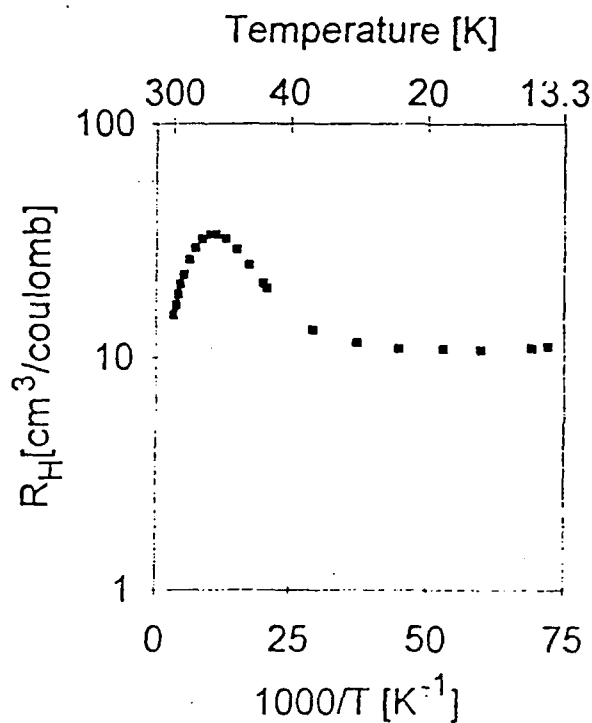


Figure 2. Hall Constant vs. $1/T$ for our highest mobility GaN Film

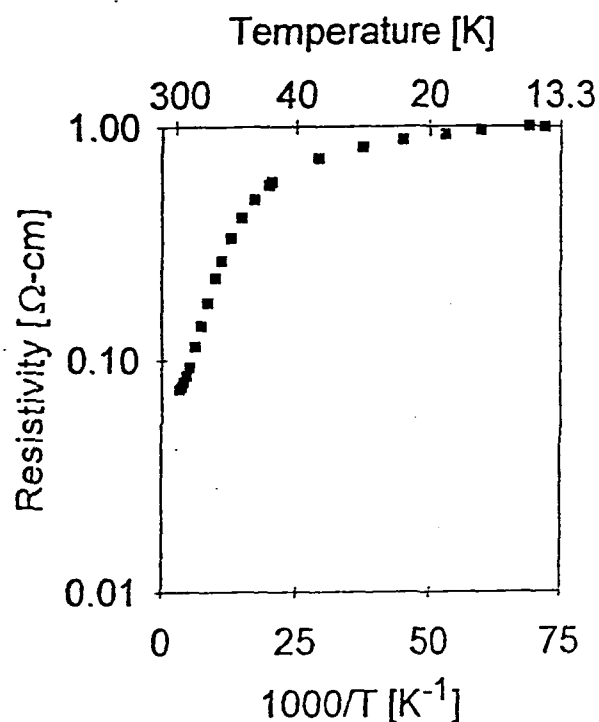


Figure 3. Resistivity vs. $1/T$ for the same GaN film discussed in Figure 2.

The temperature dependence of the electron mobility for the film discussed in Figures 2 and 3 is shown in Figure 4. The high temperature data in this Figure are characteristic of transport in the conduction band, while the low temperature correspond to transport in the band of the autodoping centers.

CONCLUSIONS

We have demonstrated the growth of high mobility GaN-films grown by the method of Electron Cyclotron Resonance assisted Molecular Beam Epitaxy. The relation between mobility and net carrier concentration also predicts the results on GaN films grown by CVD methods as well as anticipates the values of electron mobility for purer and relatively defect free GaN films. For GaN films with carrier concentrations larger than 10^{17}cm^{-3} transport in the autodoping center becomes dominant at temperatures below 300K.

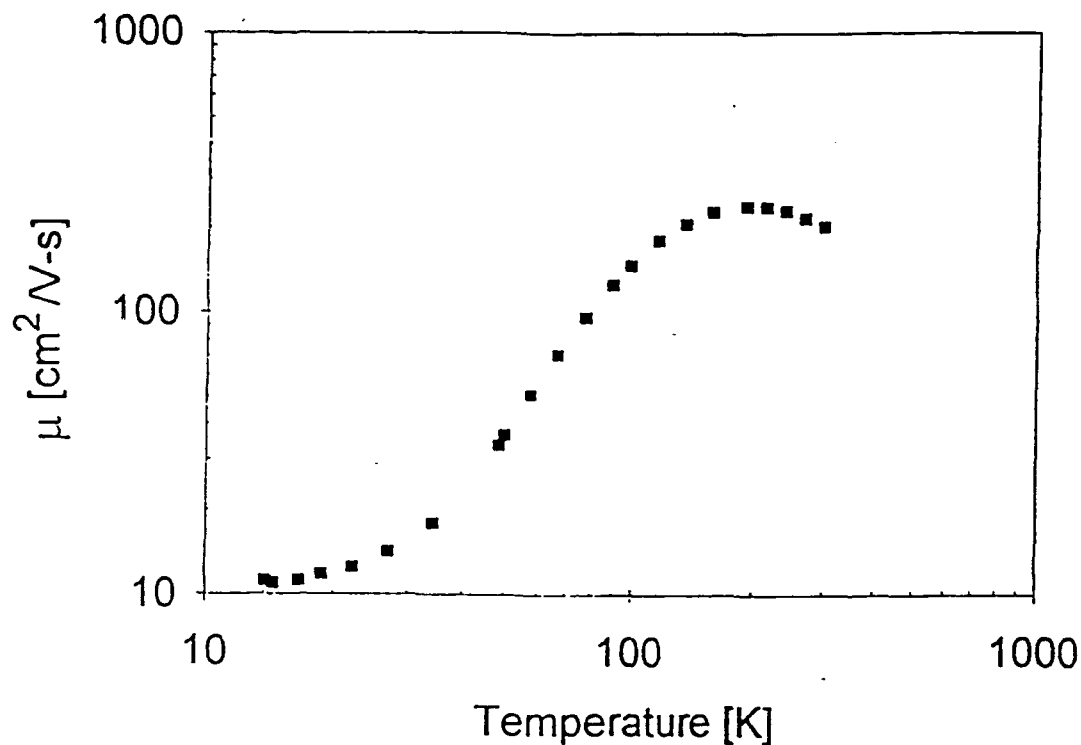


Figure 4. Temperature dependence of the electron mobility for the film discussed in Figures 2 and 3

Acknowledgements

This work was supported by the Office of Naval Research (Grant Number N00014-92-J-1436). We acknowledge the collaboration with Olga Razumovsky and James Foresi.

REFERENCES

1. J.I. Pankove, *Mat. Res. Soc. Symp. Proc.*, vol. 162, 515 (1990).
2. I. Akasaki and H. Amano, *Mat. Res. Soc. Symp. Proc.*, vol. 242, 383 (1992).
3. S. Nakamura, T. Mukai, and M. Senoh, *J. Appl. Phys.*, 71, 5543 (1992).
4. T.D. Moustakas, R.J. Molnar, T. Lei, G. Menon, and C.R. Eddy Jr., *Mat. Res. Soc. Proc.*, vol. 242, 427 (1992).
5. T.D. Moustakas, T. Lei, and R.J. Molnar, *Physica B; Condensed Matter* (accepted for publication).
6. M. Hegems, *J. Crystal Growth*, 13/14, 360 (1972).
7. R.J. Molnar, T. Lei, and T.D. Moustakas, *Appl. Phys. Lett.*, 62 (Jan. 1993).

Appendix D:

Electron Transport Mechanism in Gallium Nitride
Published in *Applied Physics Letters* **62**, 72 (1993).

Electron transport mechanism in gallium nitride

R. J. Molnar, T. Lei, and T. D. Moustakas

*Molecular Beam Epitaxy Laboratory, Department of Electrical Computer and Systems Engineering,
Boston University, Boston, Massachusetts 02215*

(Received 23 July 1992; accepted for publication 20 October 1992)

The electron transport mechanism in autodoped gallium nitride films grown by electron cyclotron resonance microwave plasma-assisted molecular beam epitaxy was investigated by studying the temperature dependence of the Hall coefficient and resistivity on samples with various concentrations of autodoping centers. The Hall coefficients go through a maximum as the temperature is lowered from 300 K and then saturate at lower temperatures. The resistivities in the same temperature range initially increase exponentially and then saturate at lower temperatures. These findings are accounted for if a significant fraction of electron transport, even at room temperature, takes place in the autodoping centers and that conduction through these centers becomes dominant at lower temperatures. The activation energy of these centers was found to be on the order of 20–30 meV. When the concentration of the autodoping centers becomes smaller than that of deep compensating defects, the material becomes semi-insulating and transport by hopping in the compensating defects becomes dominant.

Gallium nitride (GaN) is one of the most promising wide-band-gap semiconductors for the development of high efficiency UV-vis photonic devices due to its direct band gap. The majority of reported work indicates that the GaN films are autodoped *n*-type, a result generally attributed to nitrogen vacancies.^{1,2} In general, the defect structure of GaN films is poorly understood and very difficult to control experimentally, resulting in difficulties in doping this material *p*-type.^{2,3}

GaN films produced by a variety of deposition methods were generally found to have low electron mobilities ($< 100 \text{ cm}^2/\text{V s}$) and high carrier concentration ($> 10^{18} \text{ cm}^{-3}$),^{2,3} although there have been reports^{4,5} of mobilities $\sim 600 \text{ cm}^2/\text{V s}$ and carrier concentration $\sim 10^{16} \text{ cm}^{-3}$. Some other workers^{6,7} reported semi-insulating films. One would expect that more lightly doped films would have higher Hall mobilities. However, such films generally do not have measurable Hall coefficients, suggesting low carrier mobilities,^{6,7} while highly conductive (even degenerate) samples readily have mobilities $> 20 \text{ cm}^2/\text{V s}$. This anomaly has not yet been accounted for.

In this letter, we report on Hall measurements performed on a number of GaN thin films grown on the (0001) plane of sapphire by the electron cyclotron resonance microwave plasma assisted molecular beam epitaxy (ECR-MBE) method. The data is analyzed by taking into account that conduction through defects makes a significant contribution to the electrical transport. The proposed model also accounts for the low mobility in the semi-insulating films.

The films were deposited by the two-step growth process in which a GaN buffer is grown first at relatively low temperatures and the rest of the film is grown at higher temperatures.^{7–12} This method is capable of producing either conductive or insulating films. The conductive films, which are reported here, are generally grown under conditions (high substrate temperature, low nitrogen overpressure) which are believed to lead to the introduction of nitrogen vacancies.^{1,2} These films tend to be covered at the

end of the run with microscopic Ga droplets, due to phase separation of excess Ga in the GaN films. To study the transport properties in these films the Ga droplets are etched by immersing them in concentrated HCl. The insulating films, which are grown at high nitrogen overpressure are free of Ga droplets.

The structure and surface morphology of these films were reported elsewhere.¹⁰ X-ray diffraction studies indicate that the films are high-quality single crystals with full width at the half-maximum of the θ -rocking curves found to be ~ 10 –20 min.

The films were grown at a deposition rate of $0.2 \mu\text{m/h}$ and were 1–2- μm thick. The samples were abrasively etched into Van der Pauw lamella and ohmic contacts were made by annealing indium pads. The transport coefficients were measured from 10 to 300 K in a closed loop helium cryostat. The magnitude of the magnetic field was varied up to 7 kG and the current through the sample was varied from 10^{-5} to 10^{-3} A.

The resistivities of the investigated samples at 300 K are shown in Table I. All the samples are *n*-type and their room temperature resistivities vary from 0.01 to 0.12 $\Omega \text{ cm}$. Figure 1 shows the Hall coefficient vs $1/T$ for the investigated samples. For the more resistive samples (118, 119, 110, 115) the Hall coefficient goes through a maximum. The temperature at which this maximum occurs is higher for samples with lower resistivity. The Hall coefficients for all the samples saturate to constant values at low temperatures. The resistivity vs $1/T$ of the investigated films is shown in Fig. 2. In all samples the resistivity initially increases as the temperature is lowered and then saturates to a constant value.

The observed decrease in the Hall coefficient at low temperatures is not typical for semiconductors.¹³ Similar behavior has been observed for GaN films grown by chemical vapor deposition.^{14,15} The data of Figs. 1 and 2 bear resemblance to behavior observed in *p*-type and *n*-type Ge,¹⁶ where a model involving transport in both the defect centers and the conduction band was introduced to explain

TABLE I. Room temperature resistivities of the investigated samples.

Sample	Thickness [μm]	Type	Resistivity at 300 K [$\Omega \text{ cm}$]
118	1.9	<i>n</i>	0.121
119	1.7	<i>n</i>	0.074
110	1.8	<i>n</i>	0.038
115	1.8	<i>n</i>	0.025
114	1.1	<i>n</i>	0.012

the phenomenon. The conduction in the defect centers may be either diffusive, due to the small but finite overlap of the localized electron wave functions of the defect centers or hopping.¹⁷ Therefore the defect band mobility is expected to be small compared to the conduction band mobility, and defect band conduction only becomes dominant when carriers in the conduction band become negligible.

The results of Figs. 1 and 2 can be fitted to such a two-band model in order to determine the relative concentration and the corresponding mobilities of electrons in the autodoping centers and the conduction band. Let us assume that the donor concentration in our films is N_d with an activation energy ΔE_d , and that the concentration of deep compensating centers (due to defects such as dislocations) is N_a . At a given temperature, a portion of the net carrier concentration ($N_d - N_a$) is excited into the conduction band and has mobility μ_c and concentration n_c . The unexcited carriers remain in the defect states with a much lower mobility μ_d and concentration n_d . The net carrier concentration of the conducting carrier is

$$N_0 = n_c + n_d = N_d - N_a \quad (1)$$

Taking both these contributions into account, the Hall coefficient, R_H can be expressed as¹⁶

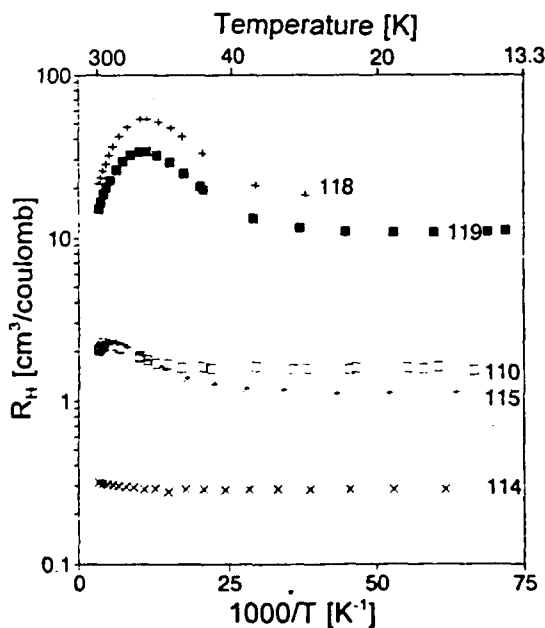


FIG. 1. Hall coefficient vs $1/T$.

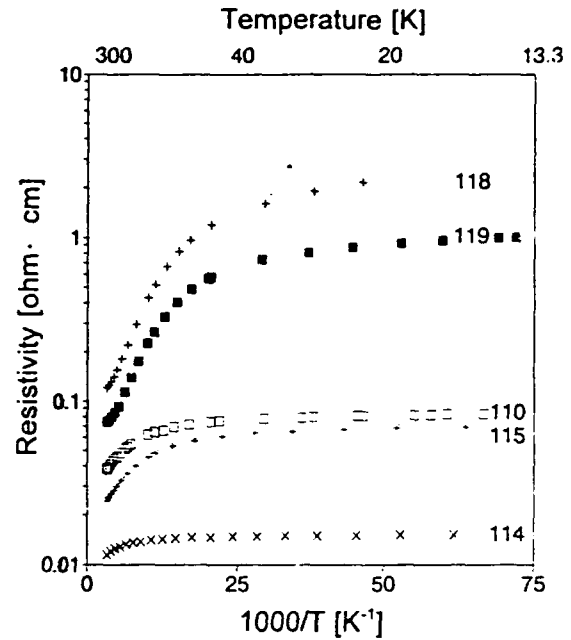


FIG. 2. Resistivity vs $1/T$.

$$R_H = \frac{n_d \mu_c^2 + (N_0 - n_c) \mu_d^2}{[n_d \mu_c + (N_0 - n_c) \mu_d]^2} \quad (2)$$

and the measured resistivity is

$$\rho = \frac{1}{\sigma} = \frac{1}{n_c e \mu_c + (N_0 - n_c) e \mu_d} \quad (3)$$

Letting $b = \mu_d / \mu_c$ we have

$$eR_H = \frac{(1 - b^2)n_c + N_0 b^2}{[(1 - b)n_c + N_0 b]^2} \quad (4)$$

$$\rho = \frac{1}{\mu_c [(1 - b)n_c + N_0 b] e} \quad (5)$$

Note that if n_c is much larger than n_d (the high temperature limit), the expression for R_H reduces to the expression used for one-band conduction. However, for $\mu_d \neq 0$, as the temperature is lowered the carriers in the conduction band will decrease to the point where conduction through the defect states will dominate. It is also apparent from Eq. (4) that eR_H at both temperature limits is the same and equal to $1/N_0$. If b is not a strong function of temperature, it can be shown that eR_H in Eq. (4) has a maximum

$$eR_{H_{\text{max}}} = \frac{(1 + b)^2}{4N_0 b} \quad (6)$$

when

$$n_c = \frac{N_0 b}{(1 + b)} \quad (7)$$

Then the expression of R_H in Eq. (4) qualitatively predicts the shape of the experimental curves shown in Fig. 1.

The parameters μ_d , μ_c , n_c , and n_d are related to R_H and ρ by Eqs. (4) and (5). However, at each temperature, there are three unknowns for the two equations. Hung

TABLE II. Values of N_0 and ΔE_d for samples studied.

Sample	N_0 [carrier/cm ³]	ΔE_d [meV]
118	4.75×10^{17}	19.09
119	5.80×10^{17}	18.82
110	4.00×10^{18}	32.16
115	5.56×10^{18}	31.31
114	2.19×10^{19}	...

*et al.*¹⁶ analyzed the Ge data by assuming that the measurements at high temperatures were dominated by the conduction band electrons and extrapolated the carrier concentration curve to low temperatures to predict n_c at low temperatures. However, we found that in our case, the defect band conduction is not negligible even at room temperature and therefore we did not adopt this approach.

In the case of a well-defined activation energy ΔE_d , the carrier concentration in the conduction band is expected to change exponentially with temperature. The parameters N_0 , ΔE_d , and μ_c , μ_d at each temperature can be extracted using Eqs. (4)–(7).¹² The extracted values of N_0 and ΔE_d for each of the samples are listed in Table II.

Figure 3 shows the temperature dependence of μ_c and μ_d calculated for sample No. 119. The temperature dependence of μ_c is typical of semiconductors. The scattering is dominated at low temperatures by ionized impurities and at high temperatures by phonon scattering. Figure 4 shows the temperature dependence of n_c and n_d calculated for the same sample (119).

If the concentration of donors is smaller than the deep defects known to exist in GaN films, the material will be fully compensated with its Fermi level pinned by these defects. In such a material, transport is dominated by hop-

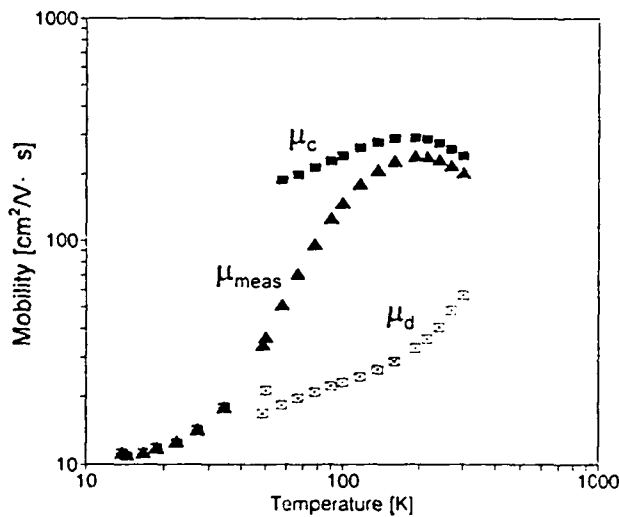


FIG. 3. Temperature dependence of μ_{meas} , μ_c and μ_d .

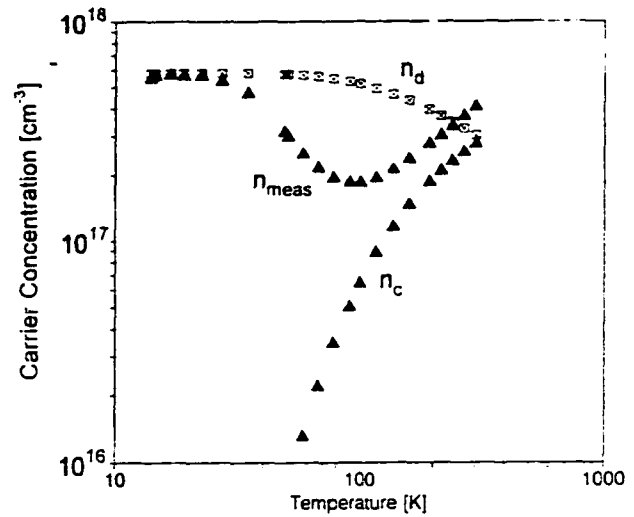


FIG. 4. Temperature dependence of n_{meas} , n_c , and n_d .

ping in the compensating centers leading to low electron mobilities.

In conclusion, we studied the transport mechanism of a number of GaN films produced by the ECR-MBE method. The experimental results were accounted for by invoking conduction both through the conduction band and the autodoping centers at 20–30 meV below the conduction band. When the concentration of the autodoping centers becomes smaller than the deep compensating defects, the material becomes semi-insulating and the transport is determined by electron hopping through the deep compensating defects. This accounts for the low electron mobility of the semi-insulating GaN films. The nature of the autodoping centers is assumed to be nitrogen vacancies, and their energy levels are found to be 20–30 meV.

We would like to thank M. Yoder for his encouragement in this effort. This work was supported by the Office of Naval Research (Grant No. N00014-92-J-1436).

¹H. P. Maruska and J. J. Tietjen, Appl. Phys. Lett. 15, 327 (1969).

²J. I. Pankove, Mater. Res. Symp. Proc. 162, 515 (1990).

³R. F. Davis, Proc. IEEE 79, 702 (1991).

⁴M. Ilegems, J. Cryst. Growth 13/14, 360 (1972).

⁵S. Nakamura, Jpn. J. Appl. Phys. 30, L1705 (1991).

⁶R. C. Powell, G. A. Tomasch, Y. W. Kim, J. A. Thornton, and J. E. Greene, Mater. Res. Symp. Proc. 162, 525 (1990).

⁷G. Menon, M. S. thesis, Boston University, 1990.

⁸T. Lei, M. Fanciulli, R. J. Molnar, T. D. Moustakas, R. J. Graham, and J. Scanlon, Appl. Phys. Lett. 59, 944 (1991).

⁹T. Lei, T. D. Moustakas, R. J. Graham, Y. He, and S. J. Berkowitz, J. Appl. Phys. 71, 4933 (1992).

¹⁰T. D. Moustakas, T. Lei, R. J. Molnar, Phys. B (to be published).

¹¹T. D. Moustakas, R. J. Molnar, T. Lei, G. Menon, and C. R. Eddy, Jr., Mater. Res. Symp. Proc. 242, 427 (1992).

¹²T. Lei, Ph.D. dissertation, Boston University, 1992.

¹³C. Kittel, Introduction to Solid State Physics, 6th ed. (Wiley, New York, 1986).

¹⁴M. Ilegems and H. C. Montgomery, J. Phys. Chem. Solids 34, 885 (1973).

¹⁵I. Akasaki and H. Amano, Mater. Res. Symp. Proc. 242, 383 (1991).

¹⁶C. S. Hung and J. R. Gliessman, Phys. Rev. 96, 1226 (1954).

¹⁷N. F. Mott and T. D. Twose, Adv. Phys. 10, 107 (1961).

¹⁸T. L. Tansley and R. J. Egan, Mater. Res. Symp. Proc. 242, 395 (1992).

Appendix E:

Metal Contacts to Gallium Nitride
Published in *Applied Physics Letters* 62, 2859 (1993).

Metal contacts to gallium nitride

J. S. Foresi and T. D. Moustakas

Molecular Beam Epitaxy Laboratory, Department of Electrical, Computer, and Systems Engineering, Boston University, Boston, Massachusetts 02215

(Received 19 October 1992; accepted for publication 9 March 1993)

We report measurements on the nature of aluminum and gold contacts to GaN. The GaN films were deposited onto the *R*-plane of sapphire substrates by molecular beam epitaxy and are autodoped *n*-type. Metal contacts were deposited by evaporation and were patterned photolithographically. Current-voltage characterization shows that the as-deposited aluminum contacts are ohmic while the as-deposited gold contacts are rectifying. The gold contacts become ohmic after annealing at 575 °C, a result attributed to gold diffusion. The specific contact resistivity of the ohmic aluminum and gold contacts were found by transfer length measurements to be of device quality (10^{-7} – 10^{-8} Ω m²). The results of these studies suggest a direct correlation between barrier height and work function of the metal, consistent with the strong ionic character of GaN.

Gallium nitride (GaN) is a direct, wide band-gap semiconductor ($E_g=3.4$ eV) whose conduction band structure allows for a high saturation velocity (3×10^7 cm/s).^{1,2} Due to these unique properties GaN is expected to find applications in optical devices (LEDs, lasers, detectors) operating in the spectral region from the blue to near-UV and in electronic devices such as high temperature, high power, and high frequency transistors.

GaN films are generally *n*-type³ with carrier concentrations between 10^{18} and 10^{20} cm⁻³ and electron mobilities of about 20 cm²/V s. The *n*-type autodoping is attributed to nitrogen vacancies. The most important recent development is the discovery that AlN⁴ and GaN⁵⁻¹⁰ buffers lead to lateral growth which significantly improves the surface morphology and the electrical properties of the films.

In this letter, we report our initial investigation of metal/GaN contacts. Metals investigated include Al and Au. Current-voltage (*I-V*) measurements and transfer length measurements (TLM) of the specific contact resistivity are presented.

The GaN films used in this study were grown by the ECR-MBE method without a GaN buffer layer.^{11,12} All films were deposited on sapphire substrates with *R*-plane orientation. X-ray diffraction studies show that the films have the wurtzitic crystal structure with (11 $\bar{2}$ 0) orientation, which leads to a faceted surface morphology.¹² The faceted surface makes these films unsuitable for planar devices, however, the metal contact results presented in this letter should be applicable to GaN films grown on other substrates and orientations. The transport coefficients were determined by Hall effect measurements using the Van der Pauw configuration. The investigated films were *n*-type with resistivities of about 10^{-1} Ω cm, carrier concentration of 3×10^{18} cm⁻³ and Hall mobilities of about 20 cm²/V s. The thickness of the films was 1.6 μ m.

The Au and Al contacts were deposited on the GaN films by thermal evaporation and patterned using photolithography and liftoff techniques.¹³ The base pressure of the evaporation unit was 10^{-7} Torr and the system was cryopumped to keep the chamber oil-free. Tungsten evapora-

tion boats were used to evaporate 99.999% pure Al and Au. The substrates were kept at room temperature during the evaporation. Prior to photolithography, the samples were degreased. Following metal deposition, the metals were patterned using liftoff techniques which consisted of ultrasonic baths in acetone and methanol. The contacts were patterned in TLM structures which consist of three square contacts separated by known distances [see Fig. 1(a)]. The same contacts were also used in pairs to evaluate the rectifying nature of the metal/semiconductor interface by *I-V* characterization. Because these pairs of contacts were deposited on the surface of the GaN films, they constituted back-to-back Schottky barrier systems.

I-V characterization was carried out by injecting up to ± 20 mA with a current source and measuring the voltage across the same contacts with an electrometer. *I-V* characterization was performed on both as-deposited metal contacts and metal contacts which had been annealed in a reducing atmosphere for 10 min at 575 °C. All of the measurements were made in atmosphere at room temperature.

Measurements of the specific contact resistivity were made using the TLM method which is employed widely in the characterization of ohmic contacts to semiconductors.¹⁴⁻¹⁶ The technique requires the formation of contacts

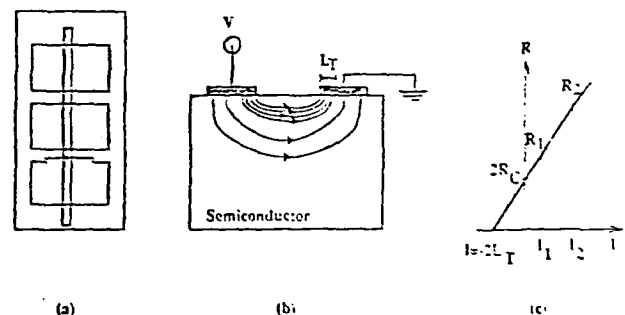


FIG. 1. (a) Sample configuration for *I-V* and TLM characterization. The thin vertical stripe is a 10 μ m wide area of exposed GaN. The three wide rectangles are metal contacts separated by 20 and 15 μ m. (b) Schematic of current flow through planar contacts. Nearly all of the current flows through one transfer length, L_T , of the contacts' front edges. (c) Plot of the measured resistance against the contact separation.

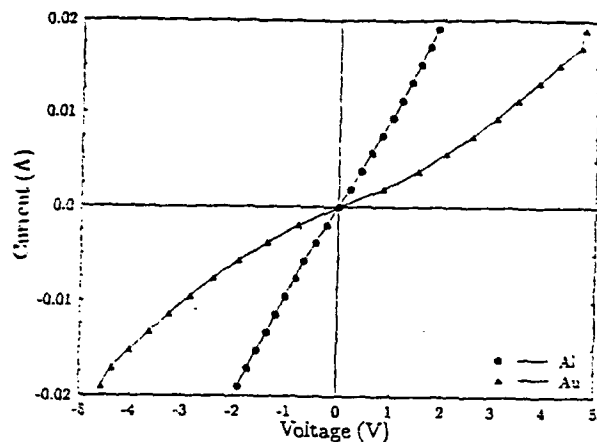


FIG. 2. I - V characteristics of as-deposited Al/ n -GaN and Au/ n -GaN structures.

with controlled geometry and evaluates the difference in resistance between equally sized pairs of contacts separated by different distances. The specific contact resistivity (ρ_c) is calculated from a measurement of the effective contact resistance (R_c), the contact width (W), and the transfer length (L_T):

$$\rho_c = R_c W L_T. \quad (1)$$

The effective contact resistance is given by:

$$2R_c = \frac{R_2 l_1 - R_1 l_2}{l_1 - l_2}, \quad (2)$$

where R_1 is the resistance measured between contacts spaced l_1 apart and R_2 is the resistance measured between contacts spaced l_2 apart. In a planar contact configuration, nearly all of the current enters the semiconductor through a small area at the edge of the contact.¹⁷ The parameter L_T is the length of this area as indicated in Fig. 1(b). This quantity is estimated by plotting the resistance of two pairs of contacts against the distance separating the individual contacts within each pair. The line connecting the points R_1 and R_2 crosses the resistance axis at the $2R_c$ point and intersects the distance axis at the $-2L_T$ point [see Fig. 1(c)].

The TLM technique relies on the assumption that the semiconductor material under the contact has not been doped differently than the bulk material, and the accuracy of the method depends on the ability to control the separation between the contacts. Due to the faceted surface morphology in our films, the determination of the contact areas was difficult and limited the accuracy of the specific contact resistivity to within an order of magnitude.

The I - V characteristics of the as-deposited Al and Au contacts are shown in Fig. 2. For both metals the I - V curves are symmetric about the origin as is expected for back-to-back Schottky barriers where the characteristic is that of a reverse-biased barrier irrespective of the current polarity.¹⁷ The Al contact I - V characteristics are linear indicating that the contact is ohmic with no apparent barrier to current flow. In contrast, the I - V characteristics of the Au contact exhibit curvature associated with the for-

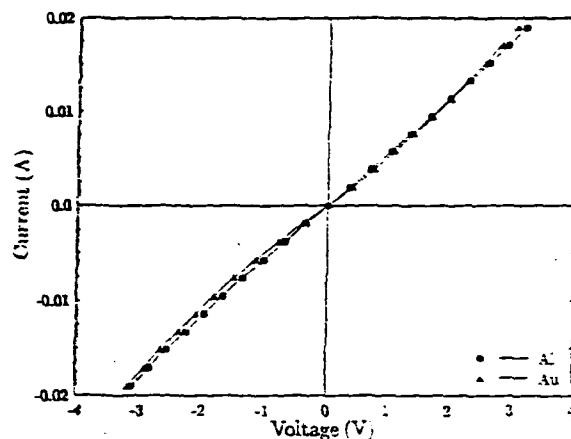


FIG. 3. I - V characteristics of annealed Al/ n -GaN and Au/ n -GaN structures.

mation of a Schottky barrier. This Schottky barrier is leaky due to tunneling effects arising from the high carrier concentration of the films and the possible existence of an interfacial native oxide layer.¹³ These results indicate that the barrier height depends on the metal used.

The I - V curves for the same contacts after annealing, shown in Fig. 3, suggest that both the Al and Au contacts have changed during annealing. The I - V curves of the Al contacts acquired a slight curvature and the calculated resistance increased by about 50%. These changes may be attributable to the formation of an interfacial AlN layer during the annealing process. No experimental work was performed to confirm the existence of such a layer. The I - V curves of the Au contacts became practically linear. A similar result has been observed in Au contacts to GaAs and attributed to Au diffusion in GaAs.¹⁵ Analytic measurements and electron microscopy have not been performed to confirm Au diffusion. The GaN material, however, has 10^{18} - 10^{19} cm^{-3} nitrogen vacancies which should facilitate the Au diffusion even though the material is tightly bonded.

The specific contact resistivities of Al and Au contacts were measured by the TLM method after annealing. The results in Table I show specific contact resistivities measured for a number of contact pairs on a single GaN sample. The variations in the contact resistivities can be attributed to the nonuniformity of the film. All of the contacts measured have specific contact resistances in the 10^{-7} - 10^{-8} $\Omega \text{ m}^2$ range. The lowest specific contact resistivities

TABLE I. Specific contact resistivities for Au/ n -GaN and Al/ n -GaN after annealing. Measurements correspond to different TLM studies of a single sample.

Metal	Specific contact resistivity ($10^{-7} \Omega \text{ m}^2$)	Metal	Specific contact resistivity ($10^{-7} \Omega \text{ m}^2$)
Au	1.6	Al	0.12
	2.0		4.4
	3.1		1.3
	3.0		...

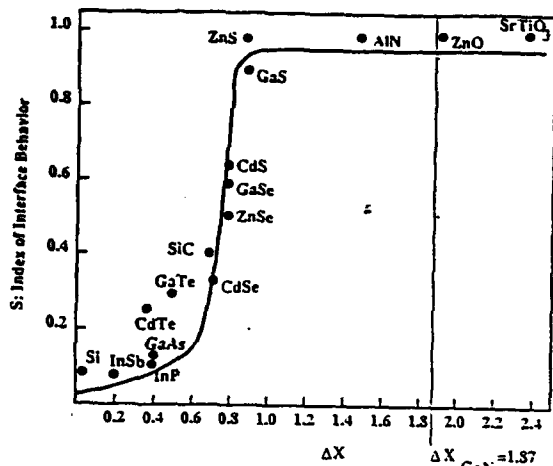


FIG. 4. Dependence of $S = d\phi_b/d\chi_m$ (change in barrier height over the change in metal work function) on the electronegativity difference between the components of the compound (after Ref. 20).

reported for GaAs are $\approx 10^{-9} \Omega \text{ m}^2$ for high quality AuGeNi contacts.¹⁸

The simplest considerations of Schottky barrier formation between metals and semiconductors rely on the difference in work functions of the two materials to predict the barrier height. For a large number of important semiconductors, Si and GaAs included, the dependence of barrier height on work function difference has not been observed, a result attributed to the existence of surface states which pin the Fermi level at the interface.¹⁹ The dependence of the barrier height on the work function difference has been correlated to the ionicity of the semiconductor by Kurtin and co-workers²⁰ as shown in Fig. 4. In this figure, the vertical axis is a parameter S which is defined as the change in barrier height over the change in metal work function ($d\phi_b/d\chi_m$) and the horizontal axis is the electronegativity difference between the components of a compound which is a measure of the compound's ionicity. The direct dependence of the barrier height on the work function for the semiconductors with large electronegativity differences results from the bunching of surface states near the band edges where they have less effect on the surface Fermi level position.¹⁷

The electronegativity difference for GaN is 1.87 eV.^{21,22} This puts GaN above the knee of the curve implying that Schottky barriers on GaN should have barrier heights which depend directly on the work function difference between the metal and GaN. The work function of GaN has been measured to be 4.1 eV.²³ Therefore, any metal with a work function equal to or lower than that of GaN should form essentially ohmic contacts to n -type GaN and any metal with a work function higher should form a rectifying contact to n -type GaN. The work function of Al is 4.08 eV (Ref. 22) putting Al in the ohmic category. The work function of Au is 4.82 eV (Ref. 22) which puts it in the rectifying category. Our results on Al and Au contacts to n -GaN are in agreement with the predictions of this model.

Based on these findings a variety of metals can be cho-

sen to form either ohmic or Schottky barriers to n - or p -type GaN. For example, Al can form ohmic contacts to n -type GaN and Au can form ohmic contacts to p -type GaN. Other factors may also play a role in choosing the proper metals for contacts to GaN. For example, Au appears to diffuse upon annealing in the GaN. Thus, the use of Au as a contact to GaN requires a thin interlayer of Ti or Cr as a diffusion barrier.¹⁵ Also, annealing of Al contacts may result in the formation of a thin insulating AlN interlayer, which will increase its contact resistance.

In conclusion, the nature of Al and Au contacts to n -GaN were investigated. It was found that the as-deposited Al- and Au-contacts are ohmic and rectifying, respectively. This result is in direct agreement with data indicating that ionic materials do not suffer from Fermi level pinning at metal/semiconductor interfaces. The lack of Fermi level pinning greatly reduces the complication of creating ohmic contacts to GaN as it is only necessary to determine metals with appropriate work functions. Measurements of the specific contact resistivities of Al and Au annealed contacts on GaN give values in the range of 10^{-7} – $10^{-8} \Omega \text{ m}^2$ which are of device quality.

The authors benefited from collaborations with R. Molnar, W. Choi, and E. DeObaldia. Suggestions and discussions with Max Yoder and Scott Dunham are greatly appreciated. The work was supported by the Office of Naval Research (Grant No. N00014-92-J-1436).

¹J. I. Pankove, MRS Symp. Proc. 162, 515 (1990).

²P. Das and D. K. Ferry, Solid-State Electron. 19, 76 (1976).

³R. F. Davis, Proc. IEEE 79, 702 (1991).

⁴I. Alkaskas and H. Amano, MRS Symp. Proc. 242, 383 (1992).

⁵G. Menon, M. S. thesis, Boston University, 1990.

⁶T. Lei, M. Fanciulli, R. J. Molnar, T. D. Moustakas, R. J. Graham, and J. Scanlon Appl. Phys. Lett. 58, 944 (1991).

⁷T. Lei, T. D. Moustakas, R. J. Graham, T. He, and J. Berkowitz, J. Appl. Phys. 71, 4933 (1992).

⁸T. D. Moustakas, T. Lei, and R. J. Molnar, Physica B 185, (1993).

⁹S. Nakamura, Jpn. J. Appl. Phys. 30, L1705 (1991).

¹⁰R. J. Molnar, T. Lei, and T. D. Moustakas, Appl. Phys. Lett. 62, 72 (1993).

¹¹C. R. Eddy Jr., M. S. thesis, Boston University, 1990.

¹²C. R. Eddy, Jr., T. D. Moustakas, and J. Scanlon, J. Appl. Phys. 73, 448 (1993).

¹³J. Foresi, M.S. thesis, Boston University, 1992.

¹⁴B. L. Sharma, Metal-Semiconductor Schottky Barrier Junctions and Their Applications (Plenum, New York, 1984).

¹⁵G. N. Maracas, Gallium Arsenide Technology, edited by D. K. Ferry (Howard W. Sams, Carmel, IN, 1989), Vol. 2.

¹⁶G. Stareev and A. Umbach, J. Electron. Mater. 20, 1059 (1991).

¹⁷H. K. Henisch, Semiconductor Contacts (Clarendon, Oxford, 1984).

¹⁸E. H. Rhoderick and R. H. Williams, Metal-Semiconductor Contacts (Clarendon, Oxford, 1988).

¹⁹J. Bardeen, Phys. Rev. 71, 717 (1947).

²⁰S. Kurtin, T. C. McGill, and C. A. Mead, Phys. Rev. Lett. 22, 1433 (1969).

²¹C. M. Wolfe, N. Holonyak, Jr., and G. E. Stillman, Physical Properties of Semiconductors (Prentice Hall, Englewood Cliffs, NJ, 1989).

²²K. W. Böer, Survey of Semiconductor Physics (Van Nostrand, New York, 1990).

²³J. I. Pankove and H. E. P. Schade, Appl. Phys. Lett. 25, 53 (1974).

Appendix F:

Heteropitaxy, Polymorphism And Faulting In GaN Thin Films on Silicon
and Sapphire Substrates

Accepted for Publication in *Journal of Applied Physics* (Oct. 1993).

Heteroepitaxy, Polymorphism And Faulting In GaN Thin Films On Silicon And Sapphire Substrates

T. Lei¹, K.F. Ludwig Jr.¹ and T.D. Moustakas^{1,2}

¹*Dept. of Physics, Boston University; Boston, MA 02215*

²*Dept. of Electrical Engineering, Boston University; Boston, MA 02215*

Abstract:

The structure of GaN films grown by electron-cyclotron-resonance-assisted MBE on Si(111), Si(001), basal-plane sapphire, a-plane sapphire and r-plane sapphire substrates was studied with four-circle x-ray diffractometry. Phase content, domain size, inhomogeneous strain and in-plane and out-of-plane domain misorientations were measured and compared for films grown on each type of substrate. Wurtzite and zincblende polymorphs were found to coexist in films grown on Si(111). The two structures grow in the (0002) and (111) orientations respectively so that they may transform into each other via stacking faults on close-packed planes. Smaller amounts of zincblende material were also found in predominately (0002) wurtzitic films on a-plane sapphire and (11 $\bar{2}$ 0) wurtzitic films on r-plane sapphire.

1. Introduction:

The growth and properties of GaN films have been under extensive investigation because of their potential applications as light-emitting devices in the blue, violet and near ultra-violet spectra [1,2]. It is known that GaN exists in two polymorphs: wurtzite and zincblende structures with direct bandgaps of 3.4 eV and 3.2 eV respectively. The two are analogous to hcp and fcc structures respectively in their stacking sequences. Since bulk GaN substrates are not available, films must be grown by heteroepitaxy on foreign substrates. The majority of GaN films reported have grown in the wurtzite structure, most commonly with the basal planes parallel to the substrate. However, epitaxial stabilization of the zincblende phase has been obtained on GaAs, MgO, SiC and Si substrates [see the citations in Ref. 1]. All substrates used have a large mismatch to GaN films.

Despite the critical role which substrate symmetry and unit cell size must play in the formation of heteroepitaxial GaN films, relatively little detailed comparative structural work has been performed. While reflective high-energy electron diffraction (RHEED) is often used to characterize films *in situ* [3-6], it probes only the surface structure of the growing film. Electron transmission microscopy (TEM) studies provide important information about the film microstructure and epitaxial orientation [7,8], but they cannot quantitatively examine the degree of orientational order between film domains or reliably detect small phase components. In contrast, x-ray diffraction examines the structure of the bulk of the film, can quantify the degree of film orientational order and can determine oriented minor phase content down to the 10^{-4} level. However, x-ray diffraction measurements limited to Bragg peaks from planes parallel to the substrate have significant limitations. Because the wurtzite and zincblende structures simply differ in their packing sequences (ABAB and ABCABC respectively), the wurtzite (0002) and zincblende (111) stacking planes have the same lattice spacing. The wurtzite (11 $\bar{2}$ 0) and zincblende (110) lattice spacings are also equal to each other. Standard θ - 2θ x-ray diffraction scans measure only the lattice plane spacings parallel to the film surface and therefore cannot distinguish

between the zincblende and wurtzite polymorphs if they have one of the above orientations. Moreover, rocking curves of these "on-axis" Bragg peaks (peaks due to lattice planes parallel to the surface) [9] show only the orientational order perpendicular to the substrate - they yield no information on the orientational order of film domains in the plane.

We report here a comprehensive x-ray diffraction study examining both the in-plane and out-of-plane structures of GaN films grown by electron-cyclotron-resonance-assisted molecular beam epitaxy (ECR-MBE) on two of the most important substrates for technological applications - silicon and sapphire. Silicon substrates were of (111) and (001) orientation. Sapphire substrates were of (0001) (basal-plane), (11 $\bar{2}$ 0) (a-plane) and (1 $\bar{1}$ 02) (r-plane) orientations. The details of the growth process have been previously reported along with brief descriptions of some of the x-ray results [10-13]. All films studied here were approximately one micron thick and included a thin (~ 200 Å) GaN buffer layer at the substrate interface. We have found that wurtzite and zincblende GaN polymorphs often coexist in these materials. This may explain the variable optical and transport measurements sometimes observed in GaN films [14].

2. Experimental Methods:

The x-ray diffraction measurements reported here used Cu K_α radiation in conjunction with a sagittally focussing graphite (002) monochromator crystal and Soller slits for low resolution measurements and a Ge (111) crystal for high resolution determination of peak widths. The higher flux graphite configuration was used for scans covering a wide range of angles and to examine weak peaks; its angular resolution is approximately 0.1° . The low flux of the Ge crystal configuration limited its application to relatively strong Bragg peaks; its angular resolution is approximately 0.01° , which is much smaller than the diffraction widths of the peaks observed from the GaN. Since most of the lineshapes observed could be fit to a lorentzian function, the instrumental resolution could be subtracted directly from the measured peak widths to yield the net peak width values cited throughout the

rest of the paper.

The experiments utilized a four-circle diffractometer which allowed access to a large volume of reciprocal space [15]. A schematic of the four-circle geometry is shown in Fig. 1. The horizontal plane M is defined by the incident and reflected beams; χ is defined as the angle between the sample surface and plane M and $\chi = 0$ when they are parallel. The angle ϕ measures the rotation around the surface normal of the substrate and 2θ is defined as the angle between the incident and reflected beam. The angle θ measures the sample rotation around the axis perpendicular to the M plane.

Several different types of scans were utilized to characterize the thin films. The simplest, θ - 2θ scans, measure the film structure along the surface normal \hat{n} , giving information on phase presence and orientation. Homogeneous strain in the film due to uniform stress or nonstoichiometric composition is reflected in Bragg peak shifts relative to the those expected from measured GaN lattice constants. Inhomogeneous strain and finite domain sizes act to broaden the θ - 2θ Bragg peaks. The full-width at half-maximum (FWHM) of a Bragg peak in a θ - 2θ scan includes both effects [16]

$$\delta\theta = \frac{\lambda}{2D \cos \theta} + \epsilon_{in} \tan \theta, \quad (1)$$

or, in reciprocal space

$$\delta k = \frac{2\pi}{D} + \epsilon_{in} k. \quad (2)$$

Here D is the average domain size, ϵ_{in} is the inhomogeneous strain, i.e. the FWHM variation of the interplanar spacing d through the film $\delta d/d$, and we assume that the finite domain size and inhomogeneous strain contributions lead to lorentzian peakshapes. The different angular dependencies of the the inhomogeneous strain and the domain size allow them to be separately determined from measurements of two or more diffraction peaks. Various factors can contribute to ϵ_{in} , including local stresses due to dislocations and mismatch as well as "stress-free" strain due to varying chemical stoichiometry through the film.

As mentioned in the introduction above, in many cases θ - 2θ measurements do not uniquely determine phase presence and orientation in GaN films. Because the wurtzite and zincblende structures are based on a simple stacking sequence analogous to hcp and fcc packings, the (0002) and (11 $\bar{2}$ 0) planes of wurtzitic GaN films have identical spacings and structure factors as do the (111) and (220) planes of zincblende GaN respectively. Thus if a film grows in one of these orientations, θ - 2θ diffraction scans of these peaks cannot distinguish between the two polymorphs. However the periodicities of the two structures are fundamentally different – the stacking sequence repeats every two planes in wurtzite; every three in zincblende. Thus there are “off-axis” diffraction peaks from planes inclined relative to the substrate which unambiguously belong to either the zincblende or the wurtzite structure. We have examined these to determine the phase contents of the films in this study.

We have also performed measurements to examine the orientational quality of the thin films. Rocking curves of θ around the “on-axis” Bragg peaks were used to examine the orientational spread of the film parallel to the surface normal. The spread of in-plane orientations as well as the epitaxial relationship between substrate and film axes in the plane were determined with ϕ scans, in which the sample was rotated about its normal while θ , 2θ and χ were held fixed at the peak position.

3. Experimental Results:

3.1 GaN on Si

A. GaN on Si(111)

X-ray θ - 2θ scans of films on Si(111) show only two peaks which are indexed as the wurtzite (0002) and/or zincblende (111) and their harmonic. The peak positions yield a d-spacing of 2.59 Å, which is consistent with previous lattice constant measurements

[1]. No other peaks were observed, ruling out the existence of other epitaxial orientations down to the 0.1% level. Since data from only two peaks are available, the separation of the peak widths into domain size and inhomogeneous strain broadening using Eq. (1) has limited accuracy. However the theta FWHM of the fundamental peak and its harmonic are 0.08° and 0.19° respectively, implying that the dominant contribution to the widths comes from an inhomogeneous strain of approximately 0.2%. The grain size estimated from the peak widths is resolution limited, so that the coherent domain size must be larger than approximately 1500 Å.

In order to better investigate the polymorph content of the film, separate diffraction scans were performed in the [0001] direction through the wurtzite ($10\bar{1}l$), ($1\bar{1}0l$) and ($11\bar{2}l$) reciprocal lattice points (Figures 2 and 3 show the scan through the ($10\bar{1}l$) peaks). The scans show that there are significant components of both wurtzite and zincblende phases in the materials. The zincblende further exists equally in its two twins corresponding to ABCABC... and CBACBA... packing. The relative heights of the zincblende and wurtzite peaks suggests that approximately 25% of the film is zincblende and the remainder is wurtzite. The in-plane orientation between the two polymorphs is wurtzite $[10\bar{1}0] \parallel$ zincblende $[1\bar{1}0]$, which is the orientation required in order for the close-packed planes of the two polymorphs to be in registry. It is noteworthy that earlier reports [17] of wurtzite formation on Si (111) could not distinguish between wurtzite and zincblende structures, so that similar polymorph coexistence may have been present there as well.

It is possible that the zincblende and wurtzite phases nucleate independently on the substrate. However, in cobalt and silicon carbide [18] it is known that the two analogous hcp and fcc polymorphs can nucleate each other at stacking faults on the close-packed planes. Moreover, twinning in metallic crystals as well as in CdTe [19] films can occur in the same way. It is therefore possible that the coexistence of the two polymorphs and of the two zincblende twins in the GaN films may be related to the presence of stacking faults. While it is difficult to definitively confirm this with x-ray diffraction, TEM studies

[21] performed after our initial reports of these results [22] have shown conclusively that wurtzite and zincblende polymorphs do nucleate each other at stacking faults in InN films.

Within each of the two phases, however, the occurrence of stacking faults *can* be examined with x-ray diffraction [20]. The faults formed during the growth process here occur mostly on the close-packed plane parallel to the substrate, i.e. the growth plane of wurtzite (0002) and zincblende (111). Therefore the on-axis wurtzite (0002) and zincblende (111) peaks themselves are insensitive to stacking faults since they represent Fourier density components perpendicular to the stacking planes. However, faults do affect certain off-axis diffraction peaks from planes inclined relative to the surface [20]. In the wurtzite structure, those diffraction peaks ($hk.l$) with $(h - k) \neq 3n$, where n is an integer, are broadened by faulting so that the FWHM of a Bragg peak for diffraction scans along the [0001] direction is

$$\delta k = \frac{2\pi}{D} + \epsilon_{in}k + \frac{2(3\alpha + 3\beta)}{c} \quad (3)$$

for even l and

$$\delta k = \frac{2\pi}{D} + \epsilon_{in}k + \frac{2(3\alpha + \beta)}{c} \quad (4)$$

for odd l . Here we assume that the predominant faults in the material are deformation faults (...ABAB|CACA...) and growth faults (...ABAB|CBCB...) with probabilities α and β of occurring in a given plane respectively, and c is the c -axis lattice constant. Measurements of the peak widths of the (10 $\bar{1}$ 3) and (10 $\bar{1}$ 4) peaks show that they both have an excess width associated with faulting of approximately 0.007 reciprocal lattice units ($2\pi/c$). Thus the dominant faults appear to be the deformation faults with $\alpha \sim 0.007$ and the distance between faults is approximately $c/\alpha \sim 800\text{\AA}$.

It is more difficult to measure faulting densities accurately from the lower intensity zincblende peaks. Those diffraction peaks (hkl) with $(-h+2k-l) \neq 6n$ would be broadened and shifted by faulting [20]. If we assume that the predominant faults are deformation faults (...ABC|BCA...) with probability γ on a given plane and twin faults (...ABCBA...)

with probability ζ , then the FWHM of a Bragg peak affected by faulting for scans in the [0001] direction is

$$\delta k = \frac{2\pi}{D} + \epsilon_{in}k + \frac{\sqrt{3}(3\gamma + 2\zeta)}{a}. \quad (5)$$

Peak positions are shifted by $\pm 3\gamma/4\pi$ reciprocal lattice units ($2\pi/a$), where a is the cubic lattice constant. The lack of shifting and excess broadening in the zincblende peaks measured with the high flux low resolution graphite monochromator limits the faulting probabilities to $\gamma, \zeta < 0.005$. The distance between faults must therefore be greater than 600 Å in the zincblende material.

In addition to the peaks which can be indexed to the wurtzite and zincblende structures, there is a very small peak not belonging to these two phases in the $(11\bar{2}l)$ and $(1\bar{1}0l)$ scans at $l = 1.66$ reciprocal lattice units. The position of a peak at a nonintegral l value suggests that it could be due to a larger superstructure. Polytypes with long repeat periods are well known in the silicon carbide system [18]. However, no other peaks attributable to a long-period polytype are observed and calculations suggest that polytypes would not have a strong reflection at this position. The origin of the peak therefore remains unclear.

The orientational quality of the films normal to the substrate was examined with θ rocking curves at the wurtzite (0002)/zincblende (111) peak. The FWHM of the rocking curve, which is a direct measure of the orientational spread of grains around the surface normal, is 0.9° . The orientational quality parallel to the substrate was measured with ϕ scans at the wurtzite $(1\bar{1}02)$ and zincblende $(\bar{1}11)$ reflections. The dominant peak in the wurtzite $(1\bar{1}02)$ scan has the sixfold symmetry expected from the hexagonal structure (see Fig. 4). However, very small peaks with slightly less than 1% of the intensity of the dominant peaks were observed at $\phi=30^\circ$ and $\phi=90^\circ$. These indicate that a small fraction of the domains have an in-plane orientation which differs by 30° from the bulk of the wurtzite component. Phi scans of the zincblende $(\bar{1}11)$ show that these 30° misoriented domains exist in that polymorph as well (see Fig. 5). The in-plane orientational spread of the wurtzite film component is 1.9° , twice as large as the out-of-plane orientational spread.

The epitaxial in-plane orientation is $\text{GaN}[11\bar{2}0] \parallel \text{Si}[\bar{1}10]$. This is the same orientation as found in earlier growth studies [17].

B. GaN on Si(001)

We have previously reported the results of θ - 2θ scans and rocking curves of GaN films on Si(001) substrates [11,12]. The dominant peaks in the θ - 2θ scans are indexed to zincblende (002) and (004). The large widths of the two peaks, 0.40° and 0.72° respectively, indicate a higher inhomogeneous strain and a smaller domain size than occurs on the Si(111) substrate. Application of Eq. (1) yields an approximate inhomogeneous strain of 0.6% and an effective domain size of 500 Å.

In addition to the dominant zincblende (002) peak and its harmonic, the θ - 2θ scan shows a small peak at the position corresponding to zincblende (111) and/or wurtzite (0002) orientations. Thus approximately 1% of the film has this orientation. Transmission electron microscopy has shown that this component develops in the early stage of the buffer layer deposition.

The rocking curve of the (002) peak is 1.6° wide – much broader than that of GaN on Si(111). The in-plane orientational order of the dominant zincblende (001) phase was examined with a ϕ scan of the (111) reflection. It shows a fourfold rotational symmetry with a spread of approximately 2.5° about the maxima. The ϕ scans show also that the epitaxial relationship between film and substrate is $\text{GaN}(100) \parallel \text{Si}(100)$.

In order to explore the existence of wurtzite and of stacking faults in the films, we have also performed a series of scans in the [111] and equivalent close-packed directions. Figure 6 shows such a scan from the (002) reciprocal lattice point to the (111) point. The size of the wurtzite peaks indicates that approximately 10% of the material is in that phase. However, twinning of the zincblende in the film is quite small – approximately 1% of the zincblende material is in the minor twin orientation. This suggests that one twin grows preferentially at the substrate interface and its orientation is maintained throughout the bulk of the film. :

Together, Fig. 6 and scans perpendicular to it show that the faulting density in the film is so high that the Bragg peak intensities are spread into a streak along the close-packed direction; the background on which this streak sits is only two on the scale of the figure. Scans along the other three equivalent [111] cubic directions show a similar behavior. Thus the material has a very high density of stacking faults on all four sets of zincblende close-packed planes, which are inclined at 54.74° relative to the growth plane of (001). In Fig. 6, the wurtzite (10 $\bar{1}$ 0) peak has approximately twice the width (0.19 wurtzite reciprocal lattice units) of the (10 $\bar{1}$ 1) peak (0.095 wurtzite reciprocal lattice units). If we assume that the average domain size of the wurtzite is much larger than the distance between stacking faults, then application of Eqs. 3 and 4 yields values of $\alpha \sim 0.05$ and $\beta \sim 0.15$. Thus the wurtzite material is indeed highly faulted - there are stacking faults every few unit cells! As Fig. 6 shows, the zincblende peaks are all much narrower than the wurtzite peaks. Their small width implies that the distance between stacking faults in the zincblende polymorph is at least 500 Å.

3.2. GaN on Sapphire Substrates

A. GaN on basal-plane sapphire

As was the case with the Si(111) substrate, the θ - 2θ scan of the GaN film on basal-plane sapphire shows two dominant peaks which correspond to wurtzite (0002) and/or to zincblende (111) and their harmonic. The widths of the two peaks are 0.06° and 0.11° , from which the grain size is estimated to be greater than 1500 Å and the homogeneous strain to be approximately 0.8%.

In order to further examine the polymorph content of the film, we also searched for ($\bar{1}$ 11) reflections of (111) oriented zincblende grains. In contrast to the case for GaN grown on Si(111), however, there is no zincblende (111) intensity down to the 10^{-4} level.

The θ -rocking curve of the film (0002) peak has a FWHM of 0.4° . This is comparable to that observed by Sasaki and Zembutsu [22] in films grown with MOCVD and by Shintani

et al. [23] using HVPE, but significantly smaller than that in MOCVD films grown on AlN buffers by Amano *et al.* [9]. Phi scans at the off-axis ($1\bar{1}02$) wurtzite reflection of GaN display the dominant reflection peak as ϕ rotates every 60 degrees, a result of the 6/m symmetry of the rotation axis, as is in the case on Si(111). However, here no in-plane misoriented domains were observed. The in-plane orientational spread is 0.8° , about twice as large as the out-of-plane orientational spread. The in-plane orientation of the film is found to be GaN ($11\bar{2}0$) || sapphire ($1\bar{1}00$). This is in agreement with previous reports on GaN films on basal-plane sapphire grown by a variety of techniques [3,4,5,6,24]. The lattice mismatch between GaN and the basal plane of the sapphire hexagonal unit cell is over 30%. However, as noted by Kosicki and Kahng [4], the mismatch is significantly less ($\sim 15\%$) between the wurtzite basal plane unit cell and a smaller hexagonal cell within the sapphire unit cell. The smaller cell of Al atoms on the basal-plane sapphire is oriented 30° away from the larger sapphire unit cell, in agreement with the GaN orientation found experimentally. Figure 7 shows that this epitaxial orientation gives relatively good agreement between the bulk atomic positions of Al atoms in the sapphire and Ga atoms in the film.

B. GaN on a-plane sapphire

As is the case for GaN grown on Si(111) and basal-plane sapphire, θ - 2θ scans of GaN film on a-plane sapphire show peaks corresponding well to previously published values of the wurtzite (0002) interplanar spacing. The FWHM of the two peaks are 0.06° and 0.11° , the same as those for GaN on c-plane sapphire, so that the grain size and inhomogeneous stress are similar. The off-axis zincblende ($\bar{1}11$) peak was examined to measure the percentage of (111) oriented cubic phase present. The peak's intensity suggests that approximately 1% of the material has the zincblende structure. A previous examination by Wickenden *et al.* [24] of GaN films deposited by vapor phase epitaxy had reported only the growth of wurtzitic material. It is unclear, however, that the study could distinguish between the wurtzite and zincblende polymorphs.

Although the domain size and inhomogeneous strains of the GaN films grown on a-

plane sapphire are similar to those for films grown on basal-plane sapphire, the θ -rocking curve of the film on a-plane sapphire has a FWHM of 0.6° , 50% larger than that of GaN on basal-plane material. Phi scans at the off-axis wurtzite ($1\bar{1}02$) reflection show no in-plane misoriented domains, as is the case with basal-plane sapphire. However, the in-plane orientational spread here is significantly larger - 1.4° . The in-plane epitaxial relationship was found to be GaN $[11\bar{2}0] \parallel$ sapphire $[1\bar{1}00]$. As Wickenden *et al.* [24] point out, in this orientation the bulk positions of the substrate and film cations lie along lines in the sapphire $[0001]$ direction (see Fig. 8). The mismatch between the substrate and film row spacings is only $\sim 0.7\%$, although many of the substrate and film cation positions do not show a good correspondence.

C. GaN on r-plane sapphire

When θ was aligned with respect to the GaN reflection, θ - 2θ scans from films grown on r-plane sapphire showed only a peak which can be indexed to the wurtzite ($11\bar{2}0$) or zincblende (110) reflections. No peak from the sapphire substrate was observed. However, when θ was aligned with respect to the substrate reflection, the scan showed only the sapphire ($2\bar{2}04$) peak. Thus the film planes are not exactly parallel to the ($1\bar{1}02$) planes of the sapphire substrate. By varying ϕ , it was found that the misorientation is approximately 1.5° and is along the GaN $[0001]$ direction. In order to better measure the phase content of the films, we examined the zincblende (111) off-axis peak. From its peak intensity, we estimate that only $\sim 1\%$ of the material is in the zincblende phase; the majority is wurtzite. Again, previous studies have reported only the growth of wurtzitic GaN on r-plane sapphire [3,5,22], but it is unclear that they had the ability distinguish between the two polymorphs.

The FWHM of the θ rocking curve at the on-axis peak is 0.6° . This is comparable to values reported by Sasaki and Zembutsu [22] on films grown by MOCVD. In order to examine the in-plane orientation, a ϕ scan was performed at the wurtzite ($1\bar{1}00$) reflection.

The scan shows a repetition every 180° in ϕ , which is a result of the 2-fold symmetry of a-plane GaN. The in-plane orientational spread is 6.7° , the largest for all of the GaN films. Phi scans show that the in-plane orientations between the two film polymorphs and the substrate are wurtzite (0002) \parallel sapphire ($1\bar{1}01$) \parallel zincblende ($1\bar{1}1$). The wurtzite epitaxial orientation is the same as that found in previous reports of films grown on r-plane sapphire [3,5,22]. Surface studies have found that corundum r-plane surfaces are quite stable and evidently do not significantly reconstruct [26]. It is therefore interesting to note the good agreement between bulk substrate and film cation positions in the experimental epitaxial orientation, as Fig. 9 shows. The lattice mismatch is only 1.3% in the sapphire [$\bar{1}101$] direction, although it is $\sim 15\%$ in the [$11\bar{2}0$] direction. The particularly small mismatch in the sapphire [$\bar{1}101$] direction may be responsible for the small tilt between the GaN planes in the film and the substrate planes. Since the film axis in this direction is slightly longer than that of the substrate, the film planes may tilt up slightly in order to better match the projection of the GaN unit cells onto the interface with the sapphire unit cells below. Because of the two-fold rotational symmetry of the sapphire r-plane unit cell, however, it is unclear why film domains grow with a misalignment in only one of the two possible directions. An alternate possibility is that the film tilt is related to a miscut of the substrate wafer. However, the tilt was observed in several films and was always oriented along the sapphire [$\bar{1}101$] direction.

4. Discussion and Conclusions:

The results of our four-circle x-ray diffractometry suggest that the coexistence of wurtzite and zincblende polymorphs in GaN thin films may be widespread. As discussed above, most previous studies would not have been able to distinguish between the two, especially if one polymorph exists only at the 1% level. Since the two have different bandgaps and possibly different doping capabilities, it is imperative that future investigators interested in optical and transport properties also evaluate their films' phase content. For this

purpose x-ray or electron diffraction measurements of off-axis Bragg peaks are both suitable, but x-ray diffraction may have somewhat greater sensitivity to small volume fractions and it requires no sample thinning.

To our knowledge, these are the first experiments which have examined the orientational quality of GaN films in the film plane. On all of the films, the range of orientation angles in the plane is 1.5 to 10 times larger than along the film normal. In-plane misorientations between domains may therefore be the more important in creating domain boundary recombination sites due to broken bonds.

It is noteworthy that the measured film lattice constants in this work are all equal to accepted literature values to within experimental error. Since the lattice parameter is sensitive to the nitrogen concentration [27], this implies that the films' compositions are not too far off stoichiometry. We have, however, observed significant variations in GaN lattice parameters with varying growth temperature which we attribute partly to the formation of large numbers of nitrogen vacancies [28]. It is widely believed that such nitrogen vacancies autodope films n-type [1]. The agreement between previously reported lattice constants and those observed here also suggests that the interfacial strain in the films relaxes on length scales significantly smaller than the film thickness. Given the large mismatches present between substrate and film, this is not surprising. For GaN on Si(111) and Si(001) substrates the lattice mismatch is $\delta=21\%$. As Figs. 7-9 show, however, films grown on sapphire orient themselves to match the bulk atomic positions of the film and substrate and decrease the effective lattice mismatch below the values for epitaxy on silicon. We note that, in fact, the GaN films do not grow directly on the sapphire substrate surfaces, but rather on very thin AlN layers which grow during the substrate N_2 plasma cleaning process [13]. However, the AlN lattice constant is quite close to that of GaN (3.11 Å versus 3.19 Å) and our RHEED measurements indicate that the AlN has the same orientation as does the GaN film which grows on top of it. Unfortunately the detailed structure of the interface is unknown so the importance of matching bulk atomic positions in the early

stages of film growth is unclear. Despite the reasonably good match of cation positions in the GaN films grown on r-plane sapphire, the orientational spread in the film plane is quite large. Clearly a better understanding of the early growth kinetics and of the interfacial structure would be quite helpful in explaining the epitaxial relationship between film and substrate.

The dominant mechanisms causing the inhomogeneous strains measured in these materials is unclear. Since the films appear to relax quickly to their bulk lattice parameter and are relatively thick, it is unlikely that ϵ_{in} could be dominated by misfit stresses from the substrate interface. However, dislocations introduced to relieve the lattice mismatch could create microstresses which would cause local variations in the lattice constant. While we know of no experimental work relating the GaN bandgap to the lattice parameter, LCAO calculations suggest that the energy matrix elements V which determine the bandgap vary as the inverse square of the separation between atoms [29]. Therefore $\delta V/V = 2\delta d/d$, and a 1% inhomogeneous strain would lead to approximately a 2% variation of the bandgap. This then could be a significant source of band tailing. Nitrogen vacancies would presumably be the principal mechanism contributing "stress-free" strain due to composition inhomogeneity. While a decrease in nitrogen stoichiometry significantly decreases the wurtzite lattice parameters [27], we know of no quantitative data relating stoichiometry and lattice constants which would allow us to interpret the inhomogeneous strain in terms of nitrogen deficiencies.

All of the films except those on Si(001) have domain sizes along the surface normal which are larger than our instrumental resolution. The very large stacking fault density in GaN films on Si(001) along with their large spread of in- and out-of-plane orientation angles and relatively large inhomogeneous strain suggest that, structurally, these are the worst films overall. The very large spread of in-plane orientations in the films on r-plane sapphire also implies that there are domain boundaries within the film with a relatively large angle of mismatch. In terms of orientation quality and domain size, then, the best

films appear to be those which grow on their close-packed planes. The films on sapphire (0002) substrates are the best of these, with relatively small in- and out-of-plane misorientation and little secondary phase. Despite their orientational quality, however, it appears likely that stacking faults are common in all of the GaN films. The impact of stacking faults on carrier mobility is unclear. Away from fault edges, their main effect will likely be to cause a local variation in the bandgap. At the fault edges, however, bonds will be broken, producing deep states in the gap. Clearly significant work is required in order to examine the relationship between stacking fault density and electrical properties and to develop approaches which minimize the formation of faults in the growth process.

Acknowledgments

We would like to thank G. Morales and Y. Xie for their help with the x-ray measurements. This work was supported by the Office of Naval Research (Grant No. N00014-92-J-1436).

References

1. R. F. Davis, Proceedings of the IEEE., V. 79, No. 5, 702(1991); R. F. Davis, Z. Sitar, B. E. Williams, H. S. Kong, H. J. Kim, J. W. Palmour, J. A. Edmond, J. Ryu, J. T. Glass and C. H. Carter, Jr., Mat. Sci. & Eng. **B1**, 77(1988).
2. J. I. Pankove, MRS Symposium Proceedings, Vol. 162, 515(1990).
3. M. Sano and M. Aoki, Jap. J. App. Phys. **15**, 1943 (1976).
4. B.B. Kosicki and D. Kahng, J. Vac. Sci. and Tech. **6**, 593 (1969).
5. S. Yoshida, S. Misawa and S. Gonda, J. Appl. Phys. **53**, 6844 (1982).
6. S. Yoshida, S. Misawa and S. Gonda, Appl. Phys. Lett. **42**, 427 (1983).
7. Z. Sitar, M.J. Paisley, B. Yan and R.F. Davis, Mat. Res. Soc. Symp. Proc. **162**, 531 (1990).
8. T.P. Humphreys, C.A. Sukow, R.J. Nemanich, J.B. Posthill, R.A. Rudder, S.V. Hattangady and R.J. Markunas, Mat. Res. Soc. Symp. Proc. **162**, 531 (1990).
9. H. Amano, N. Sawaki, I. Akasaki and Y. Toyoda, Appl. Phys. Lett. **48**, 353 (1986); I. Akasaki and H. Amano, Mat. Res. Soc. Symp. Proc. **242**, 383 (1992).
10. T. Lei, M. Fanciulli, R. J. Molnar, T. D. Moustakas, R. J. Graham and J. Scanlon, Appl. Phys. Lett. **59**, 944 (1991).
11. T. Lei, T. D. Moustakas, R. J. Graham, S. J. Berkowitz and Y. He, J. Appl. Phys. **71**, 4933(1992).
12. T. Lei, T. D. Moustakas, Mat. Res. Soc. Symp. Proc. **242**, 433 (1992).
13. T. D. Moustakas, R. J. Molnar, T. Lei, G. Menon and C. R. Eddy, Jr., Mat. Res. Soc. Symp. Proc. **242**, 427 (1992).
14. T. Lei and T. Moustakas, to be published.
15. W. R. Busing and H. A. Levy, Acta Cryst. **22**, 457(1967).

16. R.W. Vook, in *Epitaxial Growth*, ed. J.W. Matthews (Academic Press, New York, 1975), 339.
17. Y. Morimoto, K. Uchiho and S. Ushio, *J. Electrochem. Soc. Solid-State Sci. and Tech.* **120**, 1783 (1973).
18. R.W.G. Wyckoff, *Crystal Structures, Vol. 1* (Interscience, New York, 1963), 111.
19. R.D. Horning and J.-L. Staudenmann, *Appl. Phys. Lett.* **49**, 1590 (1986).
20. B.E. Warren, *X-ray Diffraction* (Addison-Wesley, Reading, 1969).
21. S. Strite, D. Chandrasekhar, D.J. Smith, J. Sariel, H. Chen, N. Teraguchi, and H. Morkoc, preprint.
22. T.D. Moustakas, T. Lei and R.J. Molnar, *Physica B* **185**, 36 (1993).
23. T. Sasaki and S. Zembutsu, *J. Appl. Phys.* **61**, 2533 (1987).
24. H. Shintane, Y. Takano, S. Minagawa and M. Mari, *J. Electrochem. Soc.* **125**, 2076 (1978).
25. D.K. Wickenden, K.R. Faulkner, R.W. Brander and B.J. Isherwood, *J. Cryst. Growth* **9**, 158 (1971).
26. V.E. Henrich, *Rep. Prog. Phys.* **48**, 1481 (1985).
27. O. Lagerstedt and B. Monemar, *Phys. Rev. B* **19**, 3064 (1979).
28. C.R. Eddy, Jr., T.D. Moustakas and J. Scanlon, *J. Appl. Phys.* **73**, 448 (1993).
29. W.A. Harrison, *Electronic Structure and the Properties of Solids* (W.H. Freeman, San Francisco, 1980), 149.

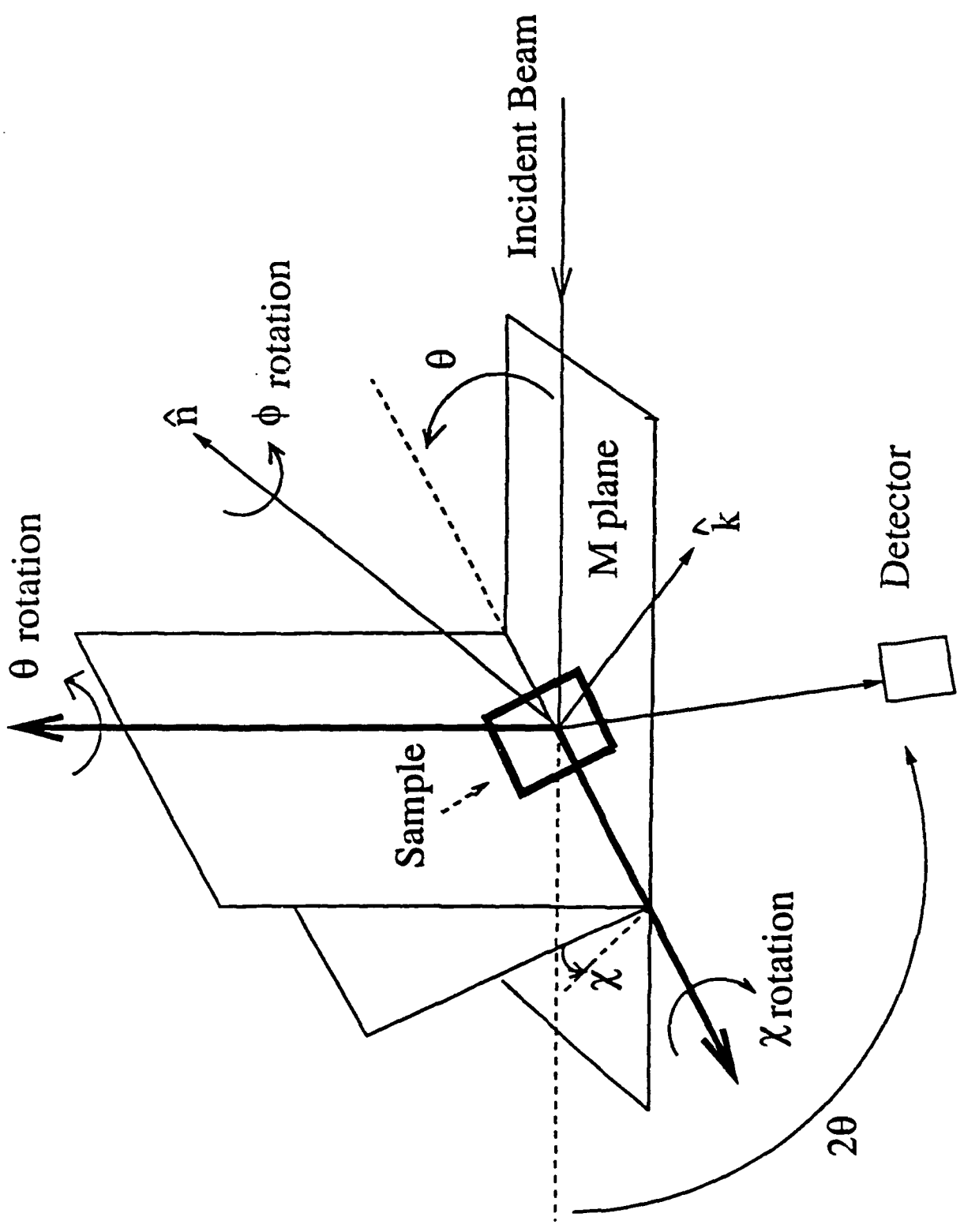
Figure Captions

1. Schematic of the Eulerian four-circle diffraction geometry.
2. Schematic of reciprocal space showing a scan along the $[10\bar{1}l]$ direction. The dots are allowed wurtzite reflections and the triangles show the allowed zincblende reflections for each of the two twins (primed and unprimed). The off-axis zincblende reflections are labelled with respect to the cubic cell, but the graph units are wurtzite reciprocal lattice units (r.l.u.).
3. A diffraction scan along the wurtzite $[10\bar{1}l]$ direction. The l reciprocal lattice unit values refer to the wurtzite c -axis and the wurtzite and zincblende peaks are labeled. The origin of the small peak at 2.66 r.l.u. is unclear.
4. A ϕ scan at the wurtzite $(1\bar{1}02)$ peak for a film on Si(111).
5. A ϕ scan at the zincblende $(\bar{1}11)$ peak for a film on Si(111).
6. A scan along the $[11\bar{1}]$ direction from the (002) peak to the (111) peak for a film grown on Si(100). The stacking fault density is sufficiently high that the Bragg peak intensity is smeared into a streak in this direction (the background to the streak is approximately 2 on this scale). The x -axis refers to the l component of the scan and is in reciprocal lattice units referenced to the zincblende lattice constant. Peaks due to the two zincblende twins (primed and unprimed) and to the wurtzite polymorph are indicated.
7. Projection of bulk basal-plane sapphire and GaN cation positions for the observed epitaxial growth orientation. The dots mark aluminum atom positions and the dashed lines show the sapphire basal-plane unit cells. The open squares mark gallium atom positions and the solid lines show the GaN basal-plane unit cells. The aluminum atoms on the sapphire plane sit at positions approximately 0.5 Å above and below the plane position.
8. Projection of bulk a -plane sapphire and basal-plane GaN cation positions for the

observed epitaxial growth orientation. The dots mark aluminum atom positions and the dashed lines show the sapphire a-plane unit cell. The open squares mark gallium atom positions and the solid lines show the GaN basal-plane unit cells.

9. Projection of bulk r-plane sapphire and a-plane GaN cation positions for the observed epitaxial growth orientation. The dots mark aluminum atom positions and the dashed lines show the sapphire r-plane unit cell. The open squares mark gallium atom positions and the solid lines show the GaN a-plane unit cells.

Figure 1



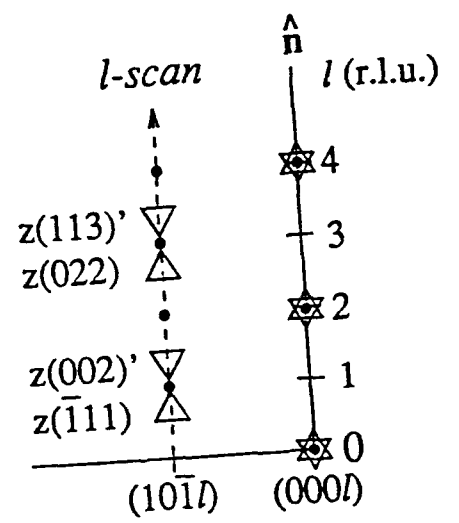


Figure 2

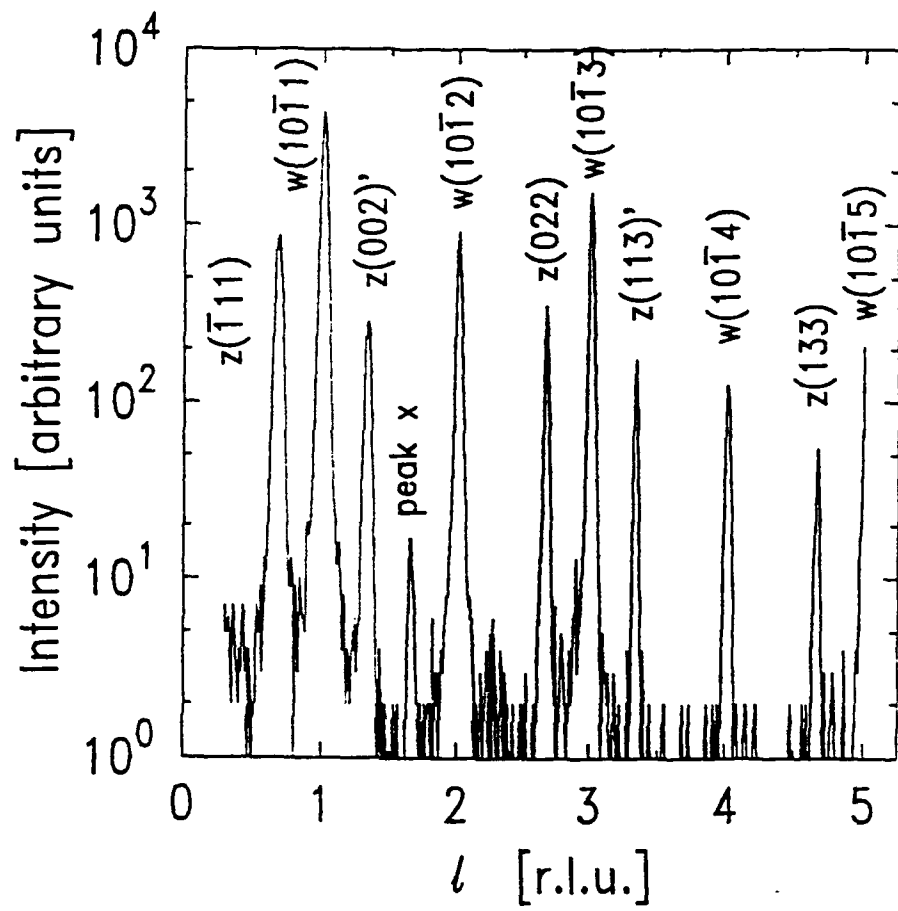


Figure 3

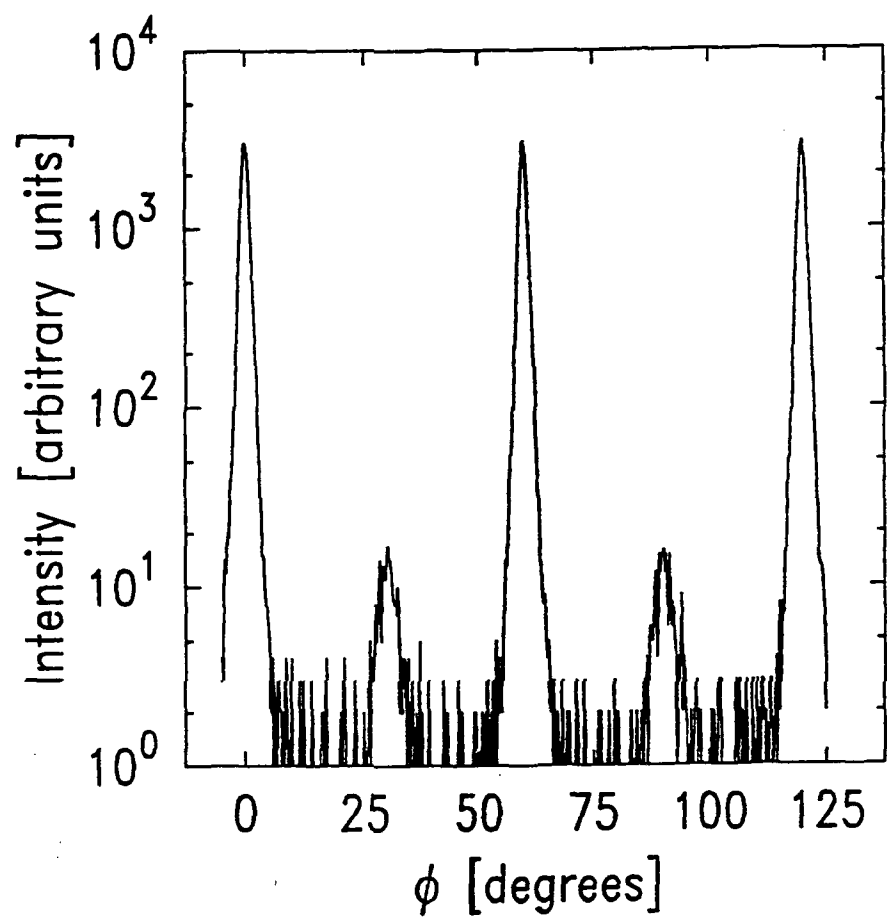


Figure 4

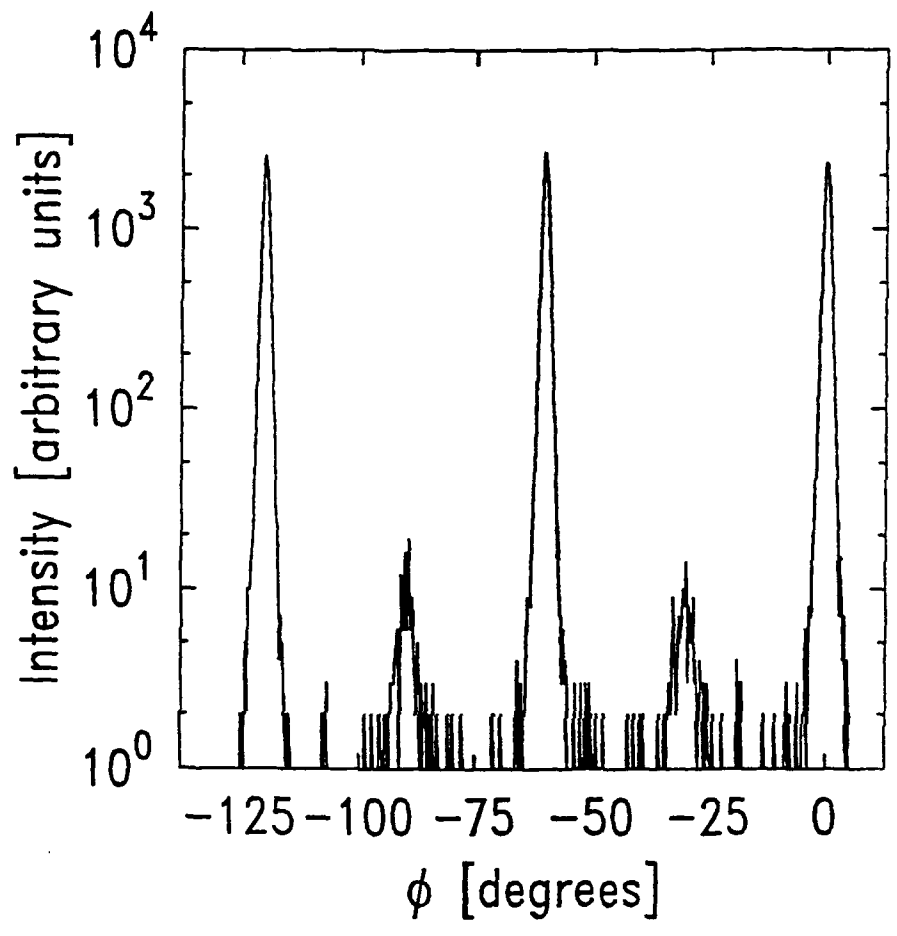


Figure 5

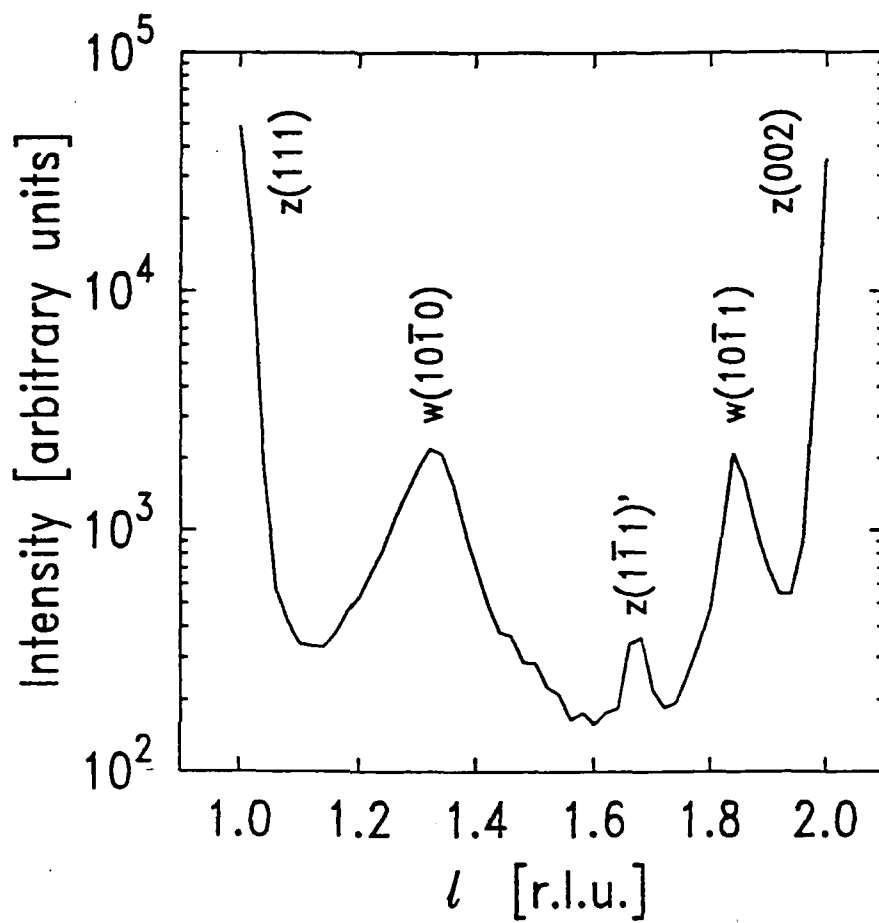


Figure 6

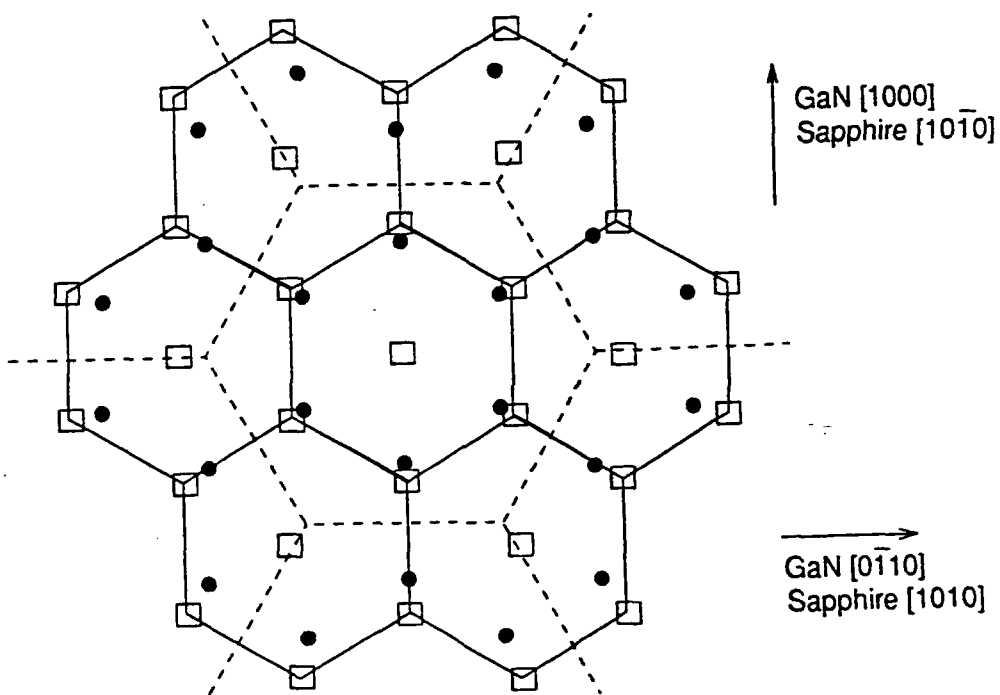


Figure 7

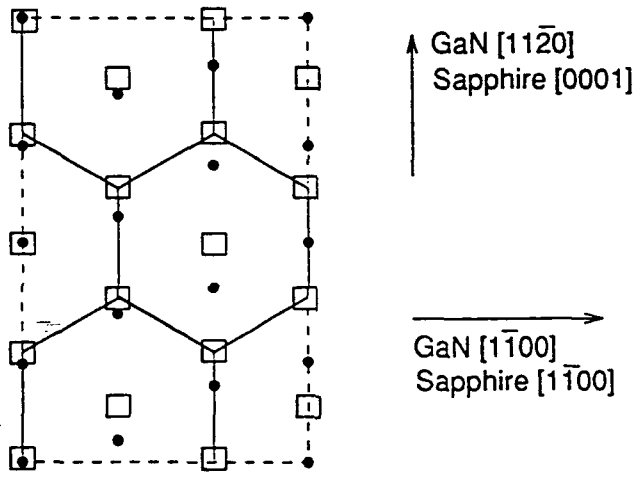


Figure 8

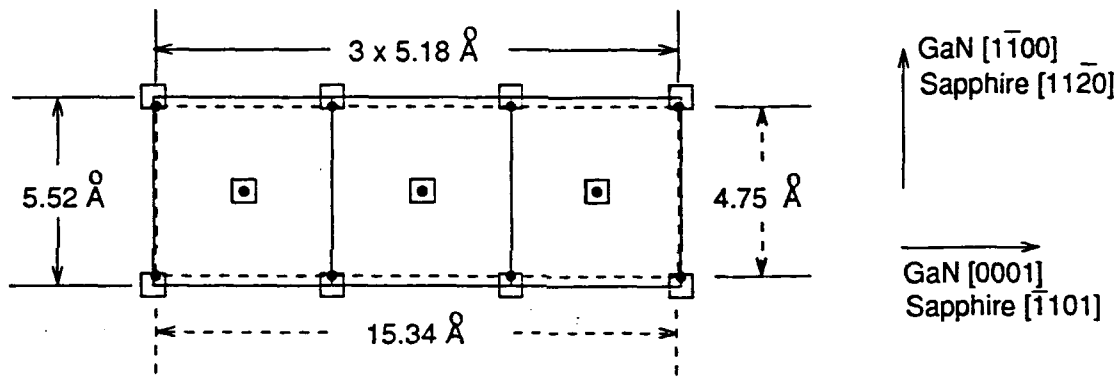


Figure 9

Appendix G:

Conduction Electron Spin Resonance in Zinc-Blende GaN Thin Films
Submitted to *Physical Review B*.

Conduction Electron Spin Resonance in Zinc-Blende GaN Thin Films

M. Fanciulli⁽¹⁾, T. Lei⁽¹⁾ and T.D. Moustakas ^(1,2)

⁽¹⁾ Department of Physics

⁽²⁾ Department of Electrical, Computer and Systems Engineering
Boston University, Boston MA 02215.

We report for the first time electron spin resonance measurements on zinc-blende GaN. The observed resonance has an isotropic g -value of 1.9533 ± 0.0008 independent of temperature, a Lorentzian line shape and a line width which increases with temperature. The spin lattice relaxation time at 10 K was estimated to be $T_{1e} = (2.0 \pm 0.8) \cdot 10^{-5}$ sec. Using a five-band model a conduction electron effective mass ($m^*/m_0 = 0.15 \pm 0.01$) and a g -value consistent with the experimental results were obtained. The observed signal, together with conductivity data, was attributed to non-localized electrons in a band of auto-doping centers and in the conduction band.

PACS numbers: 76.30.Pk, 71.25.Jd, 71.55.Eq

1. Introduction. Gallium Nitride is a wide band gap semiconductor which is anticipated to find applications for optical devices (LED's, lasers, detectors) in the near U.V. region of the electromagnetic spectrum and electronic devices for high power, high frequency and high temperature applications. GaN was found to exist in two allotropic forms. The wurtzitic structure is the thermodynamically stable phase and has an optical gap of 3.5 eV [1,2], while the zinc-blende structure is a metastable phase which can be formed by epitaxial stabilization [3,4] and has an optical gap of 3.2 eV [4]. In both cases the material is found to be heavily auto-doped n-type, a result attributed to nitrogen vacancies [5]. In general the electron concentration is in the range

of 10^{17} - 10^{20} cm^{-3} .

In this paper we report for the first time electron spin resonance (ESR) studies in auto-doped n-type zinc-blende GaN thin films. The data were correlated with electrical conductivity measurements and from their analysis the nature of the resonance and the conduction electron effective mass were determined.

2. Experimental Results. The GaN films were grown by Electron Cyclotron Resonance microwave plasma assisted Molecular Beam Epitaxy (ECR-MBE). Epitaxial stabilization of the zinc-blende structure was accomplished by using a two temperature step process on Si (100). In this process a 200 Å GaN buffer was grown at 400°C and the rest of the film, $4\mu\text{m}$ thick, was grown at 600°C . Both heavily auto-doped and semi-insulating GaN films were fabricated and investigated. Transport studies in these films [6] show that the conductivity is dominated by the high quality top layer rather than by the GaN buffer. Details on the growth are given elsewhere [3,4]. Structural studies (RHEED, electron diffraction and XRD) show that the films are single crystals having the zinc-blende structure with lattice constant 4.5 \AA [3,4].

To conduct optical, transport and spin resonance measurements self standing GaN flakes were obtained by dissolving the Si substrate with a solution of HNO_3 and HF. The optical gap of the films was determined by transmission measurements and found to be 3.2 eV [4]. The electrical resistivity of one of the investigated films, determined by four probe measurements using sputtered Al contacts, is shown as a function of $1/T$ in figure 1.

ESR measurements were performed at different temperatures in a Varian E9 spectrometer at 9.3 GHz, 100 KHz modulation frequency and 0.5-1.0 G modulation amplitude. A α, α' -diphenyl- β -picrylhydrazyl (DPPH) reference was used to evaluate the g-value and the spin concentration. Figure 2 shows the ESR spectrum at 10 K of the same sample discussed in figure 1. This resonance has an isotropic g-value of 1.9533 ± 0.0008 independent of temperature. The shape of the line is Lorentzian and

the peak to peak line-width ($\Delta H_{pp} = 18 \pm 1$ G at 10 K) has a temperature dependence shown in figure 3. Similar behavior has been observed in heavily doped silicon [7]. The broadening of the line with the increase in temperature prevented us of observing the resonance at temperatures higher than 100 K. The concentration of spins was estimated to be $(10 \pm 3) \cdot 10^{17} \text{ cm}^{-3}$ and the intensity of the EPR signal was found to be almost independent of temperature. From the saturation behavior of the resonance we estimated a spin-lattice relaxation time, at 10 K, of $(2.0 \pm 0.8) \cdot 10^{-5}$ sec. The ESR signal was not observed in semi-insulating GaN films.

2. *Discussion.* The temperature dependence of the resistivity, in figure 1, is consistent with transport in the conduction band at high temperatures (> 100 K) and transport in the band of the auto-doping centers at lower temperatures (< 50 K) as recently discussed in another paper [6]. From these data an activation energy for the auto-doping centers of 20 meV was evaluated and by comparison with our previous analysis [6] the concentration of these centers was estimated to be $10^{17} - 10^{18} \text{ cm}^{-3}$. Thus the electron wavefunctions overlap and form a band. Similar temperature dependence of the resistivity has been observed for impurity conduction in many semiconductors [8].

Tight binding calculations by Jenkins and Dow [9] show that the neutral unrelaxed N vacancy is a shallow donor with its singly occupied p-like level (T_2) in the conduction band and its doubly occupied s-like level (A_1) in the band gap close to the conduction band edge. It is anticipated that lattice distortion should pull the singly occupied level down in the energy gap. Our experimental results, interpreted in this model, put the p-like level 20 meV below the conduction band edge. The level is sufficiently shallow to apply the hydrogenic model and calculate the conduction electron effective mass

$$E = 13.6 \frac{m^*}{m_0 \epsilon^2} \quad (1)$$

In polar materials there is an ambiguity concerning whether the high frequency (ϵ_∞) or the low frequency (ϵ_0) dielectric constant should be used in eq.(1). The criterion is that

ϵ_0 should be used if $E \ll h\nu_{TO}$, while ϵ_∞ should be used in the opposite case [10]. In our case since $E = 20$ meV and $h\nu_{TO} = 68.9$ meV [11] ϵ_0 should be used. From eq.(1) with $\epsilon_0 = 10 \pm 0.5$ [12], we obtain an electron effective mass $m^*/m_0 = 0.14 \pm 0.02$. The polaron correction is small and would increase the value to $m^*/m_0 = 0.15 \pm 0.02$.

To discuss the nature of the observed resonance we should first rule out that such signal is not due to either plasma resonance or cyclotron resonance. Plasma resonance is ruled out based on Dresselhaus et al. prediction [13] that the resonance moves to lower magnetic field as the frequency is increased. To test this we varied the microwave frequency in our experiment from 9.3 GHz to 9.5 GHz and observed that the resonance moved to higher magnetic field instead. Electron cyclotron resonance also is ruled out since from the previously calculated effective mass the resonance should occur at a magnetic field ~ 7 times smaller than it was actually observed.

The following findings provide evidence that the observed ESR signal is due to electrons predominantly in the band of the auto-doping centers at low temperatures (< 50 K) and in the conduction band at higher temperatures: a) the intensity of the EPR signal does not satisfy the Curie-Weiss law suggesting that the electrons responsible for the observed resonance are delocalized. b) no hyperfine or super-hyperfine structure, expected for localized electrons, was resolved, c) no resonance was observed for highly resistive films, d) the calculated spin density agrees with the carrier concentration determined from transport measurements, e) the electrical conductivity data define the temperature ranges where transport is dominated by electrons in the band of the auto-doping centers or in the conduction band. The fact that we did not observe a change in the g-value as a function of temperature suggests that, to within the experimental accuracy, the g-value is the same in both bands.

The possible interaction mechanisms responsible for the spin-lattice relaxation rates of conduction electrons have been discussed by several authors [14-16]. As pointed out by Yafet [16] the dominant relaxation process, at least at not too low temperatures

where the spin-current interaction should dominate, is the phonon modulation of the spin-orbit coupling. This mechanism gives the following spin-lattice relaxation rate [16]

$$T_{1e}^{-1} \sim \frac{2}{\pi^{3/2} \hbar} \frac{D^2}{\rho u^2} \left(\frac{2m^* kT}{\hbar^2} \right)^{5/2} \quad (2)$$

where ρ is the density, u the sound velocity and, for a polar semiconductor, $D \sim C f \delta g (\hbar^2 / am^* E_0)$ with C being the deformation potential, f the relative strength of the crystal potential that is odd under inversion, δg the g -shift, a a parameter of the order of the lattice constant and E_0 the optical gap. Using values appropriate to cubic GaN ($\rho = 6.1 \text{ g cm}^{-3}$, $u = 6.9 \cdot 10^3 \text{ ms}^{-1}$, $C \sim 13 \text{ eV}$ [17], $f=1$ [18]) we find $T_{1e} \sim 9 \cdot 10^{-5} \text{ s}$ at 10 K in general agreement with our experimental result. The analysis of the matrix elements which contribute to T_{2e}^{-1} shows the same \vec{k} and \vec{q} dependence as the matrix elements used for T_{1e}^{-1} . Therefore T_{1e} and T_{2e} have the same temperature dependence [16]. This qualitatively accounts for the increase of the resonance line width with temperature, since $\Delta H_{pp} \propto T_{2e}^{-1}$.

It is interesting to compare our experimental results of the electron effective mass and g -value with theoretical predictions based on the five band model [18-21]. According to this model the effective mass and the g -value are given by the expressions

$$\frac{m_0}{m^*} - 1 = \frac{P^2}{3} \left(\frac{3E_0 + 2\Delta_0}{E_0(E_0 + \Delta_0)} - \lambda^2 \frac{3(E'_0 - E_0) - 2\Delta'_0}{(E'_0 - E_0)(E'_0 - E_0 - \Delta'_0)} \right) \quad (3)$$

$$\frac{g^*}{g_e} - 1 = -\frac{P^2}{3} \left(\frac{\Delta_0}{E_0(E_0 + \Delta_0)} + \lambda^2 \frac{\Delta'_0}{(E'_0 - E_0)(E'_0 - E_0 - \Delta'_0)} \right) \quad (4)$$

where $\Delta_0 = \Gamma_{8v} - \Gamma_{7v}$, $\Delta'_0 = \Gamma_{8c} - \Gamma_{7c}$, $E'_0 = \Gamma_{8c} - \Gamma_{8v}$ and according to Chadi et al [20]

$$P^2 = \frac{2}{m_0} |\langle \Gamma_{1c} | p_x | \Gamma_{5c,x} \rangle|^2 \quad (5)$$

$$\lambda^2 P^2 = \frac{2}{m_0} |\langle \Gamma_{1c} | p_x | \Gamma_{5v,x} \rangle|^2 \quad (6)$$

Hermann and Weisbuch [21] presented an estimate of P^2 based on simplified linear

combination of atomic orbitals

$$P_{sst}^2 = \frac{\hbar^2 \eta^2}{a^2 m_0} \left(\frac{(1 - \alpha_p^2)^{1/2} - S}{2(1 - S^2)} \right)^2$$

where α_p is the polarity and S is the overlap term [22] and η is a best fit parameter $\eta = (1.04 \pm 0.07) \cdot 10^3$ [21]. From this expression, with $\alpha_p = 0.63$ [22] and $S = 0.5$ [21] one obtains for GaN $P_{sst}^2 = 2S = 2$ eV. With the following values $E_0 = 3.2$ eV, $\Delta_0 = 0.000 - 0.016$ eV [23], $\Delta'_0 = 0.06 - 0.1$ eV [24], $E_g = 9.0 \pm 0.3$ eV [25], $\lambda^2 = 0.4$ [20], we obtained $m^*/m_0 = 0.15 \pm 0.01$ and $g^* = 1.95 \pm 0.01$ in agreement with our experimental results. The difference in the g-shift between electrons in the band of auto-doping center and electrons in the conduction band is to within the accuracy of the calculation.

3. *Conclusions.* In conclusion we reported the observation for the first time of an electron spin resonance in zinc-blende gallium nitride thin films produced by the Electron Cyclotron Resonance microwave plasma assisted MBE method. The EPR signal was attributed to electrons predominantly in the band of auto-doping centers (N vacancies) at low temperatures and in the conduction band at higher temperatures. The electron g-value was found to be 1.9533 ± 0.0008 . From the saturation behavior of the resonance line a spin-lattice relaxation time of the order of 10^{-5} sec. at 10 K was estimated in general agreement with the theoretical value predicted considering the phonon modulation of the spin-orbit interaction as the relaxation mechanism. The increase of the resonance line width with temperature was interpreted in the same fashion. Using a five-band model and appropriate parameters for GaN an effective mass $m^*/m_0 = 0.15 \pm 0.01$, consistent with the value obtained from electrical measurements, was evaluated and a g-value $g^* = 1.95 \pm 0.01$ in agreement with the experimental value was calculated.

Acknowledgment

This research was supported by the Office of Naval Research (Grant No. N00014-92-J-1436). We are indebted to Prof. Hans Van Willigen of the University Of Massachusetts for the use of the ESR facilities.

References

1. J.I. Pankove, H.P. Maruska and J.E. Berkeyheiser, *Appl. Phys. Lett.* 5, 197 (1970)
2. J.I. Pankove, *Mater. Res. Soc. Symp. Proc.* Vol. 162, 515 (1990)
3. T. Lei, M. Fanciulli, R. Molnar, T.D. Moustakas, R.J. Graham and J. Scanlon, *Appl. Phys. Lett.* 58, 944 (1991)
4. T.Lei, T.D. Moustakas, R.J. Graham, Y.He and S. Berkowitz, *J. Appl. Phys.* 71, 4933 (1992)
5. J.I. Pankove, S. Bloom and G. Harbeke, *RCA Rev.* 36, 163 (1975)
6. R.J. Molnar, T. Lei and T.D. Moustakas, *Appl. Phys. Lett.* 62, 72 (1993)
7. A.M. Portis, A.F. Kip, C. Kittel and W.H. Brattain, *Phys. Rev.* 90, 988 (1953)
8. N.F. Mott and W.D. Twose, *Adv. in Physics* 10, 107 (1961)
9. D.W. Jenkins and J.D. Dow, *Phys. Rev. B* 39, 3317 (1989)
10. B.K. Ridley, *Quantum Processes in Semiconductors*, Oxford University Press, p. 62 (1982)
11. S. Mururgkar, R. Merlin, T. Lei and T.D. Moustakas, *Bull. Am. Phys. Soc.* 37, 556 (1992)
12. A.S. Barker and M. Ilegems, *Phys. Rev. B* 7, 743 (1973)
13. G. Dresselhaus, A.F. Kip and C. Kittel *Phys. Rev.* 100, 618 (1955)
14. A.W. Overhauser, *Phys. Rev.* 89, 689 (1953)

15. R.J. Elliott, *Phys. Rev.* 96, 266 (1954)
16. Y. Yafet, *Solid State Physics* 14, 1 (1963)
17. Estimated from the general trend of other semiconductors.
18. M. Cardona, in *Semiconductors and Semimetals*, Academic Press, New York. Vol. 3, p. 125 (1967)
19. L.M. Roth, B. Lax and S. Zwerdling, *Phys. Rev.* 114, 90 (1959).
20. D.J. Chadi, A.H. Clark and R.D. Burnham, *Phys. Rev. B* 13, 4466 (1976)
21. C. Hermann and C. Weisbuch, *Phys. Rev. B* 15, 823 (1977)
22. W.A. Harrison and S. Ciraci, *Phys. Rev. B* 10, 1516 (1974)
23. R. Dingle, D.D. Sell, S.E. Stokowki and M. Ilegems, *Phys. Rev. B* 4, 1211 (1971)
24. Estimated from the general trend of other Ga-V compounds. close to GaP [18]. (D.J. Chadi private communication).
25. S. Bloom, G. Harbeke, E. Meier and I.B. Ortenburger, *Phys. Stat. Sol.* 66, 161 (1974)

Figures Captions

Figure 1. Resistivity of GaN as a function of $1000/T$.

Figure 2. First derivative absorption resonance line at 10 K and Lorentzian best fit.

Figure 3. Peak to peak line-width ΔH_{pp} as a function of temperature.

